3-2-2018

Chemotherapeutic Applications of Rhodamine Based NanoGUMBOS

Nimisha Bhattarai

Louisiana State University and Agricultural and Mechanical College, nimishabhattarai@gmail.com

Recommended Citation

CHEMOTHERAPEUTIC APPLICATIONS OF RHODAMINE BASED NANOGUMBOS

A Dissertation

Submitted to the Graduate Faculty of the
Louisiana State University and
Agricultural and Mechanical College
in partial fulfillment of the
requirements for the degree of
Doctor of Philosophy

in

The Department of Chemistry

by
Nimisha Bhattarai
B.S. University of Central Missouri, 2013
May 2018

To my mentor, Prof. Warner, thank you so much for your endless support, insightful guidance and inspiration for my future endeavors.

AKNOWLEDGEMENTS

TABLE OF CONTENTS

LIST OF TABLES

LIST OF FIGURES

LIST OF ABBREVIATIONS

2HP-α-CD	2-Hydroxypropyl Alpha cyclodextrin
2HP-β-CD	2-Hydroxypropyl Beta cyclodextrin
γ-CD	Gamma cyclodextrin
Asc	Ascorbate
BETI	Bis(pentafluorethane)sulfonamide
DCM	Dichloromethane
DMSO	Dimethylsulfoxide
DLS	Dynamic light scattering
FTIR	Fourier transform infrared spectroscopy
GUMBOS	Group of Uniform Materials Based on Organic Salts
MTT	(3-(4,5 dimethylthiazol-2yl)-2,5-diphenyltetrazolium bromide)
nanoGUMBOS	Nanoparticles fabricated from GUMBOS
NMR	Nuclear magnetic resonance spectroscopy
OTf	Sodium Trifluoromethanesulfonate
PBS	Phosphate buffered saline
R110	Rhodamine 110
R123	Rhodamine 123
R6G	Rhodamine 6G
RB	Rhodamine B
SNAFR	Seminapthofluorone
TPB	Tetraphenylborate
UV-Vis	Ultraviolet-visible

ABSTRACT

The work presented in this dissertation employs nanomaterials derived from a *g*roup of *u*niform *m*aterials *b*ased on *o*rganic *s*alts (GUMBOS) for selective chemotherapeutic applications. GUMBOS, similar to ionic liquids, are organic salts consisting of a bulky cationic and anionic moiety. In contrast to ionic liquids, these materials have melting points ranging from 25–250 °C, making them solid phase at room temperature. Similar to ionic liquids, GUMBOS display tunable properties, such as hydrophobicity and solubility, through counter ion variation. These tunable properties provide a variety of applications for these GUMBOS, including selective chemotherapeutics applications. The work in this dissertation evaluates the chemotherapeutic behavior of a series of nanomaterials, i.e, nanoGUMBOS, derived from rhodamine dyes to examine the role of both anion variation as well as cation structure on the therapeutic efficacy of the nanoparticle. Firstly, the mechanism of selective toxicity of previously investigated rhodamine 6G (R6G) nanoGUMBOS was determined. Interestingly, these R6G nanoGUMBOS displayed internalization via endocytosis in cancer cells while they lacked endocytic internalization in normal cells. This variation in internalization pathways ultimately resulted in the observed selective behavior of these R6G nanoGUMBOS. In my second project, the role of cyclodextrin (CD) templating on the size and selective chemotherapeutic behavior of these R6G nanoGUMBOS was evaluated. These CD-templated nanoGUMBOS displayed a remarkable two to three-fold increase in toxicity with no effect on selectivity. In my latter two chapters, the therapeutic efficacy of nanoGUMBOS derived from various rhodamine dyes is examined to assess the role of cation structure on selective chemotherapeutic behavior. Intriguingly, a significant difference was found in the selective behavior of GUMBOS derived from ester and carboxylic acid derivatives. In this regard, nanoGUMBOS derived from ester derivatives displayed selective chemotherapeutics

toxicity similar to that of R6G nanoGUMBOS. In contrast, GUMBOS derived from carboxylic acid rhodamines displayed non-selective behavior, suggesting that the selectivity was structure dependent. Further examination of a triple nanoGUMBOS structure corroborated these results as modification of the carboxylic acid structure led to complete selectivity of these nanoGUMBOS under examined conditions. Moreover, these studies demonstrate the promising therapeutic potential and advantages of rhodamine based nanoGUMBOS for selective chemotherapeutic applications.

CHAPTER 1
INTRODUCTION

1.1. CHARACTERISTICS OF CANCER

As reported by the National Cancer Institute, despite the development of several treatment methods, cancer remains the second leading cause of death in the United States in 2017.[1-2] Cancer is defined as the uncontrolled replication of cells that ultimately leads to formation of a tumor that can damage the body's healthy cells. These tumors are typically classified as either benign or malignant.[3-4] Benign tumors are a mass of cells that lack the ability to travel or metastasize to neighboring tissue. In contrast, malignant tumors are a mass of cells that continuously grow and travel to neighboring tissues resulting in disrupted oxygen and nutrient flow to the surrounding normal tissues.[5] These malignant tumors form as a result of genetic mutations within normal cells, which ultimately leads to conversion of the normal to cancer cells through a phenomenon known as oncogenesis.[6] In the case of normal cells, replication can be controlled through a cellular defense mechanism termed apoptosis. Apoptosis refers to programmed cell death to maintain proper conditions of tissues and organs and eradicate the dysfunctional cells. In cancer cells, several genetic mutations leads to formation of oncogenes that cause significant changes in the normal cell processes.[7-8] Specifically, oncogenes that inhibit apoptosis result in an imbalance between cell growth and cell death; thus, leading to uncontrolled cell growth and eventual conversion of the normal cell into an immortal cancer cell.[9]

This process of oncogenesis can be triggered by a variety of either genetic or environmental/lifestyle factors. Genetic factors include inherited DNA mutations, hormone imbalance and immune conditions. External/lifestyle factors include consumption of tobacco and alcohol, diet, exposure to radiation, and environmental pollution. In this regard, the majority (90-95%) of most cancer causes are attributed to environmental factors, while genetic factors only

correspond to about five to ten percent of these cases. Furthermore, the majority of these environmental/lifestyle factors include tobacco consumption, diet and infections. Other environmental factors such as stress, environmental pollutants and exposure to radiation only play a minor role.[10-11] High risk lifestyles and inherited genetic mutations can lead to the DNA mutations that trigger oncogenesis and ultimately leading to the formation of a tumor. Moreover, cancer caused by these environmental factors can be prevented through lifestyle modifications can minimize exposure to these toxic substances. Furthermore despite several advancements in detection techniques, due to their unique characteristics, some cancer are only detected after 10 years of exposure to the toxin that triggered oncogenesis.[11]

These unique characteristics of cancer cells that distinguish them from normal cells develop from the physiological changes they undergo doing oncogenesis. In their studies, Hanahan and Weinberg described these physiological changes as the eight hallmarks of cancer.[12] Firstly, the alteration during oncogenesis allows cancer cells to stimulate self-growth as a mechanism to bypass the needs of a normal tissue for continual growth. This self-growth is stimulated by self-secretion of growth hormones through autocrine signaling, permanent activation of pathways that stimulate growth, destruction of negative feedback that prevents uncontrolled growth, and other mechanisms of autocrine signaling.[13-14] Secondly, within the cancer cells, modifications of tumor suppressor proteins results in their insensitivity towards growth regulation pathways.[15-16] These modifications in the tumor suppressor proteins inactivate the p53 and pRb proteins responsible for regulation of apoptosis and other natural cell death mechanisms. This gives cancer cells the ability to evade cell death due to apoptosis and biological aging, which are the third and fourth hallmarks of cancer.[17-18] These first four hallmarks ultimately result in immortality of cancer cells body as they are able to continuously grow undisturbed from the normal cell processes that would eradicate

mutated or dysfunctional cells. As these cancer cells continuously grow into a tumor mass, their demand for nutrients escalates. In this regard, angiogenesis, the development of new blood vessels, is initiated by the cancer cells as a mechanism to avoid starvation due to continuous growth; this is the fifth hallmark of cancer.[19-20] The sixth distinguishing hallmark of cancer is its ability to invade other cells through these newly formed blood vessels, resulting in tumor metastasis.[21] This continual growth of tumor cells is further stimulated by its seventh hallmark, its ability to exploit both aerobic and anaerobic pathways of glucose synthesis as compared to normal cells which are limited to only aerobic mechanism.[22-23] Lastly, while the immune system of the human body typically recognizes and eliminates disease causing entities, cancer cells have the ability to escape immune system recognition.[12]

1.1.1. Cancer Treatment

Currently, no cure has been developed for cancer. However, several treatment techniques have been developed to control the disease. These treatment techniques include surgery, radiation, immunotherapy, and chemotherapy. An overview of these techniques is presented in Figure 1.1. Surgery involves the excision of the tumor from the body. Radiation therapy refers to the use of x-rays or gamma rays to shrink the tumor. Immunotherapy, a newly developed treatment, uses the cells involved in the body's immune response to attack the tumor cells. Chemotherapy is the most common treatment for cancer and involves the use of medication to treat the cancer.[24-25] Other treatment techniques such as targeted therapy and hormone therapy have been developed as well, but they are used less frequently as compared to the other discussed therapeutics.[26]
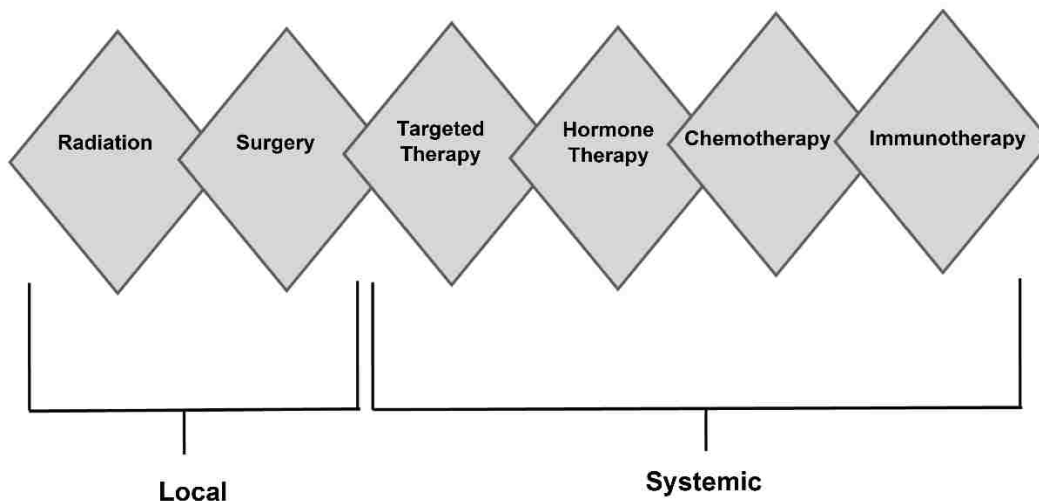
Figure 1.1. Overview of current cancer therapeutics

These current treatments have shown great promise; however, several challenges arise with these therapeutics. As cancer cells continue to grow, their mutations continue to multiply making them susceptible to drug resistance.[27] In addition, while treatments such as radiation therapy, chemotherapy and immunotherapy have shown success in killing tumor cells, they also have harmful effects to normal cells causing many adverse side effects.[28-30] For example, radiation therapy many times can result in nausea, shortness of breath, hair loss and infertility depending on the location the therapy is applied.[30-32] Chemotherapy has similar side-effects to radiotherapy in addition to urinary/bladder changes and kidney malfunction due to toxicity of the drugs.[28, 33] Immunotherapy, hormone therapy and targeted therapy comprise of biomolecules that activate the body's immune system to attack the tumor; thus, they cause less severe side-effects as compared to radiation and chemotherapy.[26, 34] However, the application of these treatment techniques is limited to only certain types of cancer.[29] Thus, design of easily tunable targeted therapeutics becomes essential to minimize systemic toxicity and drug resistance.

4

In this regard, nanomedicine has been widely investigated for targeted therapeutic applications.[35-37] Conventional nanomedicines serve as nanocariers consisting of an outer shell prepared from materials such as polymers and organic-inorganic nanomaterials and a hollow core for drug loading.[37] As compared to conventional therapeutics, nanomaterials provide several distinct advantages. Firstly, several studies have shown that these nanocarriers provide protection of the drug from biodegradation. Secondly, the nanoscale size of the nanocarrier allows enhanced permeation into cells, ultimately enhancing the therapeutic efficacy of the drug. Furthermore, these nanocarriers can be functionalized with various targeting ligands to reduce systemic toxicity.[38-41]

Current research on chemotherapeutic application of nanomaterials have mainly focused on carrier free nanodrugs. Drugs such as doxorubicin and paclitaxel have been self-assembled into nanomaterials through hydrophobic interactions using polymer or inorganic materials as a matrix.[42-43] These carrier free nanodrugs are synthesized via a simple reprecipition reaction where limited organic solvent is used; thus, eliminating the use of toxic organic solvents for formation of nanocarriers. Furthermore, as these nanodrugs are engineered through intramolecular interactions within the drug, high drug loading and release is seen.[44-45] Many nanocarriers suffer from low drug loading due to inadequate interaction between the carrier and the drug, reducing the therapeutic efficacy of these therapeutics. In addition, those nanocarriers that have strong interactions with the drug have low drug release at the tumor site again reducing the efficacy. This reduced drug release can be attributed to the interface between the tumor site and the nanodrug being the nanocarrier rather than the drug. [40, 46-47] In contrast, in these "carrier free" nanodrugs, the interface between the nanodrug and the tumor site is the nanoparticle assembly of the drug itself; thus, allowing for enhanced drug release.[48-49] In this regard, many of these new nanodrugs have been employed for

clinical applications due to their enhanced therapeutic efficacy. Moreover, development of a highly tunable carrier free nanodrug can provide for an interface for rapid synthesis of an array of highly effective therapeutics to combat problems such as systemic toxicity and drug resistance. [50]

In this regard, our research group has developed highly tunable nanomaterials, i.e. nanoGUMBOS, derived from a *g*roup of *u*niform *m*aterials *b*ased on *o*rganic *s*alts (GUMBOS). GUMBOS are comprised of both a cationic and anionic entity and can be synthesized via a simple ion exchange reaction. The simple and rapid synthesis makes these GUMBOS highly tunable for various applications.[51] Anticancer GUMBOS can be designed through the use of either an anticancer cation or anion, and this counter-ion variation can lead to numerous unique properties. Furthermore, GUMBOS can be synthesized using counter-ions that aid in evading biological processes leading to drug resistance and systemic toxicity in order to combat these problems in current therapeutics. This dissertation focuses on synthesis, characterization of and chemotherapeutic examination of rhodamine based nanoGUMBOS.

1.2. ANTICANCER APPLICATIONS OF RHODAMINE DYES

Chemotherapeutic applications of various rhodamine dyes have been examined due to their ability to penetrate the cell membrane and induce mitochondrial dysfunction. These dyes bind to the mitochondrial membrane and block oxidative phosphorylation, which serves as the major pathway of ATP production within the cell.[52] The lipophilic characteristic of these rhodamine dyes allows for enhanced penetration of dye into the cell through interactions with the phospholipid bilayer. Previous investigation of various hydrophobicity of several cationic structures indicated a more selective accumulation of rhodamine dyes as compared to triarylmethane dyes such as methyl and crystal violet. In addition, the cationic charge on some rhodamine derivatives such as rhodamine 6G (R6G) and rhodamine 123 (R123) provide an electrostatic interaction of the dye

with the net negative charge of the cell membrane. The combination of both the lipophilic and cationic characteristics of these rhodamine dyes resulted in partially selective uptake of these dyes into the mitochondrion of cancer cells.[53-54] In-vivo applications of both dyes indicated substantial toxicity of R6G and R123 at high concentrations to healthy tissue limiting their chemotherapeutic application.[52] While the latter has progressed to clinical trials, the high toxicity of the dye ultimately prevented its further use. In addition to R6G and RB, rhodamine 110 (R110) and rhodamine B (RB) have been examined for anticancer applications; however, permeation of the dye into the cell was hindered due to the zwitterion structure. In addition, for R110 the hydrophilic nature of the dye resulted in non-selective uptake of the dye such that intracellular localization was observed in both the cytosol and the mitochondria.[55-56] Further investigations indicated encapsulation of these zwitterion dyes into nanocarriers enhanced therapeutic toxicity since the interface of the cell membrane is now the nanocarrier rather than the dye. In this dissertation, chemotherapeutic applications of R6G, R123, R110 and RB based nanoGUMBOS to enhance the therapeutic potential of these dyes through ion variations.[57-58]

1.3. GUMBOS

GUMBOS (*g*roup of *u*niform *m*aterials *b*ased on *o*rganic *s*alts) are a new class of ionic materials developed by the Warner Research Group.[51] They are organic salts primarily comprising of bulky organic or inorganic cationic and anionic moieties that can be tuned via a simple metathesis reaction. GUMBOS are solid at room temperature with melting point ranges 25-250°C, in contrast to ionic liquids which have melting points below 100°C. Similar to ionic liquids, ion variation of GUMBOS can lead to various changes in their chemical and physical properties, giving them their tunable nature.[51] Furthermore, the simple and rapid synthetic route of these materials give them a distinct advantage over materials requiring lengthy and complex synthesis.

The cationic or anionic moiety typically determines the application of the compound, making these materials inherently task-specific for a variety of applications, including cancer therapy, mass spectrometry, optoelectronic devices, sensors, protein separation, and nanotechnology. These applications arise from the tunable nature of GUMBOS, which allows for modification of hydrophobicity, solubility, thermal stability, and photophysical properties through ion variation. Herein, this dissertation focuses on chemotherapeutic applications of GUMBOS.[51]

Biomedical applications of GUMBOS have been examined through replacement of the cation or anionic moiety with a therapeutic ion. The Warner research group has reported antimicrobial applications of GUMBOS derived from the combination of antibiotic and antiseptic ions. Intriguingly, the combination of both therapeutic ions into a single GUMBOS led to reduced toxicity at examined conditions and a synergistic effect between the antibiotic and antiseptic was observed.[59] Similar applications can be examined for chemotherapeutic applications as well. For example, a targeted therapeutic ion can be combined with a fluorescent probe for fluorescent aided surgery applications. In this regard, the targeted ion serves to drive the GUMBOS to the tumor site, and the fluorescence ion will aid in identification of the tumor.[38, 60] This allows for more precise removal of tumor tissue, in addition to treatment of any residual tumor. Furthermore, targeted therapeutic ions can be combined with other currently toxic therapeutics to create a targeted compound with dual anticancer properties. Moreover, the tunable nature of GUMBOS provides an interface for rapid synthesis of innovative combinations of therapeutics that could aid in reduction of severe side effects and drug resistance.

1.4. NANOGUMBOS

Nanomaterials derived from GUMBOS, i.e. nanoGUMBOS, incorporate the advantages of GUMBOS into a compact nanoscale material, further broadening the application of these organic

salts. These nanoGUMBOS have been employed for various applications such as cancer therapy and biomedical imaging.[51, 61-62] In contrast to conventional nanomaterials used in biomedical applications, these nanoGUMBOS serve as the drug/probe themselves, eliminating the need for lengthy and complex examination of drug loading/release profiles. In addition, the rapid synthesis and tunable nature of nanoGUMBOS allows for easy modification to avoid drug resistance.[62]

1.4.1. Synthesis of NanoGUMBOS

The hydrophobic nature of GUMBOS allows rapid formation of nanoGUMBOS in aqueous media through various methods. For this dissertation, nanoGUMBOS were prepared using reprecipitation and ion-association methods depicted in figure 1.2. For the reprecipitation method, the compound was first dissolved in organic solvent, and a small amount of this solution was rapidly injected into an aqueous medium, such as water or cell media, under sonication for 5 minutes. After sonication, nanoGUMBOS were left to grow for 30 minutes before further use.[62] In the case of ion-association method, both cation and anion were dissolved in an aqueous solvent. Subsequently, the two solutions were mixed under ultrasonication to develop nanoGUMBOS. These nanomaterials were then centrifuged, and dried *in vacuo* to form a nanoparticle pellet.[61] In contrast to reprecipitation, the ion association method provides rapid synthesis of nanomaterials through integration of GUMBOS and nanoGUMBOS formation in one step.
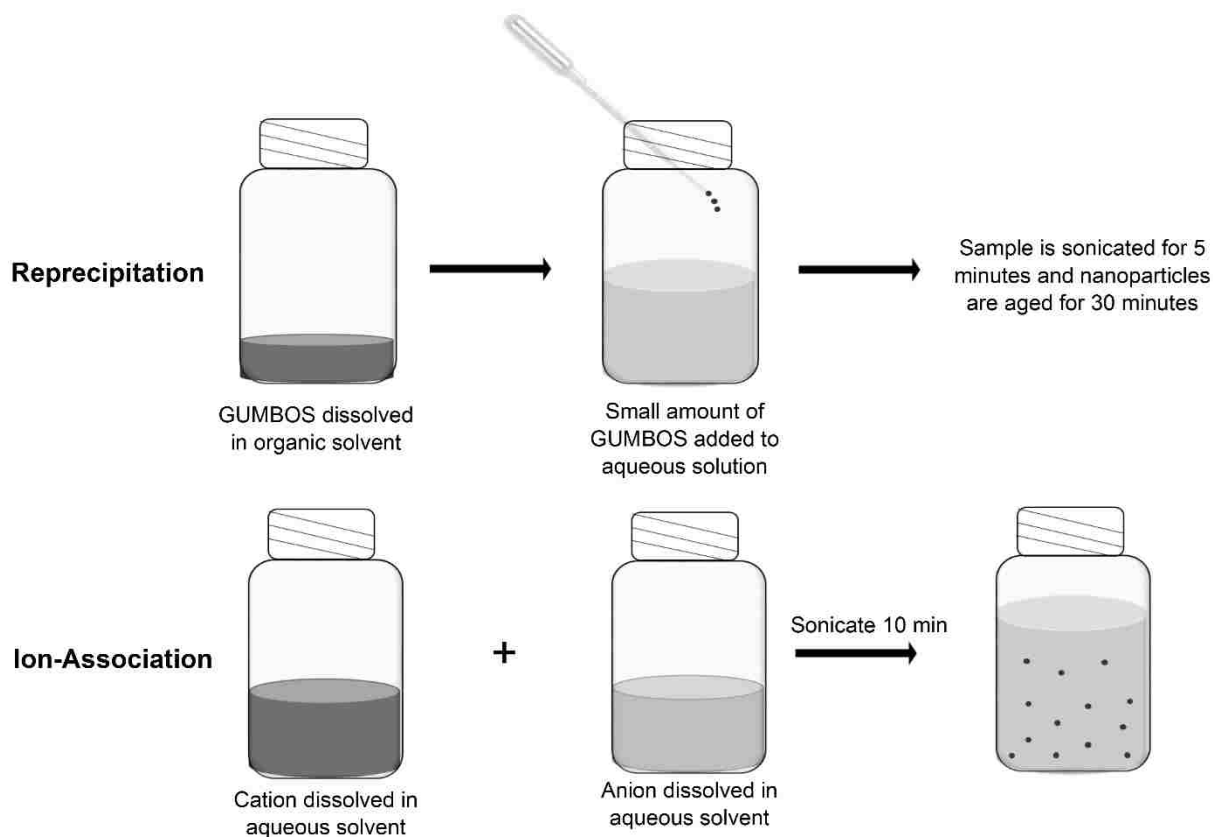
Figure 1.2. Schematic of repreciation and ion association methods for synthesis of nanoGUMBOS

1.5. SELECTIVE CHEMOTHERAPEUTIC APPLICATIONS OF R6G NANOGUMBOS

Recently in our research group, selective chemotherapeutic applications were examined for R6G based nanoGUMBOS.[62] As indicted in the earlier discussion of anticancer applications of rhodamine dyes, the R6G dye has been previously examined for anticancer applications by others; however, its application was limited due to its high toxicity towards normal cells.[63] In our research group, we have found that conversion of the R6G dye into nanoGUMBOS led to selective toxicity towards cancer cells, with no toxicity to normal cells under examined conditions. Examination of cellular uptake indicated a profound increase in cellular internalization of dye into cancer cells as compared to normal cells. Intriguingly, despite minor cellular uptake into normal cells, no toxicity

to normal cells was observed within the explored experimental parameters. Evaluation of the hydrophobicity of these compounds indicated selective toxicity of the two most hydrophobic GUMBOS. These results suggested a dependence of the selective toxicity on the hydrophobicity of the compound. Additional examinations of more hydrophilic GUMBOS indicated non-selective toxicity further corroborating this hypothesis.[62] This dissertation involves a detailed examination of the mechanism of selective toxicity of these rhodamine 6G nanoGUMBOS and further examines other rhodamine derivatives for similar selective chemotherapeutic behavior.

1.6. ANALYTICAL TECHNIQUES

1.6.1. Ultraviolet-Visible Spectroscopy

Ultraviolet visible (UV-Vis) spectroscopy is a powerful analytical technique to quantitate the attenuation of a beam of light due to molecular absorption of the analyte as light passes through a sample. UV-Vis spectroscopy can be used for a variety of applications, ranging from simple examination of photochemistry of a molecule to biomedical applications using colorimetric assays. The working principle of a conventional UV-Vis spectrophotometer is presented in figure 1.3. When a beam of light is released from the source, it first passes through a monochromator, where the light is filtered for a desired wavelength. Subsequently, a beam splitter splits the light into two paths. One of these beams passes through the sample, and another one that passes through a reference cell. Finally, a detector then records the amount of light either absorbed or transmitted by the sample. Typically, molecules that absorb light in the ultraviolet and visible region of the electromagnetic spectrum will have a characteristic peak that corresponds to the wavelength of light absorbed. Beer-Lambert's Law (Beer's Law) correlates the absorbance to the sample concentration (c), molar absorptivity (ϵ), and path length of the cuvette (b). This is typically expressed as A= ϵbc.[64]

In this dissertation, absorbance measurements were used to determine cell viability and cellular uptake following incubation of the synthesized drug. Cell viability measurements were carried out in either a 96 or 24 well plate; thus, a microplate reader was used in place of a conventional spectrophotometer. These two instruments operate based on identical principles, with a slight variation in beam direction. The beam of this microplate reader has a vertical light beam in contrast to the horizontal light beam of a conventional spectrophotometer. In regards to Beer's law, the sample volume replaces the path length in these measurements due to this modification in beam direction. For the cellular uptake studies, a conventional UV-Vis spectrophotometer is used to determine the concentration of internalized drug using several calibration standards. A comparison of the working principle of a multichannel microplate reader to the conventional UV-Vis spectrophotometer is presented in Figure 1.3.[64-65]
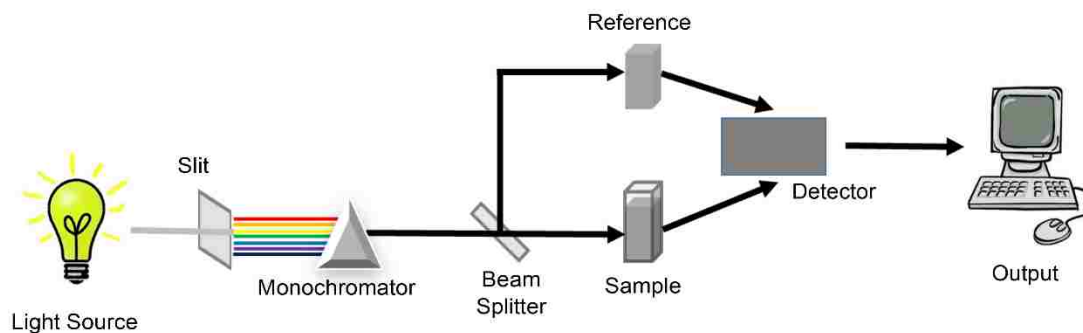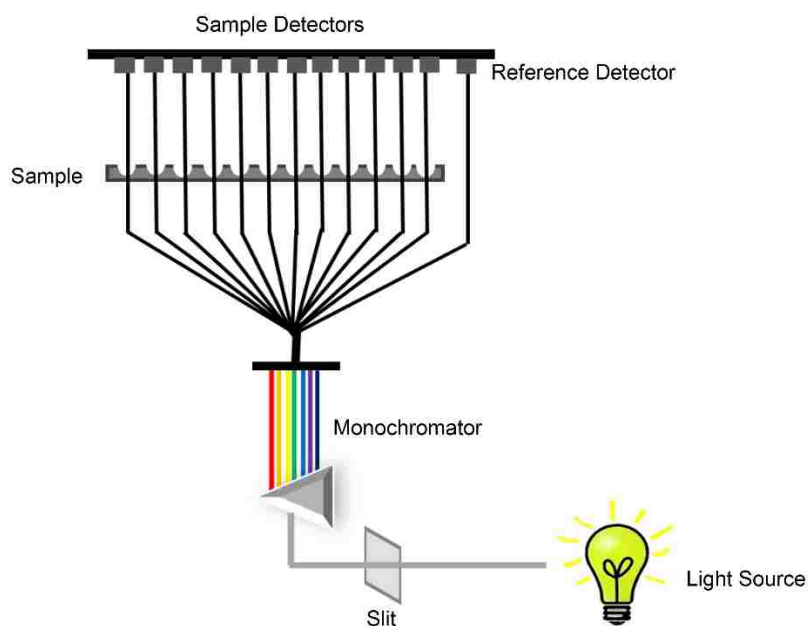
Figure 1.3. Working principles of a conventional UV-Vis spectrophotometer and UV-Vis Microplate Reader

1.6.2. Cytotoxicity Assay

Cytotoxicity assays are typically employed to assess the effect of biological probes or drugs on the function of various cell processes. Furthermore, examination of cell viability provides insight into both therapeutic efficacy and biocompatibility of developed compounds. While several colorimetric assays with varying detection methods have been developed, detection of formazan dyes is the most common technique.[66] Typically, a tetrazolium salt is cleaved into formazan

through metabolic reductase enzymes. Since these reductase enzymes are only active in live cells, the absorbance of the formazan can then be used to ascertain cell viability. The measurements are dependent upon several factors such as cell type, incubation time, type of assay used and number of cells.[67] Compounds that have an overlap in the absorbance wavelength range with the assay can cause skewed results, as the absorbance will come from both the formazan and the compound. Thus, the developed assays come in a variety of detection wavelengths to minimize this background absorbance. In addition, absorbance of just MTT (3-(4,5 dimethylthiazol-2yl)-2,5-diphenyltetrazolium bromide) dye and drug without cells can be used as background absorbance to remove compound interference as well. In this dissertation, the MTT toxicity assay was used to access the cytotoxicity of developed GUMBOS. In the presence of live cells, the yellow MTT dye is cleaved into insoluble purple formazan crystals through the reaction presented in Figure 1.4. Subsequently, a sodium dodecyl sulfate dimethylformamide solution is used to solubilize the crystals to create a homogenous purple solution with an absorbance at 570 nm. The absorbance of this solution is proportional to the number of live cells, as only the cells that are alive will have the reductase enzyme that causes this purple color.[68]
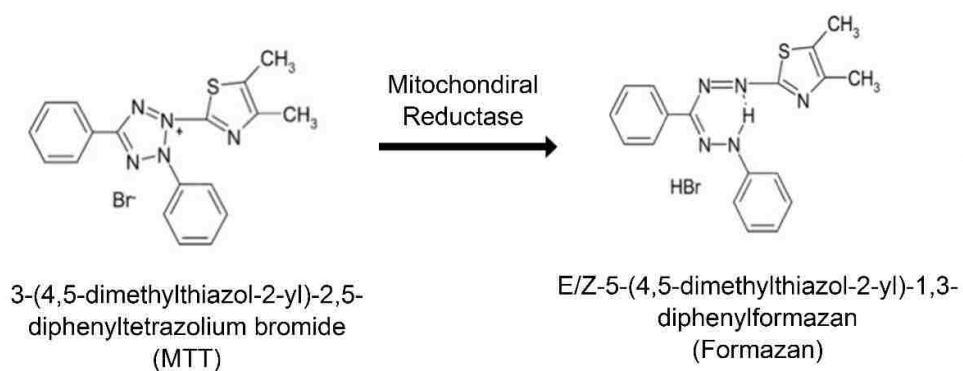
Figure 1.4. Enzymatic reaction of the cleavage of MTT to formazan in the presence of mitochondrial reductase

1.6.3. Fluorescence Spectroscopy

In addition to absorbance spectroscopy, fluorescence spectroscopy can also be used to characterize compounds that absorb light in the ultraviolet and visible range of the electromagnetic spectrum. However, in fluorescence spectroscopy, the amount of light emitted by a molecule as it decays back to ground state from an excited state is measured, rather than the amount of light absorbed by a molecule. This phenomenon is typically symbolized using a Jablonski diagram (Figure 1.5). As the molecule absorbs a photon of light, it is excited from the ground state to an excited state. Fluorescence is the radiative decay of a molecule from the first excited state, S1, back to the ground state. Phosphorescence is a radiative decay process that competes with fluorescence; however, it is less probable. When a molecule in S1 undergoes intersystem crossing (ISC) to an excited triplet state before it decays to the ground state, that molecule undergoes phosphorescence. In the case that the fluorophore is excited to an excited state higher than S1, it must undergo non-radiative decay via internal conversion (IC) to return to S1 prior to fluorescence. When a photon undergoes IC, it emits less energy than it originally absorbed. Thus, the emission wavelength of a molecule is always at a longer wavelength as compared to that of excitation. This shift in the excitation and emission wavelengths is known as Stokes shift.[65]
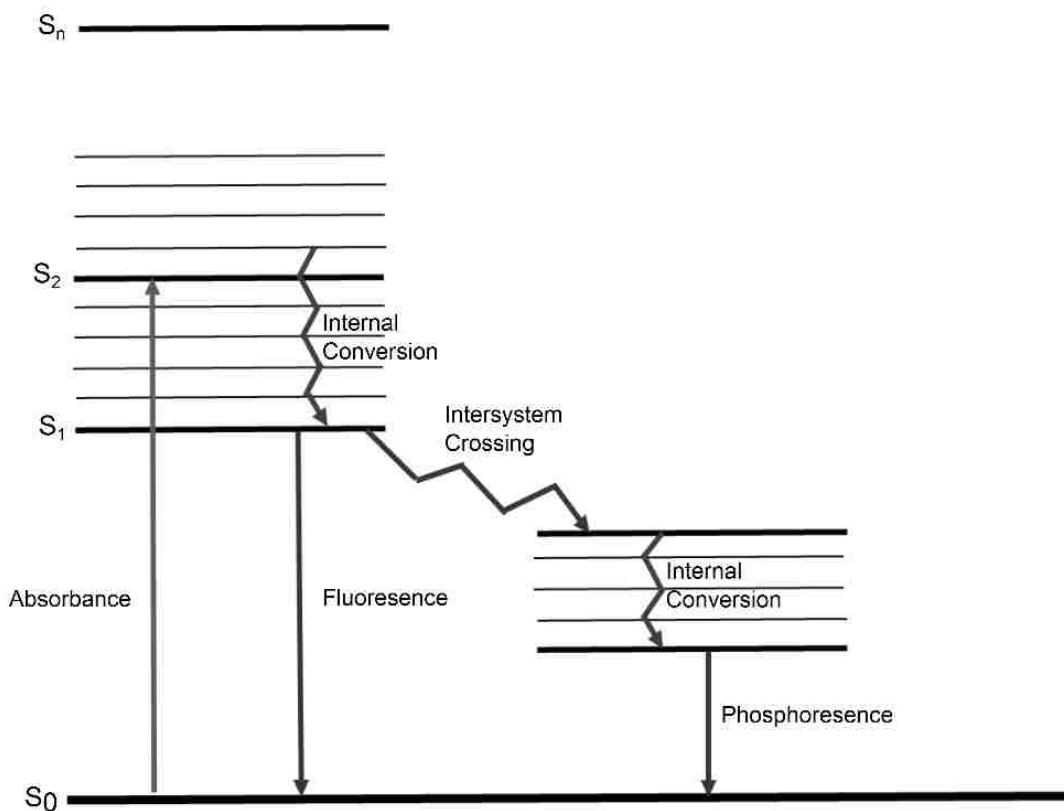
Figure 1.5 Graphical representation of the Jablonski diagram

A typical fluorimeter consists of an excitation and emission monochromator, sample chamber and detector. Briefly, as the light source releases a beam of light, it is first passed through an excitation monochromator where it is filtered for a desired wavelength. As the beam of light passes through the sample, the emitted light is collected perpendicular to the excitation light beam to prevent interference of the incident light with the sample fluorescence. This emitted light is then passed through an emission monochromator, which filters stray light for better detection of the desired wavelength, prior to reaching the detector. As compared to absorbance, all sides of a fluorescence cuvette must be polished as the emitted light is collected perpendicular to the beam of incident light, rather than in a straight line. Figure 1.6 shows a graphical representation of this working principle.[65]
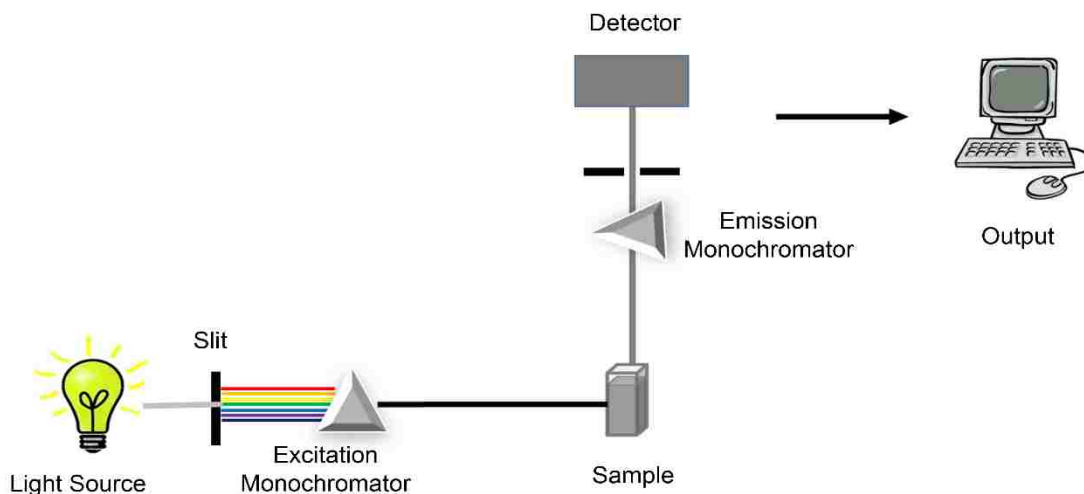
Figure 1.6. Working principle of conventional fluorimeter

1.6.4. Fluorescence Microscopy

Biomedical applications of fluorescence typically rely on the integration of the fluorescence concept described above into a microscope that can aid in visualization of microstructures within the cell. In contrast to bright field microscopy, that only examines the sample with white light, fluorescence microscopy can help increase resolution of fine structures within the cell.[69] In this regard, fluorescence microscopy is typically used in conjunction with staining techniques to examine organelles within the cell. In addition, this technique can also be employed to examine internalization and cellular localization of fluorescent probes or drugs within the cell. Furthermore, while fluorescence microscopy is typically used for qualitative detection of fluorophores within cells, development of new software now allows for quantitation of the observed fluorescence.[70]

A fluorescence microscope consists of a light source, excitation filter, emission filter, and detector. Similar to a fluorescence spectrometer, the excitation and emission filters are used to filter light for the desired wavelengths. In contrast to a conventional fluorescence spectrometer,

17

due to the upright geometry of the microscope, a dichroic beam splitter is used to reflect the excitation light onto the sample, and then transmit the emitted light to the detector. A schematic representation of this instrument is shown in Figure 1.7.[69-71]
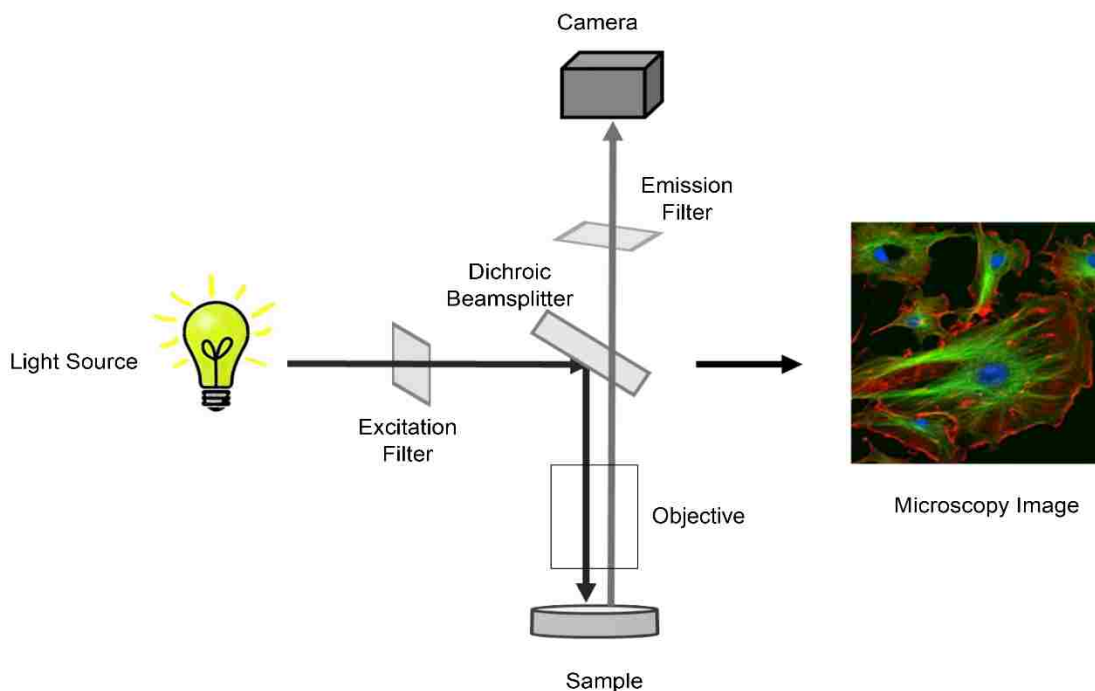
Figure 1.7. Working principle of an upright fluorescence microscope

1.6.5. Transmission Electron Microscopy

Transmission electron microscopy (TEM) is an analytical technique typically used to characterize the size and morphology of dried-state nanoparticles. The superior resolution of TEM enables its use in biological applications to image intracellular organelles as a complimentary technique to light microscopy.[72] In this dissertation, TEM microscopy was employed to characterize the developed nanoGUMBOS. Typical sample preparation involves the deposition of a small volume (4-8 uL) of nanoparticle solution onto a copper coated grid. Other metals such as gold, molybdenum and platinum can be used as well depending on the requirements of the sample; however, copper is the most common. The working principle of TEM is similar to that of a light

microscope; however, electrons are used to generate the final image rather than light.[72-73] A schematic of a TEM microscope is presented in Figure 1.8.

Briefly, electrons are first accelerated out from the electron gun due to a difference in potential of the cathode (heated tungsten filament) and anode components. The beam of electrons is then passed through the sample, resulting in scattering and subsequent transmission of the electrons. Transmission of electrons is primarily dependent upon sample thickness. Typically, 100 nm samples are considered electron transparent, as the thickness allows for the transmitted electrons to pass through the entire sample. After passing through the sample, these electrons are focused onto a fluorescent screen or detector, and where intermediate and projector lenses are used to enlarge the final image.[74-75]
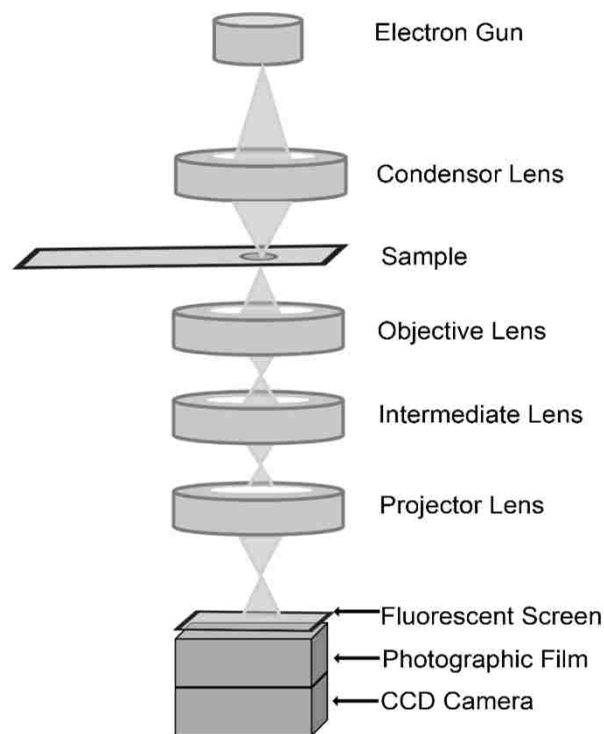
Figure 1.8. Working principle of a transmission electron microscope

1.6.6. Dynamic Light Scattering and Zeta Potential

Dynamic light scattering (DLS) and zeta potential are the two most common methods to characterize nanoparticle size and stability, respectively, in solution state. In contrast to TEM, DLS uses mathematical algorithms to determine the size of the nanomaterials, rather than produce a visual representation.[76-77] Briefly, as a laser beam irradiates a sample, Brownian motion of the nanomaterials within the sample causes scattering of the light and subsequent fluctuations of the intensity of scattered light. The rate of Brownian motion and the rate of fluctuations for the scattered light is largely dependent upon the size of the particle (i.e., smaller particles cause more rapid fluctuations in intensity). In this regard, the correlation function generated from the DLS measurements is based upon the time needed for decay of this signal. The mathematical algorithms then determine the relative size of the nanoparticle from the signal decay time.[78]

In addition to size, stability of nanomaterials also plays a major role in their application, therefore zeta potential measurements are frequently performed to determine nanoparticle stability.[79] The surface charge of the nanoparticle causes a degree of electrostatic repulsion between adjacent and similarly charged particles, which can ultimately prevent the nanoparticle from aggregation and precipitation. In this regard, as the surface charge increases, this repulsion also increases, thus a direct correlation can be made between surface charge and nanoparticle stability. Typically, zeta potential measurements are representative of the nanoparticle charge at the interfacial layer between the dispersion medium and the nanoparticle. This interfacial layer, typically known as the electrical double layer, is generated as the surface charge of the nanoparticle attracts a thin layer of oppositely charged ions.[80] This electrical double layer consists of an inner stern layer where the oppositely charged ions are strongly adhered on the surface of the nanoparticle and an outer diffuse region. As a voltage is applied across the sample, a potential is

generated on the slipping plane of the electrical double layer and the nanoparticle begins to travel towards the electrode of opposite charge of this potential. This potential is said to be zeta potential and can be determined from the velocity of the nanoparticles as they migrate through the sample. Usually, a zeta potential of greater than +30 mV or less than -30 mV indicates a relatively stable solution.[81] In contrast, a zeta potential close to 0 would indicate a high degree of precipitation of the nanoparticles due to unstable conditions.[82]

1.7. OVERVIEW OF DISSERTATION

In the presented work, a series of based nanoGUMBOS were synthesized and examined for their chemotherapeutic properties. Firstly, the previously investigated R6G nanoGUMBOS were further examined to ascertain the mechanism of selective toxicity. Furthermore, these nanomaterials were then employed in athymic nude mice to examine in-vivo therapeutic efficacy, as well as kinetics. Subsequently, in the third chapter, α-HP-CD, β-HP-CD, and γ-CD cyclodextrin was used to template these nanoGUMBOS in order to reduce their size. The effect of this size reduction on the toxicity and selective behavior the nanoparticles was then examined in-vitro studies.

The fourth and fifth chapters of this dissertation examine various rhodamine derivatives and assess their selective chemotherapeutic properties. In Chapter 4, rhodamine 123 was examined for its chemotherapeutic applications in breast and pancreatic cancer cells. This dye has previously been employed for clinical applications; however, its poor toxicity towards cancer cells halted further testing. Since the R6G nanoGUMBOS displayed selective anticancer applications, similar examinations for R123 were conducted to give further insight to its potential clinical use. In Chapter 5, chemotherapeutic applications of GUMBOS based on other rhodamine derivatives such as rhodamine 110 and rhodamine B were examined. As indicated earlier, due to their zwitterion

structure, these rhodamine decreased cellular uptake ultimately limiting their use as therapeutics. Furthermore, while typical rhodamine, such as R123 and R6G, have selective accumulation into the mitochondria, the acid-base properties of the carboxylic acid group in the zwitterion structure of rhodamine B and rhodamine 110 causes non-selective accumulation of these compounds. Previous literature indicated the profound role of hydrophobicity on this selective mitochondrial uptake. Variation of hydrophobicity through counter-ion exchange could provide more insight to tuning these compounds for more selective uptake of these dyes into the mitochondria of cancer cells and enhance their therapeutic potential. GUMBOS are easily tunable organic salts that are ideal for this application due to their rapid synthetic route. Thus, in Chapter 5, GUMBOS derived from these zwitterion rhodamines were examined for enhanced chemotherapeutic efficacy as compared to the respective parent dyes.

1.8. REFERENCES

1.   Siegel, R. L.; Miller, K. D.; Jemal, A., Cancer statistics, 2015. *CA: A Cancer Journal for Clinicians* **2015,** *65* (1), 5-29.

2.   Cancer Statistics - National Cancer Institute. **2017**.

3.   What Is Cancer? - National Cancer Institute. **2017**.

4.   WHO | Cancer. *WHO* **2017**.

5.   Clark, W. H., Tumour progression and the nature of cancer. *British Journal of Cancer* **1991,** *64* (4), 631-644.

6.   Fearon, E. R.; Vogelstein, B., A genetic model for colorectal tumorigenesis. *Cell* **1990,** *61* (5), 759-767.

7.   Vogelstein, B.; Kinzler, K. W., The multistep nature of cancer. *Trends in Genetics* **1993,** *9* (4), 138-141.

8.   Tomasetti, C.; Li, L.; Vogelstein, B., Stem cell divisions, somatic mutations, cancer etiology, and cancer prevention. *Science* **2017,** *355* (6331), 1330-1334.

9.   Oncogenes and tumor suppressor genes | American Cancer Society. **2017**.

10.   Anand, P.; Kunnumakara, A. B.; Sundaram, C.; Harikumar, K. B.; Tharakan, S. T.; Lai, O. S.; Sung, B.; Aggarwal, B. B., Cancer is a Preventable Disease that Requires Major Lifestyle Changes. *Pharmaceutical Research* **2008,** *25* (9), 2097-2116.

11.   Trichopoulos, D.; Li, F. P.; Hunter, D. J., What Causes Cancer? *Scientific American* **1996,** *275* (3), 80-87.

12.   Hanahan, D.; Weinberg, Robert A., Hallmarks of Cancer: The Next Generation. *Cell 144* (5), 646-674.

13.   Sporn, M. B., Autocrine growth factors and cancer. *Nature* **1986,** *313*, 745-747.

14.   DeBerardinis, R. J.; Lum, J. J.; Hatzivassiliou, G.; Thompson, C. B., The Biology of Cancer: Metabolic Reprogramming Fuels Cell Growth and Proliferation. *Cell Metabolism* **2008,** *7* (1), 11-20.

15.   Toshiyuki, M.; Reed, J. C., Tumor suppressor p53 is a direct transcriptional activator of the human bax gene. *Cell* **1995,** *80* (2), 293-299.

16.   Negrini, S.; Gorgoulis, V. G.; Halazonetis, T. D., Genomic instability—an evolving hallmark of cancer. *Nature Reviews Molecular Cell Biology* **2010,** *11* (3), 220-228.

17.   Garner, E.; Raj, K., Protective mechanisms of p53-p21-pRb proteins against DNA damage-induced cell death. *Cell Cycle* **2008,** *7* (3), 277-282.

18.   Campisi, J., Aging, Cellular Senescence, and Cancer. *Annual review of physiology* **2013,** *75*, 685-705.

19.   Nishida, N.; Yano, H.; Nishida, T.; Kamura, T.; Kojiro, M., Angiogenesis in Cancer. *Vascular Health and Risk Management* **2006,** *2* (3), 213-219.

20.   Hanahan, D.; Folkman, J., Patterns and Emerging Mechanisms of the Angiogenic Switch during Tumorigenesis. *Cell* **1996,** *86* (3), 353-364.

21.   Gupta, G. P.; Massagué, J., Cancer Metastasis: Building a Framework. *Cell* **2006,** *127* (4), 679-695.

22.   Dang, C. V.; Semenza, G. L., Oncogenic alterations of metabolism. *Trends in Biochemical Sciences* **1999,** *24* (2), 68-72.

23.   Hsu, P. P.; Sabatini, D. M., Cancer Cell Metabolism: Warburg and Beyond. *Cell* **2008,** *134* (5), 703-707.

24.   Comprehensive Cancer Information - National Cancer Institute. **2017**.

25.   Types of Cancer Treatment | American Cancer Society. **2017**.

26.   Abou-Jawde, R.; Choueiri, T.; Alemany, C.; Mekhail, T., An overview of targeted treatments in cancer. *Clinical Therapeutics* **2003,** *25* (8), 2121-2137.

27.   Pastan, I.; Gottesman, M., Multiple-Drug Resistance in Human Cancer. *New England Journal of Medicine* **1987,** *316* (22), 1388-1393.

28.   Burstein, H. J., Side Effects of Chemotherapy. *Journal of Clinical Oncology* **2000,** *18* (3), 693-693.

29.   Couzin-Frankel, J., Cancer Immunotherapy. *Science* **2013,** *342* (6165), 1432-1433.

30.   Al-Mefty, O.; Kersh, J. E.; Routh, A.; Smith, R. R., The long-term side effects of radiation therapy for benign brain tumors in adults. *Journal of Neurosurgery* **1990,** *73* (4), 502-512.

31.   Bentzen, S. M., Preventing or reducing late side effects of radiation therapy: radiobiology meets molecular pathology. *Nature Reviews Cancer* **2006,** *6* (9), 702-713.

32.   Dearnaley, D. P.; Khoo, V. S.; Norman, A. R.; Meyer, L.; Nahum, A.; Tait, D.; Yarnold, J.; Horwich, A., Comparison of radiation side-effects of conformal and conventional radiotherapy in prostate cancer: a randomised trial. *The Lancet* **1999,** *353* (9149), 267-272.

33.   Attar, E. C.; Ervin, T.; Janicek, M.; Deykin, A.; Godleski, J., Side Effects of Chemotherapy. *Journal of Clinical Oncology* **2000,** *18* (3), 697-697.

34.   Jaffee, E. M., Immunotherapy of cancer. *Annals of the New York Academy of Sciences* **1999,** *886* (1), 67-72.

35.   Brannon-Peppas, L.; Blanchette, J. O., Nanoparticle and targeted systems for cancer therapy. *Advanced drug delivery reviews* **2004,** *56* (11), 1649-1659.

36.   Cho, K.; Wang, X.; Nie, S.; Shin, D. M., Therapeutic nanoparticles for drug delivery in cancer. *Clinical cancer research* **2008,** *14* (5), 1310-1316.

37.   Peer, D.; Karp, J. M.; Hong, S.; Farokhzad, O. C.; Margalit, R.; Langer, R., Nanocarriers as an emerging platform for cancer therapy. *Nature nanotechnology* **2007,** *2* (12), 751-760.

38.   Liu, Y.; Miyoshi, H.; Nakamura, M., Nanomedicine for drug delivery and imaging: a promising avenue for cancer therapy and diagnosis using targeted functional nanoparticles. *International journal of cancer* **2007,** *120* (12), 2527-2537.

39.   Kawasaki, E. S.; Player, A., Nanotechnology, nanomedicine, and the development of new, effective therapies for cancer. *Nanomedicine: Nanotechnology, Biology and Medicine* **2005,** *1* (2), 101-109.

40.	Wicki, A.; Witzigmann, D.; Balasubramanian, V.; Huwyler, J., Nanomedicine in cancer therapy: Challenges, opportunities, and clinical applications. *Journal of Controlled Release* **2015,** *200*, 138-157.

41.	Danhier, F.; Feron, O.; Préat, V., To exploit the tumor microenvironment: passive and active tumor targeting of nanocarriers for anti-cancer drug delivery. *Journal of Controlled Release* **2010,** *148* (2), 135-146.

42.	Zhang, R.; Xing, R.; Jiao, T.; Ma, K.; Chen, C.; Ma, G.; Yan, X., Carrier-free, chemophotodynamic dual nanodrugs via self-assembly for synergistic antitumor therapy. *ACS applied materials & interfaces* **2016,** *8* (21), 13262-13269.

43.	Zhang, J.; Li, Y.; An, F.-F.; Zhang, X.; Chen, X.; Lee, C.-S., Preparation and size control of sub-100 nm pure nanodrugs. *Nano letters* **2014,** *15* (1), 313-318.

44.	Kasai, H.; Murakami, T.; Ikuta, Y.; Koseki, Y.; Baba, K.; Oikawa, H.; Nakanishi, H.; Okada, M.; Shoji, M.; Ueda, M., Creation of pure nanodrugs and their anticancer properties. *Angewandte Chemie International Edition* **2012,** *51* (41), 10315-10318.

45.	Zhou, M.; Zhang, X.; Yang, Y.; Liu, Z.; Tian, B.; Jie, J.; Zhang, X., Carrier-free functionalized multidrug nanorods for synergistic cancer therapy. *Biomaterials* **2013,** *34* (35), 8960-8967.

46.	Moghimi, S. M.; Hunter, A. C.; Murray, J. C., Nanomedicine: current status and future prospects. *The FASEB journal* **2005,** *19* (3), 311-330.

47.	Huang, P.; Wang, D.; Su, Y.; Huang, W.; Zhou, Y.; Cui, D.; Zhu, X.; Yan, D., Combination of Small Molecule Prodrug and Nanodrug Delivery: Amphiphilic Drug–Drug Conjugate for Cancer Therapy. *Journal of the American Chemical Society* **2014,** *136* (33), 11748-11756.

48.	Chen, F.; Zhao, Y.; Pan, Y.; Xue, X.; Zhang, X.; Kumar, A.; Liang, X.-J., Synergistically Enhanced Therapeutic Effect of a Carrier-Free HCPT/DOX Nanodrug on Breast Cancer Cells through Improved Cellular Drug Accumulation. *Molecular Pharmaceutics* **2015,** *12* (7), 2237-2244.

49.	Li, Y.; Lin, J.; Huang, Y.; Li, Y.; Yang, X.; Wu, H.; Wu, S.; Xie, L.; Dai, L.; Hou, Z., Self-Targeted, Shape-Assisted, and Controlled-Release Self-Delivery Nanodrug for Synergistic Targeting/Anticancer Effect of Cytoplasm and Nucleus of Cancer Cells. *ACS Applied Materials & Interfaces* **2015,** *7* (46), 25553-25559.

50.	Zhao, Y.; Chen, F.; Pan, Y.; Li, Z.; Xue, X.; Okeke, C. I.; Wang, Y.; Li, C.; Peng, L.; Wang, P. C.; Ma, X.; Liang, X.-J., Nanodrug Formed by Coassembly of Dual Anticancer Drugs to Inhibit Cancer Cell Drug Resistance. *ACS Applied Materials & Interfaces* **2015,** *7* (34), 19295-19305.

51.   Warner, I. M.; El-Zahab, B.; Siraj, N., Perspectives on Moving Ionic Liquid Chemistry into the Solid Phase. *Analytical Chemistry* **2014,** *86* (15), 7184-7191.

52.   Fearon, K. C.; Plumb, J. A.; Burns, H. J.; Calman, K. C., Reduction of the growth rate of the Walker 256 tumor in rats by rhodamine 6G together with hypoglycemia. *Cancer research* **1987,** *47* (14), 3684-3687.

53.   Belostotsky, I.; Da Silva, S.; Paez, M.; Indig, G., Mitochondrial targeting for photochemotherapy. Can selective tumor cell killing be predicted based on n-octanol/water distribution coefficients? *Biotechnic & Histochemistry* **2011,** *86* (5), 302-314.

54.   Modica-Napolitano, J. S.; Aprille, J. R., Delocalized lipophilic cations selectively target the mitochondria of carcinoma cells. *Advanced drug delivery reviews* **2001,** *49* (1), 63-70.

55.   Jeannot, V.; Salmon, J.-M.; Deumié, M.; Viallet, P., Intracellular accumulation of rhodamine 110 in single living cells. *Journal of Histochemistry & Cytochemistry* **1997,** *45* (3), 403-412.

56.   Lampidis, T. J.; Castello, C.; Del Giglio, A.; Pressman, B. C.; Viallet, P.; Trevorrow, K. W.; Valet, G. K.; Tapiero, H.; Savaraj, N., Relevance of the chemical charge of rhodamine dyes to multiple drug resistance. *Biochemical pharmacology* **1989,** *38* (23), 4267-4271.

57.   El Baraka, M.; Deumié, M.; Viallet, P.; Lampidis, T. J., Fluorescence properties and partitioning behaviour of esterified and unesterified rhodamines. *Journal of Photochemistry and Photobiology A: Chemistry* **1991,** *62* (2), 195-216.

58.   *Frontiers in Nanomedicine*. Bentham Science Publishers: Sharjah, UAE, 2017; Vol. 2.

59.   Cole, M. R.; Hobden, J. A.; Warner, I. M., Recycling antibiotics into GUMBOS: A new combination strategy to combat multi-drug-resistant bacteria. *Molecules* **2015,** *20* (4), 6466-6487.

60.   Lee, J. E.; Lee, N.; Kim, H.; Kim, J.; Choi, S. H.; Kim, J. H.; Kim, T.; Song, I. C.; Park, S. P.; Moon, W. K., Uniform mesoporous dye-doped silica nanoparticles decorated with multiple magnetite nanocrystals for simultaneous enhanced magnetic resonance imaging, fluorescence imaging, and drug delivery. *Journal of the American Chemical Society* **2009,** *132* (2), 552-557.

61.   Hamdan, S.; Dumke, J. C.; El-Zahab, B.; Das, S.; Boldor, D.; Baker, G. A.; Warner, I. M., Strategies for controlled synthesis of nanoparticles derived from a group of uniform materials based on organic salts. *Journal of colloid and interface science* **2015,** *446*, 163-169.

62.   Magut, P. K.; Das, S.; Fernand, V. E.; Losso, J.; McDonough, K.; Naylor, B. M.; Aggarwal, S.; Warner, I. M., Tunable cytotoxicity of rhodamine 6G via anion variations. *Journal of the American Chemical Society* **2013,** *135* (42), 15873-15879.

63.   Kutushov, M.; Gorelik, O., Low concentrations of Rhodamine-6G selectively destroy tumor cells and improve survival of melanoma transplanted mice. *Neoplasma* **2013,** *60* (3), 262-73.

64.   Skoog, D. A., *Principles of Instrumental Analysis*. 6th ed.; Thomas Brooks/Cole: Belmont, CA, 2007.

65.   Lakowicz, J., *Principles of Fluoresence Spectroscopy*. 3rd ed.; Springer Science: New York, 2006.

66.   Gerlier, D.; Thomasset, N., Use of MTT colorimetric assay to measure cell activation. *Journal of immunological methods* **1986,** *94* (1-2), 57-63.

67.   Denizot, F.; Lang, R., Rapid colorimetric assay for cell growth and survival: modifications to the tetrazolium dye procedure giving improved sensitivity and reliability. *Journal of immunological methods* **1986,** *89* (2), 271-277.

68.   van Meerloo, J.; Kaspers, G. J.; Cloos, J., Cell sensitivity assays: the MTT assay. *Cancer cell culture: methods and protocols* **2011**, 237-245.

69.   Yuste, R., Fluorescence microscopy today. *Nature methods* **2005,** *2* (12), 902-904.

70.   Lichtman, J. W.; Conchello, J.-A., Fluorescence microscopy. *Nature methods* **2005,** *2* (12), 910.

71.   Valeur, B.; Berberan-Santos, M. N., *Molecular fluorescence: principles and applications*. John Wiley & Sons: 2012.

72.   Burghardt, R. C.; Droleskey, R., Transmission electron microscopy. *Current protocols in microbiology* **2006**, 2B. 1.1-2B. 1.39.

73.   Williams, D. B.; Carter, C. B., The transmission electron microscope. In *Transmission electron microscopy*, Springer: 1996; pp 3-17.

74.   Reimer, L., *Transmission electron microscopy: physics of image formation and microanalysis*. Springer: 2013; Vol. 36.

75.   Heidenreich, R. D., Fundamentals of transmission electron microscopy. **1964**.

76.   Chu, B., Dynamic light scattering. In *Soft Matter Characterization*, Springer: 2008; pp 335-372.

77.   Berne, B. J.; Pecora, R., *Dynamic light scattering: with applications to chemistry, biology, and physics*. Courier Corporation: 2000.

78.   Pecora, R., Dynamic light scattering measurement of nanometer particles in liquids. *Journal of nanoparticle research* **2000,** *2* (2), 123-131.

79.   Zhang, Y.; Yang, M.; Portney, N. G.; Cui, D.; Budak, G.; Ozbay, E.; Ozkan, M.; Ozkan, C. S., Zeta potential: a surface electrical characteristic to probe the interaction of nanoparticles with normal and cancer human breast epithelial cells. *Biomedical microdevices* **2008,** *10* (2), 321-328.

80.   Kirby, B. J., *Micro-and nanoscale fluid mechanics: transport in microfluidic devices*. Cambridge University Press: 2010.

81.   áO'Brien, R. W., Electroacoustic studies of moderately concentrated colloidal suspensions. *Faraday Discussions of the Chemical Society* **1990,** *90*, 301-312.

82.   Hunter, R. J., *Zeta potential in colloid science: principles and applications*. Academic press: 2013; Vol. 2.

CHAPTER 2
ENDOCYTIC SELECTIVE TOXICITY OF RHODAMINE 6G BASED NANOGUMBOS

2.1. INTRODUCTION

The increasing number of side effects of current chemotherapeutics makes the development of more targeted therapeutics essential.[1] In contrast to conventional chemotherapeutics, nanodrugs allow for a more targeted therapy; thus, several nanodrugs have been engineered and examined for chemotherapeutic applications in effort to reduce this systemic toxicity.[2-5] Conventional nanodrugs serve as a nanocarrier composed of either polymeric or organic/inorganic materials with a hollow inner core for drug loading.[6-8] In contrast to conventional theraptueic techniques, these nanocarriers provide a protective veichle of transport for the drug to the tumor site. Furthermore, the nanoscale size of these carries allows for enhanced permeation into the cell, ultimately enhancing the therapeutic efficacy of the drug.[3, 6-7, 9] Moreover, these nanocarriers have enhanced the efficacy of several drugs; however, most of these nanocarriers suffer poor drug loading and release; thus, the synthetic route requires several lengthy optimizations.[10-11, 12]

Our group has developed selective chemotherapeutic nanomaterials, nanoGUMBOS, derived from a *g*roup of *u*niform *m*aterials *b*ased on *o*rganic *s*alts (GUMBOS). GUMBOS are organic salts with tunable properties, such as hydrophobicity, making them particularly suitable for several unique applications.[13] In contrast to typical nanomaterials that serve only as drug carriers, nanoGUMBOS can serve as the therapeutic drug, eliminating the need for a matrix. Our previous study demonstrated that tuning the hydrophobicity of the R6G-based GUMBOS, followed by production of nanoGUMBOS from such materials, led to selective toxicity towards the MDA-MB-231 cancer cell line over normal breast cells, despite the nonselective behavior of the parent dye, [R6G][Cl].[14] While previous studies have examined several cations of varying hydrophobicity for targeting the mitochondrial membrane, to the best of our knowledge our studies

were the first to investigate tunable hydrophobicity of a single compound for selective cytotoxicity of nanomaterials.[15-17] Subsequently, other research groups have corroborated similar findings and have begun to investigate tunable hydrophobicity through counter-ion exchanges for several applications.[18-20] In this study, we examine the mechanism of selective toxicity of these nanomaterials.

Examination of the mechanism of selectivity is essential for development of more efficient chemotherapeutics. Several studies examining selectivity of nanomaterials have attributed their selective behavior to targeting agents as well as various internalization pathways; in this work, we have focused on examination of the latter approach.[21] Internalization of nanoparticles in cells typically occurs through endocytosis.[22-30] Endocytosis can occur via two primary pathways: phagocytosis and pinocytosis. Phagocytosis is generally associated with large particles (2-3 µm), while pinocytosis is associated with nanoscale particles. Pinocytosis is further divided into three categories 1) caveolin-mediated endocytosis 2) clathrin-mediated endocytosis, and 3) micropinocytosis.[22-23] In cancer cells, overexpression of certain endocytic proteins is often observed.[24] The nanoparticle size, charge, and shape can be modified for cellular uptake using the pathways associated with these overexpressed proteins.[25] Therefore, a detailed understanding of the internalization pathway can aid in systematic modification of nano-drugs.[26-30]

Herein, the role of endocytosis in the selective chemotherapeutic behavior of the R6G-based nanoGUMBOS was examined using MDA-MB-231 breast cancer and HMEC and Hs578Bst normal breast cell lines. Since our studies examine internalization of nanomaterials, this manuscript focuses primarily on pinocytic pathways. In these studies, cell viability as well as fluorescence microscopy measurements were used in conjunction with various pinocytosis inhibitors to examine internalization of the R6G-based nanoGUMBOS. In addition, mitochondrial

and lysosomal staining techniques were employed in order to investigate the cellular localization of the nanoGUMBOS. Lastly, *in vivo* studies of the [R6G][BETI] nanoGUMBOS were performed to evaluate bio distribution and drug efficacy.

2.2. MATERIALS AND METHODS

2.2.1. Materials

Rhodamine 6G (95%), phosphate buffered saline (10x concentrate, 0.2 uM filtered), methylene chloride, dimethylsulfoxide (DMSO), citric acid monohydrate, sodium phosphate dibasic, chlorpromazine (98%), filipin III (85%), 5 n-ethyl-n-isopropyl amiloride, 4-(2-aminoethyl) benzenesulfonyl fluoride hydrochloride and 0.2 uM nylon filters were purchased from Sigma-Aldrich (Milwaukee, WI). MitoTracker and LysoTracker dyes were purchased from Molecular Probes (Eugene, OR). Chloroquine hydrochloride was purchased from InvivoGen (San Diego, CA). Lithium bis (perfluoroethylsulfonyl) imide was obtained from Dr. Gary Baker (Oak Ridge National Laboratory, Oak Ridge, TN). Triply deionized water was obtained from an Aires High Purity Water System (Port Allen, LA). The cell viability MTT (3-[4, 5-Dimethylthiazol-2-yl]-2, 5-diphenyltetrazolium bromide) assay was purchased from Promega Corporation (Madison, WI). TEM grids were purchased from Ted Pella (Redding, CA).

2.2.2. Synthesis of GUMBOS.

The R6G based GUMBOS were synthesized using an anion exchange method outlined in Magut et.al.[1] Rhodamine 6G GUMBOS were prepared using a two-phase ion exchange method modified from literature.[7] Briefly, rhodamine 6G chloride was dissolved in dichloromethane (DCM) and mixed with an aqueous solution of lithium bis(perfluoroethylsulonyl) imide (BETI) in a 1:1 mole ratio and 2:1 volume ratio. The biphasic mixture was allowed to stir for 48 h at room temperature. After stirring for 48 h, deionized water was then used to wash the DCM layer to

remove lithium chloride by-product. Subsequently, the aqueous layer was removed and the DCM layer was rotoevaporated. The product was then dried *in vacuo* to remove trace amounts of water.

2.2.3. Synthesis and characterization of nanoGUMBOS.

R6G based nanoGUMBOS were made through a reprecipitation method outlined in Magut et.al.[1] [R6G][BETI] was dissolved was dissolved in dimethylsulfoxide (DMSO) at 2% of the total volume). Then, a 1 mM solution of nanoGUMBOS was formed by rapid injection of the DMSO solution into the cell medium under ultra-sonication for five minutes. The solution was then allowed to sit for 30 minutes, followed by dilution to 100 µM with cell medium for cell studies. TEM grids were spotted using 3 µL of nanoGUMBOS solution for characterization.

2.2.4. Study of nanoGUMBOS Dissociation.

R6G based nanoGUMBOS were made using the reprecipitation method described above. NanoGUMBOS were then diluted in either a phosphate citric acid buffer at pH seven or pH four. Buffers were made using triply de-ionized water that was filtered with 0.2 uM nylon filters.

2.2.5. Cell culture

In vitro experiments were performed using normal human breast epithelial cells (HMEC), normal human breast fibroblast breast cells (Hs578Bst) and hormone-independent human breast adenocarcinoma cells (MDA-MB-231) obtained from the American Tissue Culture Collection (ATCC, Manassas, VA). These cells were cultured according to the recommendations of the supplier. HMEC cells were cultured in Lonza Mammary Epithelial Growth Medium with Lonza MGEM Bullet Kit. MDA-MB-231 cells were cultured in Leibovitz's L-15 Medium containing 10% fetal bovine serum FBS.

2.2.6. Cell viability measurements.

Cell viability measurements were performed using 24 well plates using an MTT Assay kit

(Promega Corporation, Madison WI, USA). In each well of the 24-plate, 100,000 MDA-MB-231 cells were seeded in 0.5 mL of cell media and incubated at 37°C and 5% CO_2 for 24 h. Following the 24 h incubation, the media was then replaced with 0.5 mL of cell media containing 7 µg/mL, 3 µg/mL or 2.9 µg/mL of chlorpromazine, filipin III, and amiloride respectively. For the control wells with no inhibitor, the media was replaced with 0.5 mL of fresh cell media without inhibitor. After 2 h., the media containing the inhibitor was then replaced with 0.5 mL of nanoGUMBOS in cell media. After addition of the nanoGUMBOS, the cells were incubated for 48 h at 37°C and 5% CO_2. Following a 48 h incubation, an MTT assay was performed to observe cytotoxicity based on the Promega protocol. In brief, the MTT dye (150 µL) was added to each well and incubated for 4 h at 37°C and 5% CO_2. The MTT dye reacts with the NAPDH enzyme in live cells to form an insoluble purple formazan compound. Then, 1000 µL of the stop solution, consisting of 10% HCL in SDS buffer, were added to each well and incubated for another hour to dissolve the formazan and terminate the enzymatic reaction of the MTT dye with the NADPH enzyme. Absorbance measurements were obtained using a multichannel microplate spectrophotometer (Benchmark Plus; Bio-Rad Laboratories, Hercules, CA) at 570 nm. For cell viability calculations, the absorbance ratio was calculated between the cells treated with nanoGUMBOS and untreated cells, assuming 100% cell viability for the untreated control. A similar protocol was used for the lysosomal inhibitors with modification of concentration based on literature.

2.2.7. Fluorescence microscopy.

MDA-MB-231 breast cancer, Hs578Bst and HMEC cell lines were used for microscopy studies. In brief, approximately 10,000 cells were seeded in three mL of cell media on a 25 mm glass bottom petri dish (10 mm micro cell; Ashland, MA, USA) and incubated at 37°C for 24 h. After 24 h, cells were then pre-incubated with cell media containing 7 µg/mL, 3 µg/mL or 2.9 µM

of chlorpromazine, Filipin III, and amiloride inhibitor respectively for 2 h. For the sucrose and K^+ depletion inhibitor studies, cells were incubated with sucrose supplemented PBS, K^+ Free HEPES buffer, or the respective controls PBS buffer and K^+ Supplemented HEPES buffer for 1 h. After incubation, the inhibitor solution was removed from the cells and replaced with 25 uM of either [R6G][BETI] or [R6G][Cl], and cells incubated for another 30 minutes. Following compound incubation, the cells were washed with PBS. Fluorescence images were taken using a 40× dipping objective lens with the TRITC (excitation 535 ± 15 and emission 575 ± 15) fluorescence filter on the Leica DM RXA2 fluorescence microscope for the endocytosis studies.

For studies with MitoTracker and LysoTracker, 1 mM DMSO stock solutions of LysoTracker and MitoTracker were diluted to 15 and 10 nM in cell media respectively. NanoGUMBOS were diluted to a 25 nM working concentration in cell media. Cells were first incubated with 15 nM LysoTracker solution for 20 minutes. This solution was then removed and cells were washed with cell media to remove any excess dye. A 10 nM MitoTracker solution was then incubated with the cells for 20 minutes. Following incubation, cells were washed again with cell media to remove any excess dye. Finally, cells were incubated with the 25 nM nanoGUMBOS solution for 30 minutes. This solution was then removed and cells were washed with PBS buffer to remove excess dye. Cell media was replaced with PBS buffer for imaging.

2.2.8. *In vivo* **studies.**

Athymic nude mice were used for *in vivo* studies employing an IACUC approved protocol. Mice were injected with MDA-MB-231 cancer cells and the tumor formed was treated using R6G nanoGUMBOS. The tumor was allowed to grow for 41 days followed by subsequent injection of PBS buffer, 0.16 mg/kg [R6G][BETI] nanoGUMBOS or 1.6 mg/kg [R6G][BETI] nanoGUMBOS.

2.2.9. Statistical analysis.

A t-test was performed to ensure significant differences in cell viability with and without inhibitor and in-vivo examination. Significance was determined using p=0.05 (95% confidence level) for the inhibitor studies. In the case of in-vivo studies, significance was determined using a two-way ANOVA analysis. All results were measured in triplicate and expressed as mean cell viability % ± SD.

2.3. RESULTS AND DISCUSSIONS

2.3.1. Synthesis and Characterization of GUMBOS and nanoGUMBOS

R6G based GUMBOS were synthesized using an ion-exchange reaction reported in Magut, et.al (Figure 2.1)[15] Subsequently, nanoGUMBOS were synthesized using a reprecipitation method as outlined in the methods section of that manuscript. Endocytic uptake of nanomaterials can occur via caveolin -mediated endocytosis, clathrin-mediated endocytosis, or micropinocytosis depending upon nanoparticle size, shape and charge. Thus, characterization of nanoGUMBOS is essential to understanding the mechanism of cellular uptake. In this study, transmission electron microscopy (TEM) was used to characterize the size and shape of [R6G][BETI] nanoGUMBOS. The TEM image and histogram of the size distribution (Figure 2.2) indicate spherical nanoGUMBOS with a size of approximately 100 nm diameter. Previous literature has demonstrated that spherical nanomaterials with sizes around 100 nm are optimal for a clathrin-mediated pathway.[22] Therefore, we anticipate that uptake of our [R6G][BETI] nanoGUMBOS should occur via clathrin-mediated endocytosis.
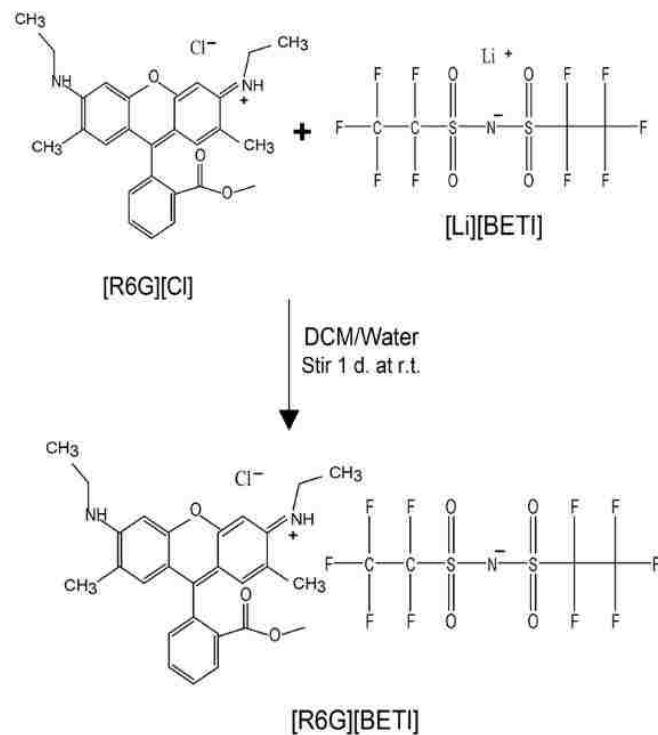
Figure 2.1. Scheme of [R6G][BETI] Synthesis
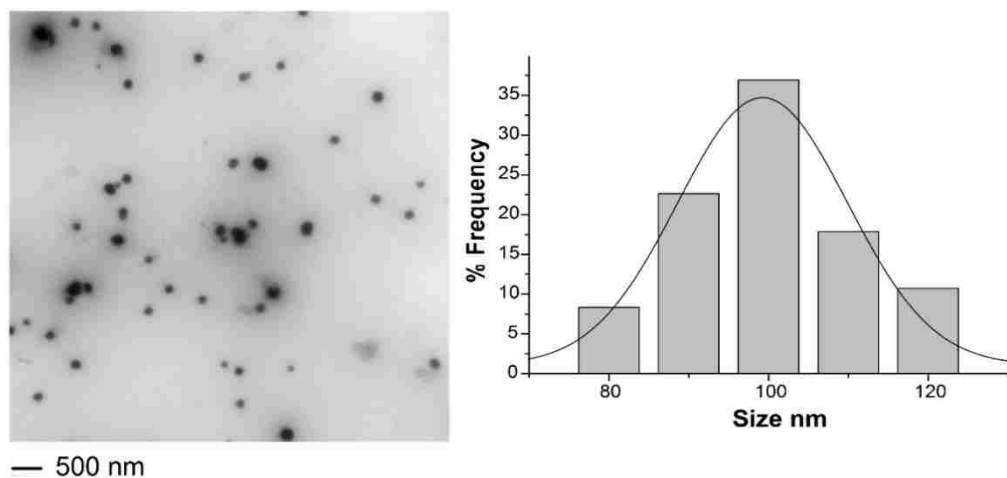
Figure 2.2. TEM Image and size distribution of [R6G][BETI] nanoGUMBOS

2.3.2. Endocytosis Studies

Following TEM characterization, the internalization mechanism of the nanoGUMBOS was

examined using cell viability assays and fluorescence microscopy. Firstly, MDA-MB-231 cancer

cells were incubated with both the nanoGUMBOS and [R6G][Cl] at low temperature (4°C) in

36

order to disrupt energy dependent internalization pathways.[31] Subsequently, fluorescence microscopy images were examined to ascertain cellular uptake of the compound. As shown in Fig. 2.3, incubation of R6G nanoGUMBOS at low temperatures resulted in diminished fluorescence intensity as compared to the control at 37 °C, demonstrating the use of an energy dependent pathway of internalization such as endocytosis. In contrast, the [R6G][Cl] fluorescence intensity was unaffected at low temperatures indicating that this compound employs an energy independent pathway of internalization such as diffusion.

[R6G][BETI]

Control 37°C   4°C

[R6G][Cl]

Control 37°   4°C
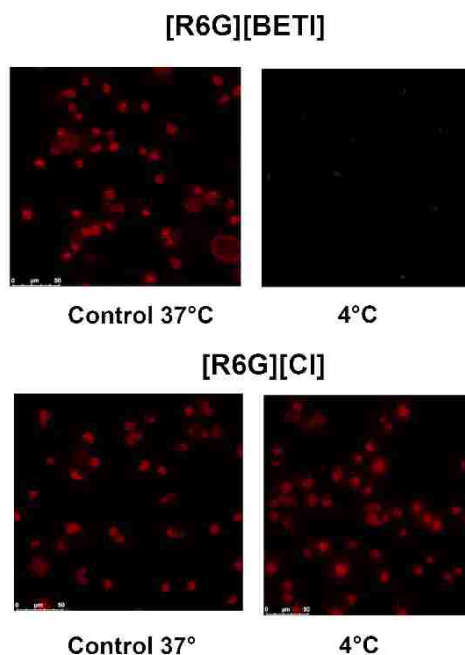
Figure 2.3. [R6G][BETI] (25 nM) and [R6G][Cl] (25 nM) incubated at 37°C and 4 °C in MDA-MB-231 cancer cells

As endocytosis is a major energy dependent pathway for internalization of nanoparticles, the role of endocytosis in the internalization for nanoGUMBOS was studied using several endocytosis inhibitors in conjunction with fluorescence microscopy. Three inhibitors [Filipin III, chlorpromazine hydrochloride, and 5 N-ethyl-N-isopropyl amiloride (amiloride)] were used to block caveolin-mediated endocytosis, clathrin-mediated endocytosis, and micropinocytosis

respectively.[32-34] As seen in Figure 2.4, cancer cells incubated with [R6G][BETI] nanoGUMBOS displayed a significant reduction in fluorescence intensity in the presence of chlorpromazine and as compared to a control with only drug. While diminished fluorescence intensity was also observed in the presence of Filipin III, an inhibitor for caveolin mediated endocytosis, this can be attributed to lack of specificity of the inhibitor. Dutta, et.al reported that Filipin III can also block clathrin mediated endocytosis in addition to caveolin mediated pathways.[35] This suggests that while the role of caveolin mediated endocytosis is unclear, uptake of these nanoGUMBOS in cancer cells occurs primarily through a clathrin-mediated pathway. Similar results were observed for the [R6G][TPB] nanoGUMBOS as well. In contrast, fluorescence intensity of [R6G][Cl], [R6G][OTF] and [R6G][Asc] was unaffected by endocytosis inhibitors indicating internalization independent of endocytosis in cancer cells.

This variation in internalization behavior between the different compounds is most likely due to a significant difference in hydrophobicity between these anion variations. Hydrophobicity of all GUMBOS were confirmed using octanol water partition coefficients and the results were consistent with that of Magut et al. In this regard, Magut et al. found that while [R6G][BETI] and [R6G][TPB] are more hydrophobic than the parent dye [R6G][Cl], [R6G][OTF] and [R6G][Asc] were more hydrophilic. Thus, while [R6G][BETI] and [R6G][TPB] GUMBOS formed nanomaterials in aqueous medium, the latter two GUMBOS were unable to form nanomaterials due to their hydrophilic nature. Additionally, Magut et al. reported that only [R6G][BETI] and [R6G][TPB] were found to display selective toxicity towards cancer cells.[15] Since only [R6G][BETI] and [R6G][TPB] employed endocytic internalization into cancer cells, this suggests that endocytic internalization might play a major role in the selective behavior.

Thus, in order to further elucidate the role of endocytosis on the selective nature of the

nanoGUMBOS, endocytic internalization of the most hydrophobic GUMBOS, [R6G][BETI], and the parent dye, [R6G][Cl], was further investigated in Hs578Bst normal breast cells (Figure 2.5). Interestingly, neither compound displayed a reduction in fluorescence intensity in the presence of endocytosis inhibitors. These results indicate endocytosis dependent internalization of the [R6G][BETI] nanoGUMBOS in cancer cells, and internalization independent of endocytosis in normal cells. In contrast, [R6G][Cl] most likely uses a passive mode of internalization for both cancer and normal cells. Subsequently, to further confirm these results, internalization [R6G][BETI] nanoGUMBOS and [R6G][Cl] was also examined in HMEC normal epithelial breast cells (Figure 2.6). Since most breast cancer arises from mutation of epithelial cells, these results will give further insight to future therapeutic use of these nanoGUMBOS.[36] Similar to the results of Hs578Bst normal cells, no change in fluorescence intensity for either compound was observed in the presence of the inhibitors suggesting internalization independent of endocytosis. Thus, these results indicate that clathrin-mediated endocytosis is the major internalization mechanism for the [R6G][BETI] nanoGUMBOS in cancer cells, while their internalization in normal cells is independent of endocytosis.
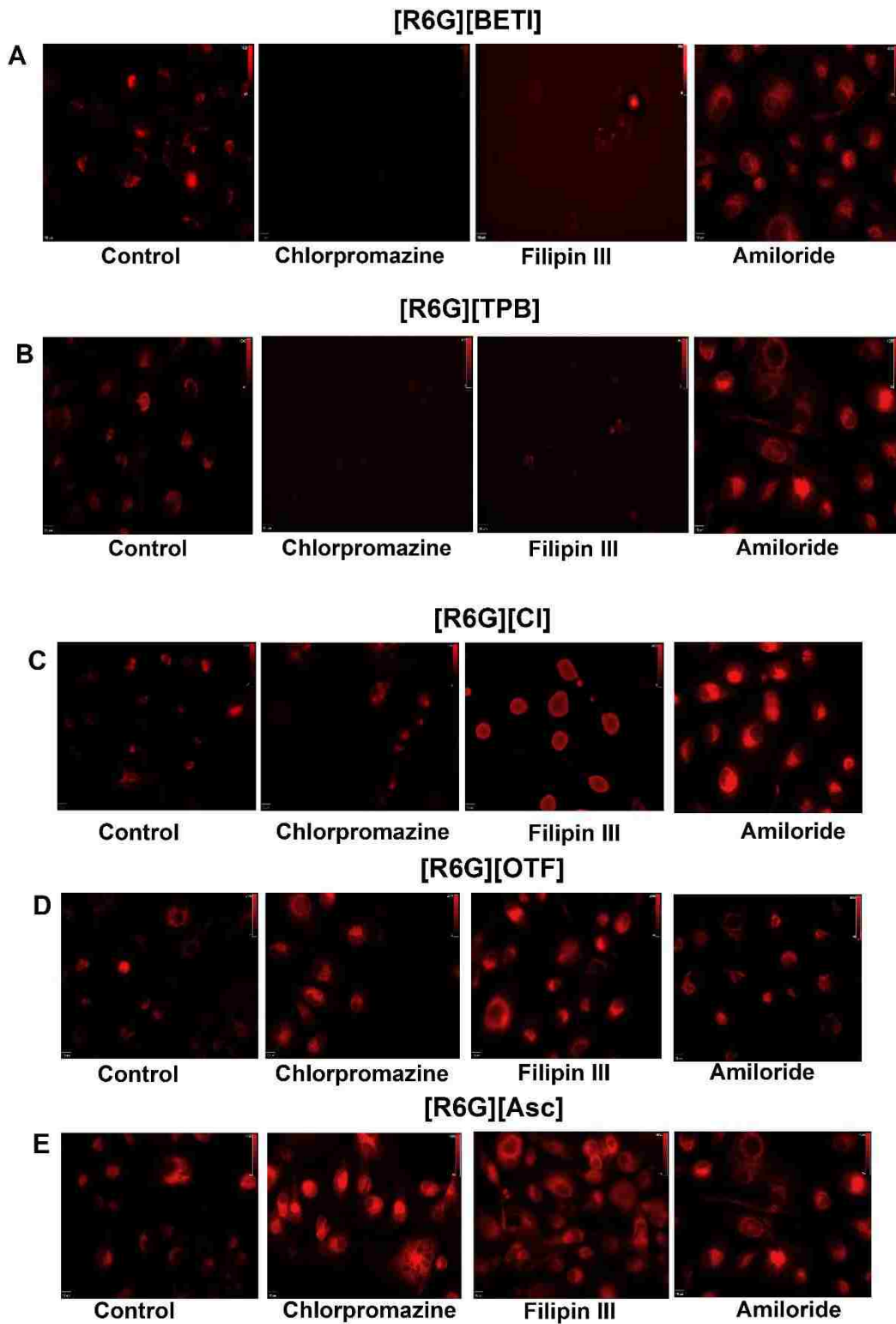
Figure 2.4. (A) [R6G][BETI], (B) [R6G][TPB], (C) [R6G][OTf], (D) [R6G][Asc], and (E) [R6G][Cl], with 3 µg/mL, 7 µg/mL, and 2.9 µg/mL of filipin III, chlorprozamine, and amiloride respectively in MDA-MB-231 cancer cells
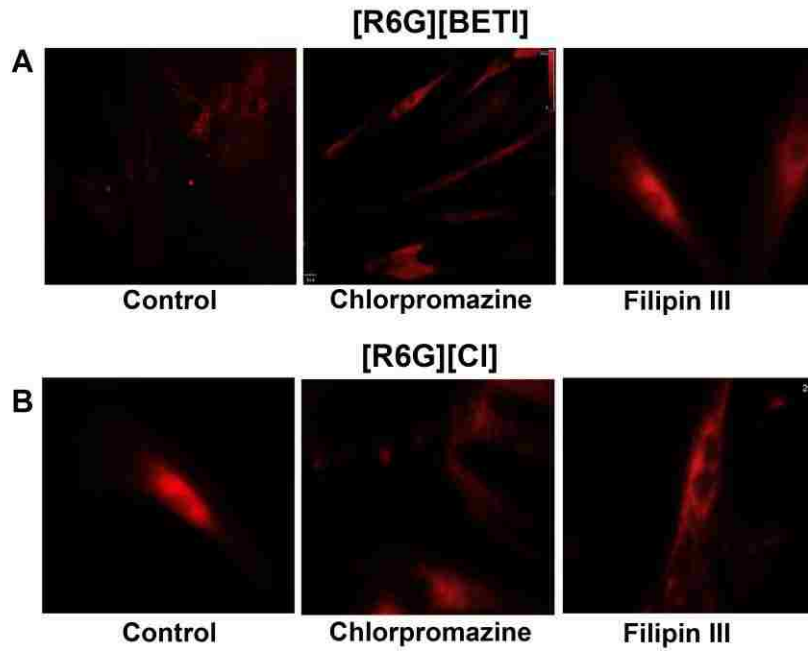
Figure 2.5. (A) R6G][BETI] and (B) [R6G][Cl]with 3 µg/mL, 7 µg/mL, and 2.9 µg/mL of filipin III, chlorprozamine, and amiloride respectively in Hs578Bst breast normal cells
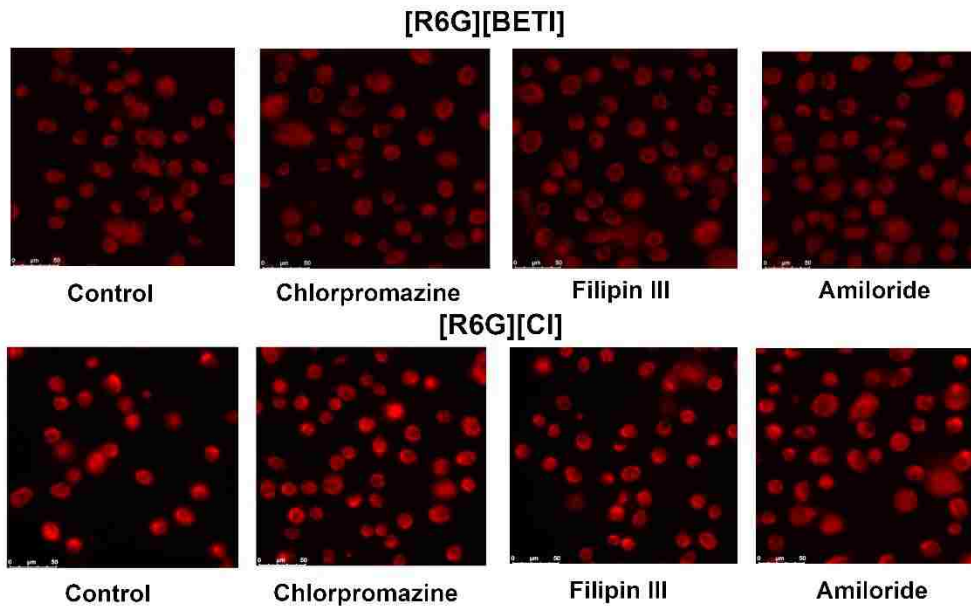
Figure 2.6. [R6G][BETI] and [R6G][Cl] with 3 µg/mL, 7 µg/mL and 2.9 µg/mL of filipin III, chlorpromazine and amiloride respectively in HMEC normal breast cells

41

In order to further confirm our observations from the endocytosis inhibitors, fluorescence microscopy of the [R6G][BETI] and [R6G][Cl] was also performed in the presence of hypertonic and potassium (K^+) depletion solutions. Previous studies have shown that hypertonic solutions and depletion of potassium can disrupt formation of clathrin coated pits.[31, 37] Here, sucrose supplemented PBS buffer and a K^+ free HEPES buffer serves as the hypertonic solution and K^+ depletion solution respectively. As depicted in Figure 2.7, a significant reduction in fluorescence intensity was observed for [R6G][BETI] nanoGUMBOS in the presence of both the hypertonic and K^+ depletion conditions as compared to their respective controls in cancer cells. These results suggest that nanoGUMBOS primarily use clathrin mediated endocytosis for internalization into cancer cells, and disruption of the clathrin coated pit formation inhibited internalization. In contrast, no change in the fluorescence intensity was observed for [R6G][Cl] as compared to the control, supporting the conclusion that [R6G][Cl] internalizes via an endocytosis independent pathway. Furthermore, no change in the fluorescence intensity was observed in the breast normal cells for either compound (Figure 2.8). These results corroborate the previous microscopy results that while [R6G][BETI] nanoGUMBOS internalize via an endocytic pathway in breast cancer cells, internalization of [R6G][BETI] into breast normal cells is independent of endocytosis.
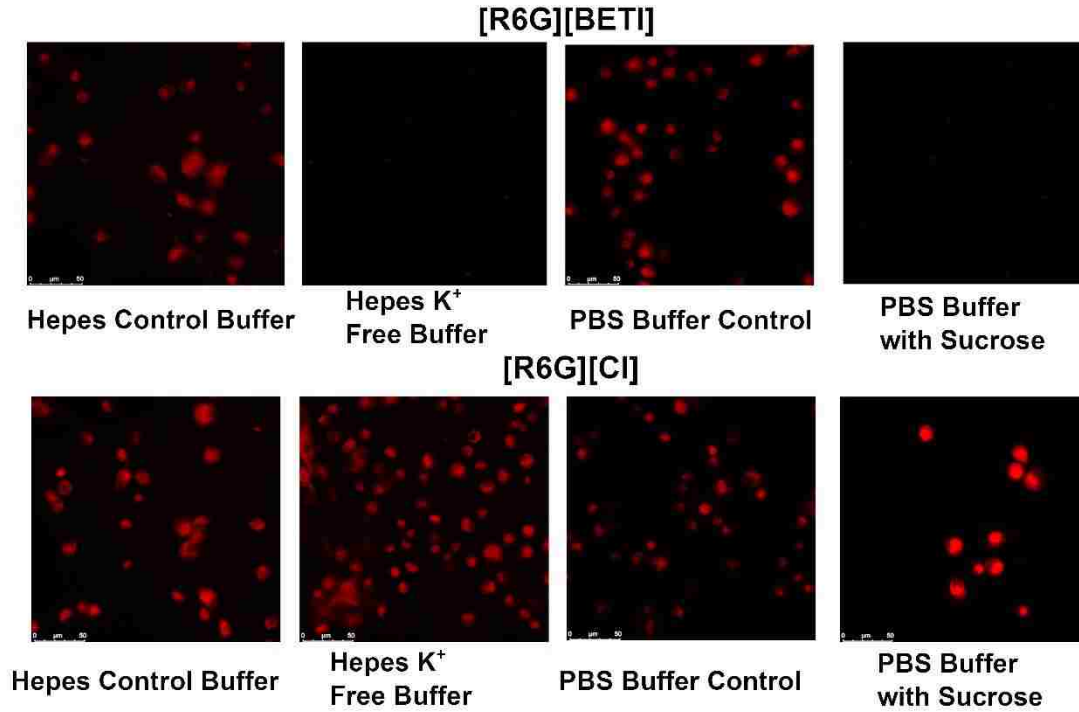
Figure 2.7. [R6G][BETI] and [R6G][Cl] incubated in MDA-MB-231 breast cancer cells in the presence of HEPES buffer with and without KCl and PBS Buffer with and without sucrose.
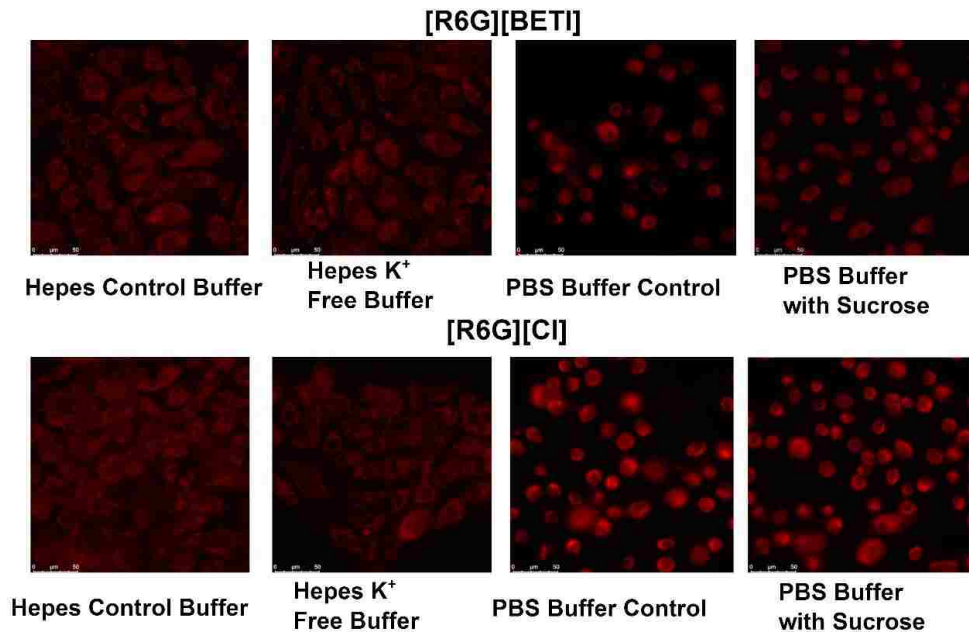
Figure 2.8. [R6G][BETI] and [R6G][Cl] incubated in HMEC normal breast cells in the presence of HEPES buffer with and without potassium chloride(KCl) and PBS Buffer with and without sucrose

43

As a final confirmation of the use of clathrin-mediated endocytosis in the internalization for the nanoGUMBOS in cancer cells, cell viability measurements were examined in conjunction with filipin III, chlorpromazine, and amiloride. Previous investigations have demonstrated toxicity of these rhodamine-based compounds towards MDA-MB-231 breast cancer cells.[15] For these studies, the cytotoxicity of [R6G][BETI] nanoGUMBOS and aqueous [R6G][Cl] were tested after blocking each endocytic pathway. An increase in cell viability in the presence of certain inhibitors could signify the use of that pathway for cellular uptake. Cell viability studies of [R6G][Cl] and [R6G][BETI] with and without inhibitors are shown in Figure 2.9. Samples containing only inhibitor and no drug were used as a control to ensure a nontoxic concentration of inhibitor. Furthermore, all samples incubated with the inhibitor were compared against a control containing only drug without inhibitor. In the presence of the chlorpromazine inhibitor, a significant increase in cell viability in cancer cells was observed with [R6G][BETI] nanoGUMBOS in contrast to the control without inhibitor. When examining the cytotoxic effect of the original dye (i.e., [R6G][Cl]), an increase was seen in cell viability in the presence of chlorpromazine as well. However, this increase is relatively small as compared to our nanoGUMBOS. No increase in cell viability was observed with filipin III or amiloride inhibitors, suggesting that nanoGUMBOS are not internalized using these pathways. Examination of these studies in HMEC normal cells, presented in Figure 2.10, shows no change in cell viability in the presence of the inhibitors, suggesting internalization independent of endocytosis in normal cells. Thus, these results are consistent with out previous results that nanoGUMBOS employ clathrin-mediated endocytosis for uptake in cancer cells while their internalization in normal cells is independent of endocytosis.
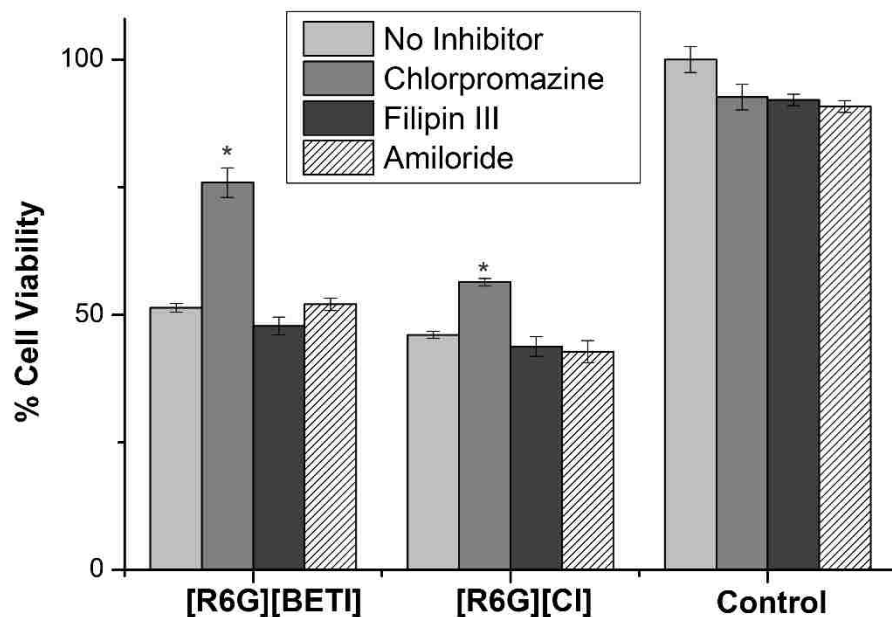
Figure 2.9. Cell viability of R6G compounds in the presence of 3 µg/mL, 7 µg/mL and 2.9 µg/mL of filipin III, chlorpromazine and amiloride respectively. The cell viability results were compared using a Student's t-test; the differences were considered statistically significant if p ≤ 0.05 (*)
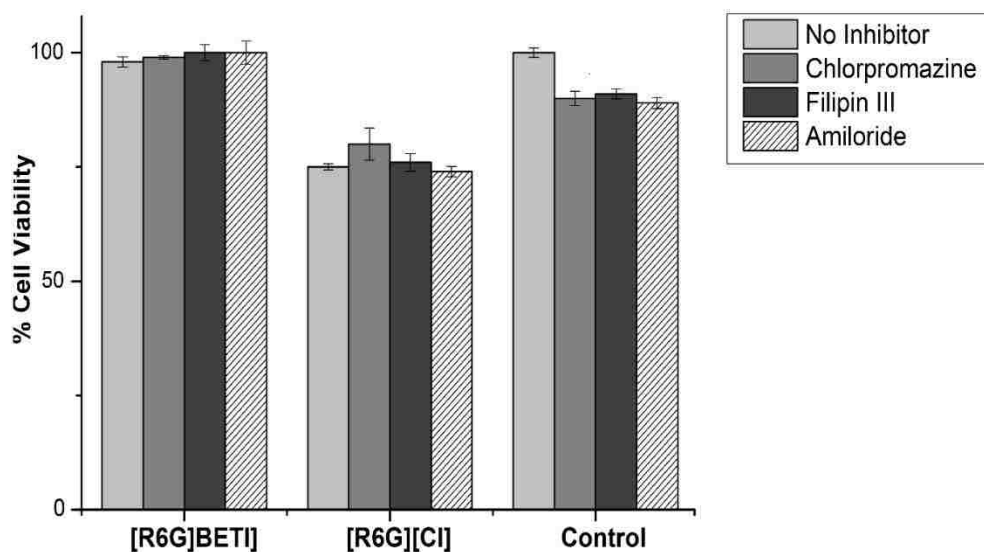
Figure 2.10. Cell viability of R6G compounds in the presence of 3 ug/mL, 7 ug/mL and 2.9 ug/mL of filipin III, chlorpromazine and amiloride respectively in HMEC normal cells

2.3.3. Examination of mitochondrial uptake using fluorescence microscopy

Results from endocytosis studies indicate that uptake of our nanoGUMBOS in cancer cells occurs primarily via a clathrin-mediated pathway. This implies that the nanoGUMBOS first pass through the lysosome and eventually accumulate in the mitochondria. Thus, to further investigate these results, fluorescence microscopy was used to examine the cellular localization of [R6G][BETI] nanoGUMBOS and [R6G][Cl] in MDA-MB-231 cancer cells as well as HMEC normal cells. A micrograph of the rhodamine compounds incubated with MitoTracker and LysoTracker in cancer cells and normal cells is shown in Figure 2.11. Colocalization of the MitoTracker with [R6G][BETI] and [R6G][Cl] in both cancer and normal cells, indicates accumulation of R6G-based compounds in the mitochondria. The merged image of the LysoTracker and the R6G-based compounds in cancer cells shows colocalization of the LysoTracker and [R6G][BETI] nanoGUMBOS, implying interaction of the nanoGUMBOS with the lysosome. However, colocalization in normal cells between the LysoTracker and the compounds is reduced as compared to that of cancer cells, suggesting that the nanoGUMBOS experience a less acidic environment in normal cells. These results further confirm the conclusions gleaned from endocytosis data.
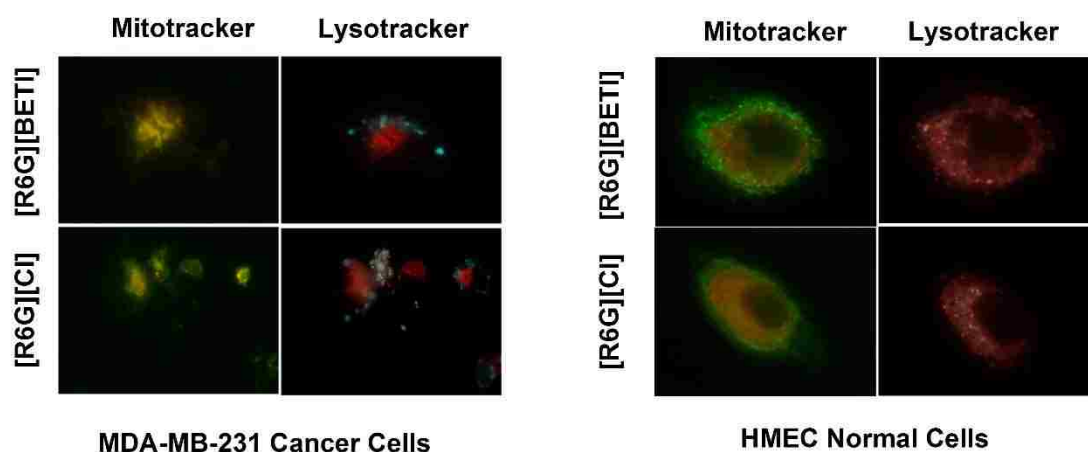
Figure 2.11. [R6G][BETI] (50 nM) and [R6G][Cl] (50 nM) with mitotracker green (10 nM) shown as green fluorescence, and lysostracker deep red (20 nM) shown as light blue fluorescence in MDA-MB-231 breast cancer cells and HMEC normal Cells

2.3.4. Lysosomal Inhibitors

As a final confirmation of the endocytosis mechanism, toxicity of the nanoGUMBOS in the presence of lysosomal inhibitors was examined. Clathrin-mediated endocytosis requires the nanoparticle to pass through the acidic lysosome before release into the mitochondria.[38] Thus, cell viability studies were examined in the presence of lysosomotrophic inhibitors to examine the role of lysosomal acidification or lysosome enzymes, such as proteases, on the nanoGUMBOS toxicity. The cell viability studies show that the toxicity of [R6G][BETI] is significantly reduced in the presence of the inhibitor chloroquine (Figure 2.12). However, the toxicity of [R6G][Cl] was unaffected by the lysosomotropic inhibitor. TEM images presented in Figure 2.13 indicate loss of nanoparticle shape, suggesting dissociation at acidic pH of the nanoGUMBOS within the lysosome. In addition, DLS results, Figure 2.14, indicate a loss of signal at acidic pH further confirming the results from TEM. Further, cytosine and serine protease enzyme inhibitors were tested to examine the effect of the associated enzymes on the toxicity of our nanoGUMBOS (Figure 2.15). The toxicity of the nanoGUMBOS was unaffected in the presence of these

47

inhibitors. Thus, these results suggest that our nanoGUMBOS dissociate in cancer cells through lysosomal acidification following endocytic uptake. However, in the case of normal cells, no dissociation would occur due to uptake using a different mechanism.
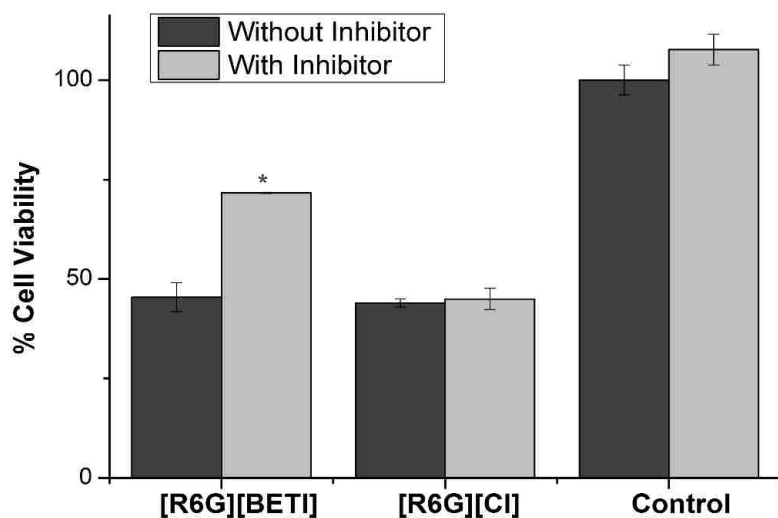
Figure 2.12. Cell viability of R6G compounds in the presence of 100 µM of chloroquine to prevent lysosomal acidification. The cell viability results were compared using a Student's t-test; the differences were considered statistically significant if p = 0.05 (*)
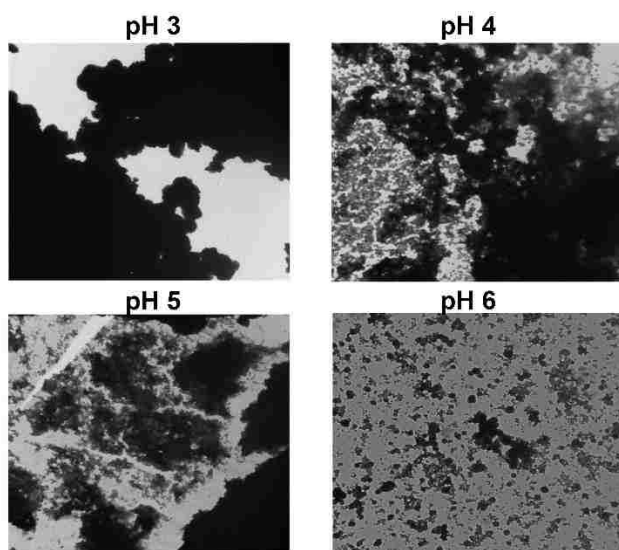
Figure 2.13. TEM Images of [R6G][BETI] in different pH buffers
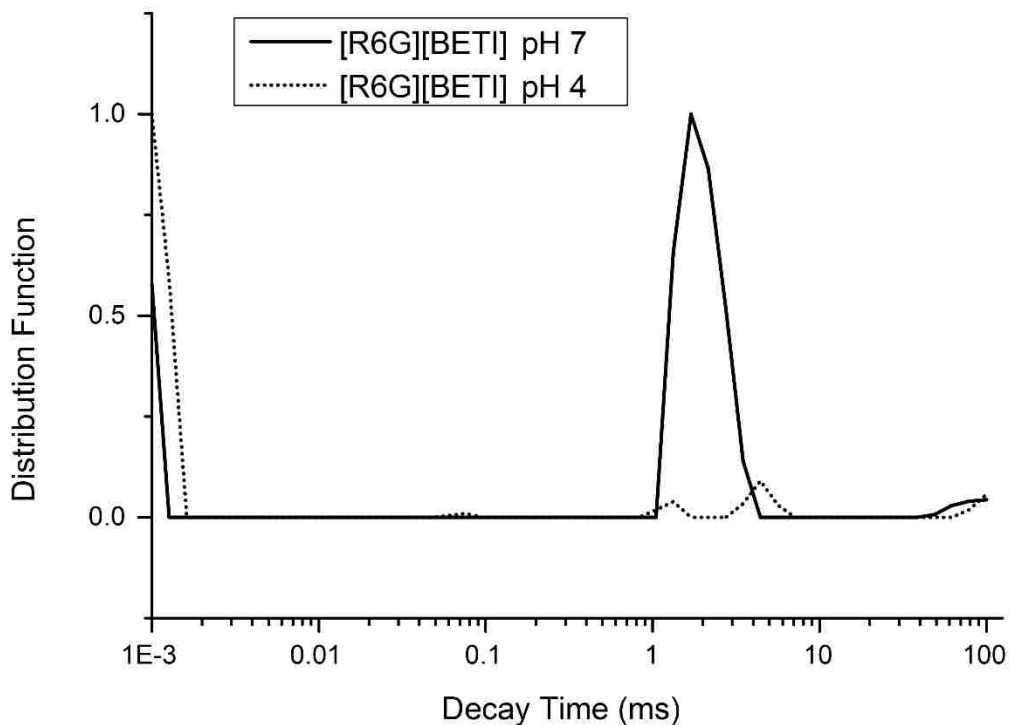
Figure 2.14. Dynamic Light Scattering (DLS) plot of particle size distribution function vs. decay time at physiological and lysosomal pH
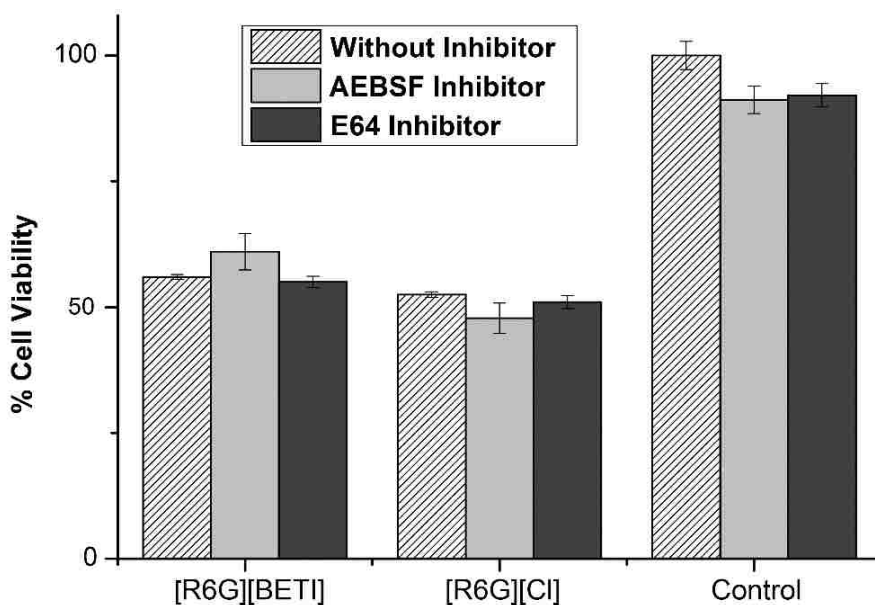
Figure 2.15. Cell viability of R6G compounds in the presence of 0.5 mM 4-(2-aminoethyl)benzenesulfonyl fluoride hydrochloride (AEBSF Inhibitor) and 100 μM E64 inhibitor that was used to block serine and cytosine proteases respectively

2.3.5. Mechanism of Selective Toxicity

Results from examination of the endocytosis studies indicate uptake of [R6G][BETI] nanoGUMBOS primarily via clathrin-mediated endocytosis in cancer cells and uptake independent of endocytosis in normal cells. While a decrease in fluorescence intensity of [R6G][BETI] in MDA-MB-231 cancer cells was observed in the presence of Filipin III, an inhibitor for caveloin-mediated endocytosis, this is attributed to the ability of the inhibitors to block some clathrin pathways as well. Thus, while the role of caveolin-mediated pathways on the internalization of nanoGUMBOS is still uncertain, one can conclude from these studies that clathrin-mediated endocytosis plays a major role in nanoGUMBOS uptake. Use of clathrin mediated endocytosis was further corroborated using lysosomal inhibitors. Our examination of lysosomal inhibitors in conjunction with cell viability analysis indicates an increase in cell viability in the presence of chloroquine, an endosomal acidification inhibitor. Thus, we were able to conclude that lysosomal acidification following endocytic uptake plays a crucial role in the selective toxicity of the nanoGUMBOS. The TEM images and DLS results (Figures 2.13 and 2.14) indicated dissociation of our nanoGUMBOS at lysosomal pH. Therefore, when clathrin-mediated endocytosis is employed for nanoGUMBOS penetration into cancer cells, the acidic pH (4.3) of the lysosome likely results in dissociation of the nanoGUMBOS, activating their toxicity to cancer cells.[38] Furthermore, uptake of the nanoGUMBOS in normal cells is independent of endocytosis; thus, no dissociation of the nanoparticle occurs, leading to their nontoxic nature towards normal cells. In the case of [R6G][Cl], no dissociation is needed to activate the toxicity due to its high solubility in aqueous systems, resulting in its inherent toxicity towards both cancer and normal cells. This overall mechanism is portrayed in figure 2.16.
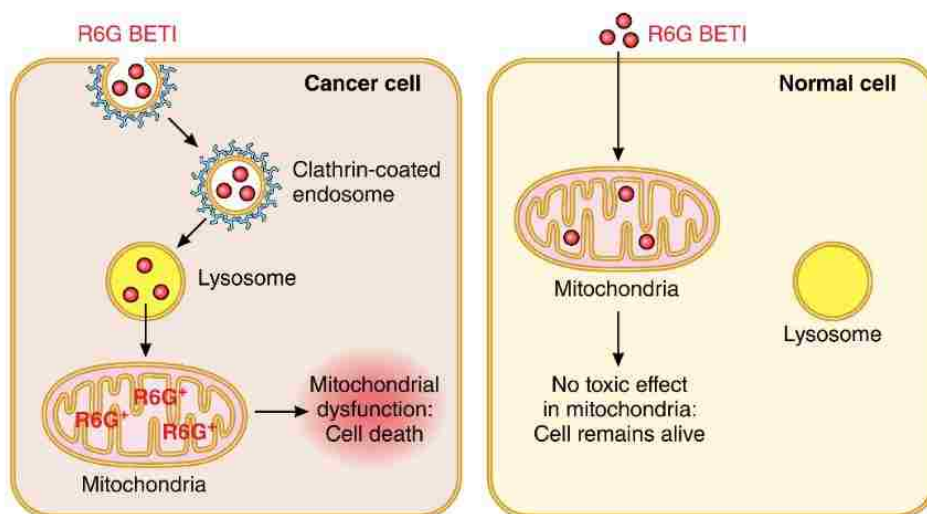
Figure 2.16. Endocytic mechanism of selective toxicity of the R6G nanoGUMBOS

2.3.6. *In vivo* examination

Following our examination of the *in vitro* mechanism of selectivity, *in vivo* kinetic and toxicity studies of [R6G][BETI] nanoGUMBOS were evaluated to further understand their potential application as chemotherapeutics. Kinetic studies were performed using both an intraperitoneal (IP) and intravenous (IV) injection to assess nanoGUMBOS accumulation within the body cavity of the mouse over time. Mice injected IP displayed a significant decrease in fluorescence intensity over time suggesting gradual excretion of the GUMBOS (Figure 2.17). However, mice injected IV displayed no change in fluorescence intensity indicating that the nanoGUMBOS are unable to easily circulate throughout the body. This is most likely due to the relatively high hydrophobicity of the nanoGUMBOS, ultimately leading to agglomeration within the blood. Furthermore, the size of the nanoparticles investigated are around 100 nm; however, literature suggests that 60-80 nm is the optimal size for biomedical applications.[3] In this regard, Chapter 3 of this dissertation employs cyclodextrin templating to aid in formation of reduced size nanoparticles.

Following kinetic studies, we also pursued *in vivo* toxicity studies of these [R6G][BETI] nanoGUMBOS to determine if therapeutic properties would be maintained *in vivo*. For our examination of tumor reduction, MDA-MB-231 cancer cells were used to produce a tumor on the right hind leg of 12 athymic nude mice. The volumes of the tumors in these mice were monitored before and after treatment with [R6G][BETI] nanoGUMBOS as shown in Figure 2.18. In these studies 0.16 mg/kg [R6G][BETI] nanoGUMBOS, and 1.6 mg/kg of [R6G]BETI] nanoGUMBOS were injected into two groups of mice respectively, with four mice per group, at the tumor site on days 41, 47 and 51. A third group of 4 mice treated only with saline solution was used as a control. Control mice showed a continuous increase in tumor volume. However, mice injected with [R6G][BETI] showed a 50% reduction in the tumor volume. These studies suggest that [R6G][BETI] nanoGUMBOS not only inhibit tumor growth but also reduce tumor volume in mice by almost 50%. In addition, similarities in therapeutic efficacy of the nanoGUMBOS with the two different doses can be attributed to saturation of the drug within the tumor at the lower dose. Furthermore, the lack of further decrease in tumor volume can most likely be attributed to the formation of necrotic tissue at the surface of the tumor; thus, preventing penetration of the nanoGUMBOS deeper in the tumor tissue. [39]

IP Injection

1 hr.   6 hr.   30 hr.

IV Injection

1 hr.   6 hr.   30 hr.
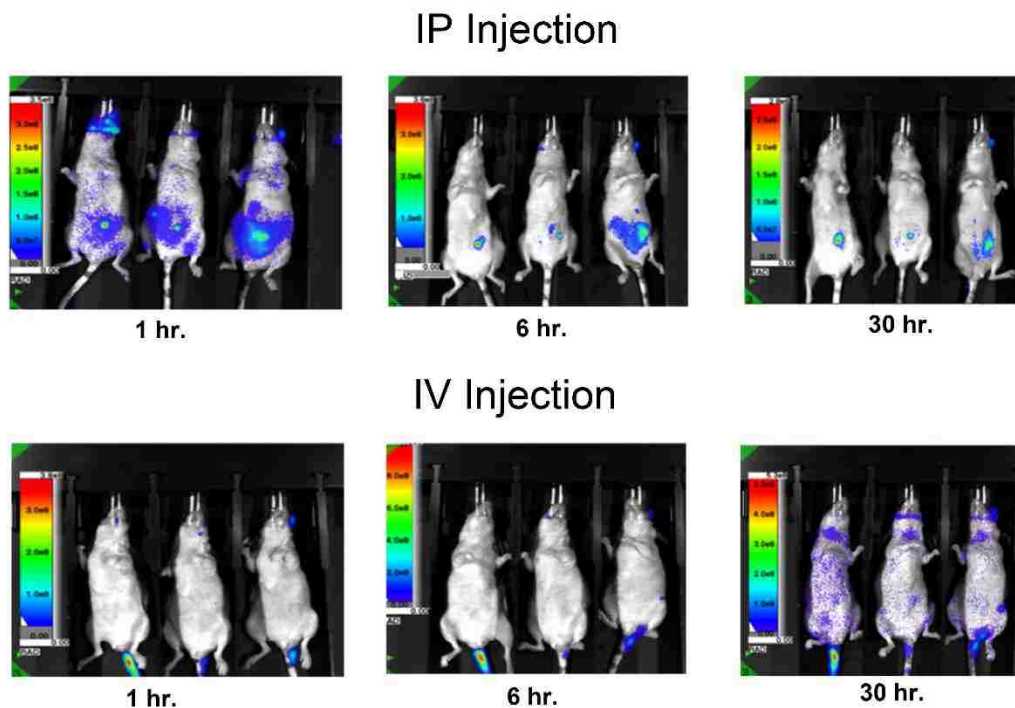
Figure 2.17 *In vivo* bio-distribution studies using IP and IV injections
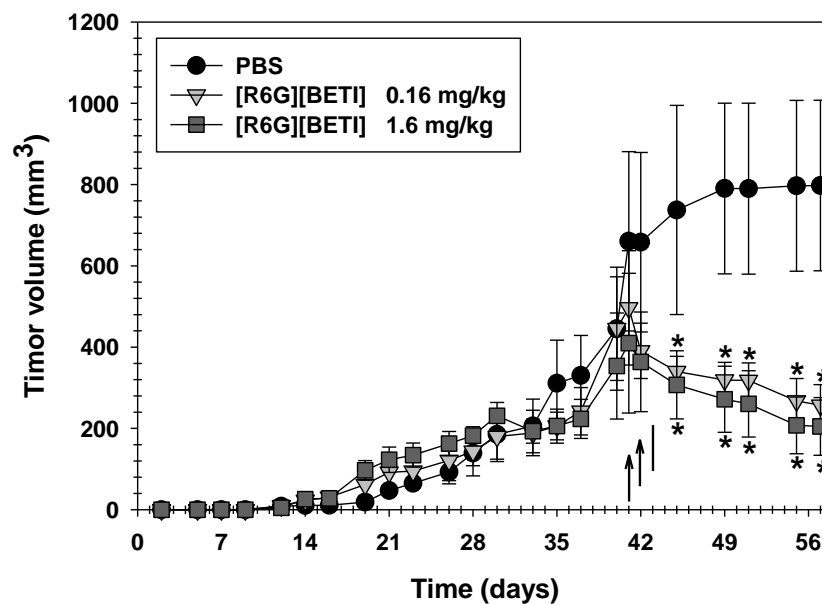
Figure 2.18 In-vivo tumor reduction using 0.16 and 1.6 mg/kg of [R6G][BETI] as compared to a saline control. Tumor measurements were compared by a two-way ANOVA and a Bonferroni post-test; the differences were considered statistically significant if p = 0.05 (*). The arrows represent days of injection for the mice

2.4. CONCLUSIONS

The studies reported here demonstrate the profound role of endocytosis in both the internalization and selectivity mechanisms of R6G nanoGUMBOS as *in vitro* therapeutic agents for cancer cells, and also confirm retained therapeutic properties *in vivo*. It was observed that use of a clathrin-mediated pathway by the nanoGUMBOS in cancer cells led to nanoparticle dissociation in the acidic environment of the lysosome, ultimately activating their toxicity. However, since the nanoGUMBOS did not employ endocytic internalization in normal cells, no dissociation of the nanoparticle occurs, resulting in their nontoxic behavior towards normal cells. After thoroughly examining this selectivity mechanism, nanoGUMBOS were employed *in vivo* to assess biodistribution and therapeutic efficacy. Remarkably, following nanoGUMBOS treatment, a 50% reduction in tumor volume was observed in athymic nude mice. Thus, we conclude that therapeutic properties of nanoGUMBOS are retained during *in vivo* applications. Moreover, these *in vitro* and *in vivo* studies have enhanced our understanding of R6G nanoGUMBOS and give further insight to the potential of these novel compounds for chemotherapeutic applications.

2.5. REFERENCES

1.   Siegel, R. L.; Miller, K. D.; Jemal, A., Cancer statistics, 2015. *CA: A Cancer Journal for Clinicians* **2015,** *65* (1), 5-29.

2.   de la Zerda, A.; Gambhir, S. S., Drug delivery: Keeping tabs on nanocarriers. *Nat Nano* **2007,** *2* (12), 745-746.

3.   Wicki, A.; Witzigmann, D.; Balasubramanian, V.; Huwyler, J., Nanomedicine in cancer therapy: Challenges, opportunities, and clinical applications. *Journal of Controlled Release* **2015,** *200*, 138-157.

4.   Peer, D.; Karp, J. M.; Hong, S.; Farokhzad, O. C.; Margalit, R.; Langer, R., Nanocarriers as an emerging platform for cancer therapy. *Nat Nano* **2007,** *2* (12), 751-760.

5.   Pérez-Herrero, E.; Fernández-Medarde, A., Advanced targeted therapies in cancer: Drug nanocarriers, the future of chemotherapy. *European Journal of Pharmaceutics and Biopharmaceutics* **2015,** *93*, 52-79.

6.   Gao, J.; Xu, B., Applications of nanomaterials inside cells. *Nano Today* **2009,** *4* (1), 37-51.

7.   Krishnamurthy, S.; Vaiyapuri, R.; Zhang, L.; Chan, J. M., Lipid-coated polymeric nanoparticles for cancer drug delivery. *Biomaterials Science* **2015,** *3* (7), 923-936.

8.   Mura, S.; Nicolas, J.; Couvreur, P., Stimuli-responsive nanocarriers for drug delivery. *Nat Mater* **2013,** *12* (11), 991-1003.

9.   Sun, T.; Zhang, Y. S.; Pang, B.; Hyun, D. C.; Yang, M.; Xia, Y., Engineered Nanoparticles for Drug Delivery in Cancer Therapy. *Angewandte Chemie International Edition* **2014,** *53* (46), 12320-12364.

10.   Farokhzad, O. C.; Langer, R., Nanomedicine: Developing smarter therapeutic and diagnostic modalities. *Advanced Drug Delivery Reviews* **2006,** *58* (14), 1456-1459.

11.   Kumari, A.; Yadav, S. K.; Yadav, S. C., Biodegradable polymeric nanoparticles based drug delivery systems. *Colloids and Surfaces B: Biointerfaces* **2010,** *75* (1), 1-18.

12.   Park, K., Facing the Truth about Nanotechnology in Drug Delivery. *ACS Nano* **2013,** *7* (9), 7442-7447.

13.   Warner, I. M.; El-Zahab, B.; Siraj, N., Perspectives on Moving Ionic Liquid Chemistry into the Solid Phase. *Analytical Chemistry* **2014,** *86* (15), 7184-7191.

14.   Kutushov, M.; Gorelik, O., Low concentrations of Rhodamine-6G selectively destroy tumor cells and improve survival of melanoma transplanted mice. *Neoplasma* **2013,** *60* (3), 262-73.

15.   Magut, P. K.; Das, S.; Fernand, V. E.; Losso, J.; McDonough, K.; Naylor, B. M.; Aggarwal, S.; Warner, I. M., Tunable cytotoxicity of rhodamine 6G via anion variations. *Journal of the American Chemical Society* **2013,** *135* (42), 15873-9.

16.   Modica-Napolitano, J. S.; Aprille, J. R., Delocalized lipophilic cations selectively target the mitochondria of carcinoma cells. *Advanced Drug Delivery Reviews* **2001,** *49* (1–2), 63-70.

17.   Belostotsky, I.; da Silva, S. M.; Paez, M. G.; Indig, G. L., Mitochondrial targeting for photochemotherapy. Can selective tumor cell killing be predicted based on n-octanol/water distribution coefficients? *Biotechnic & Histochemistry* **2011,** *86* (5), 302-314.

18.   Lou, Q.; Qu, S.; Jing, P.; Ji, W.; Li, D.; Cao, J.; Zhang, H.; Liu, L.; Zhao, J.; Shen, D., Water-triggered luminescent "nano-bombs" based on supra-(carbon nanodots). *Advanced materials* **2015,** *27* (8), 1389-94.

19.   Hu, F.; Zhang, G.; Zhan, C.; Zhang, W.; Yan, Y.; Zhao, Y.; Fu, H.; Zhang, D., Highly solid-state emissive pyridinium-substituted tetraphenylethylene salts: emission color-tuning with counter anions and application for optical waveguides. *Small* **2015,** *11* (11), 1335-44.

20.   Soulie, M.; Frongia, C.; Lobjois, V.; Fery-Forgues, S., Fluorescent organic ion pairs based on berberine: counter-ion effect on the formation of particles and on the uptake by colon cancer cells. *RSC Advances* **2015,** *5* (2), 1181-1190.

21.   Huang, Y.; He, L.; Liu, W.; Fan, C.; Zheng, W.; Wong, Y.-S.; Chen, T., Selective cellular uptake and induction of apoptosis of cancer-targeted selenium nanoparticles. *Biomaterials* **2013,** *34* (29), 7106-7116.

22.   Sahay, G.; Alakhova, D. Y.; Kabanov, A. V., Endocytosis of nanomedicines. *Journal of Controlled Release* **2010,** *145* (3), 182-195.

23.   Champion, J. A.; Walker, A.; Mitragotri, S., Role of Particle Size in Phagocytosis of Polymeric Microspheres. *Pharmaceutical research* **2008,** *25* (8), 1815-1821.

24.   Floyd, S.; De Camilli, P., Endocytosis proteins and cancer: a potential link? *Trends in Cell Biology* **1998,** *8* (8), 299-301.

25.   Jones, A. T.; Gumbleton, M.; Duncan, R., Understanding endocytic pathways and intracellular trafficking: a prerequisite for effective design of advanced drug delivery systems. *Advanced Drug Delivery Reviews* **2003,** *55* (11), 1353-1357.

26.   Iversen, T.-G.; Skotland, T.; Sandvig, K., Endocytosis and intracellular transport of nanoparticles: Present knowledge and need for future studies. *Nano Today* **2011,** *6* (2), 176-185.

27.   Bareford, L. M.; Swaan, P. W., ENDOCYTIC MECHANISMS FOR TARGETED DRUG DELIVERY. *Advanced drug delivery reviews* **2007,** *59* (8), 748-758.

28.   Sahay, G.; Kim, J. O.; Kabanov, A. V.; Bronich, T. K., The exploitation of differential endocytic pathways in normal and tumor cells in the selective targeting of nanoparticulate chemotherapeutic agents. *Biomaterials* **2010,** *31* (5), 923-933.

29.   Akinc, A.; Battaglia, G., Exploiting endocytosis for nanomedicines. *Cold Spring Harbor perspectives in biology* **2013,** *5* (11), a016980.

30.   Mellman, I.; Yarden, Y., Endocytosis and Cancer. *Cold Spring Harbor Perspectives in Biology* **2013,** *5* (12), a016949.

31.   Hu, Z.; Pan, Y.; Wang, J.; Chen, J.; Li, J.; Ren, L., Meso-tetra (carboxyphenyl) porphyrin (TCPP) nanoparticles were internalized by SW480 cells by a clathrin-mediated endocytosis pathway to induce high photocytotoxicity. *Biomedicine & Pharmacotherapy* **2009,** *63* (2), 155-164.

32.   Rejman, J.; Bragonzi, A.; Conese, M., Role of clathrin- and caveolae-mediated endocytosis in gene transfer mediated by lipo- and polyplexes. *Molecular therapy : the journal of the American Society of Gene Therapy* **2005,** *12* (3), 468-74.

33.   Watson, P.; Jones, A. T.; Stephens, D. J., Intracellular trafficking pathways and drug delivery: fluorescence imaging of living and fixed cells. *Adv Drug Deliv Rev* **2005,** *57* (1), 43-61.

34.   Schnitzer, J. E.; Oh, P.; Pinney, E.; Allard, J., Filipin-sensitive caveolae-mediated transport in endothelium: reduced transcytosis, scavenger endocytosis, and capillary permeability of select macromolecules. *The Journal of cell biology* **1994,** *127* (5), 1217-1232.

35.   Dutta, D.; Donaldson, J. G., Search for inhibitors of endocytosis: Intended specificity and unintended consequences. *Cellular Logistics* **2012,** *2* (4), 203-208.

36.   Dimri, G.; Band, H.; Band, V., Mammary epithelial cell transformation: insights from cell culture and mouse models. *Breast Cancer Research* **2005,** *7* (4), 171.

37.   Hansen, S.; Sandvig, K.; van Deurs, B., *Clathrin and HA2 adaptors: Effects of potassium depletion, hypertonic medium, and cytosol acidification*. 1993; Vol. 121, p 61-72.

38.   Mindell, J. A., Lysosomal Acidification Mechanisms. *Annual Review of Physiology* **2012,** *74* (1), 69-86.

39.   Minchinton, A. I.; Tannock, I. F., Drug penetration in solid tumours. *Nat Rev Cancer* **2006,** *6* (8), 583-592.

CHAPTER 3
ENHANCED CHEMOTHERAPEUTIC APPLICATIONS OF CYCLODEXTRIN-TEMPLATED R6G-BASED NANOGUMBOS

3.1. INTRODUCTION

Despite several advancements in treatment, cancer remains the second leading cause of death as of 2016.[1] Current chemotherapeutics suffer from numerous side effects making development of more selective therapeutics essential.[2-3] In this regard, nanomedicines have demonstrated a more targeted therapeutic delivery in comparison to conventional chemotherapeutics. Conventional nanomedicines serve as nanocarriers that encapsulate the drug to aid in therapeutic delivery.[4-6] Such nanocarriers are able to protect the drug bio-degradation and rapidly permeate the cell membrane due to nanoscale size, providing several advantages to chemotherapeutic drug delivery.[7-9] More current research on nanomedicine focuses on the development of nanodrugs fabricated from hydrophobic drugs, such as paclitaxel, in conjunction with a polymeric or inorganic matrix.[10-11] This removes the need for a carrier as the nanoparticle is primarily composed of the drug itself, while the polymeric or inorganic template simply aids in formation of the nanoparticle structure. These carrier free nanodrugs have shown promising toxicity *in vitro* and *in vivo* and are currently being employed for clinical trials as well.

Therapeutic investigations of various nanoparticles indicate a strong correlation between size, material, hydrophobicity, and surface charge of the nanodrug to its toxicity. Size, in particular, was found to play a major role in rapid uptake of nanomaterials into the tumor cells.[12] *In vivo* investigations have demonstrated enhanced permeation of the nanomaterials into tumor tissue due to the leaky tumor vasculature. In this regard, the nanoscale size of the nanoparticle allows for increased permeation into cancer cells through a phenomenon known as the enhanced permeability and retention (EPR) effect.[13-15] Additionally, i*n vitro* investigations have shown that

nanoparticles typically internalize using various size-dependent active transport pathways. In this regard, these studies have demonstrated that tuning the size of nanoparticles to around 60-80 nm led to enhanced cellular uptake and, ultimately, enhanced toxicity.[16-19] Thus, it becomes essential to develop an approach to rapidly tune size and uniformity of the nanomaterial to optimize the toxicity. However, the challenge associated with controlled size of current nanodrugs that employ polymeric and inorganic materials is the complex and labor intensive synthetic route.[20] Therefore, development of a simple method to control the size and uniformity of the nanoparticles becomes essential.

Our research group has developed nanoGUMBOS, i.e nanomaterials derived from a *group* of *u*niform *m*aterials *b*ased on *o*rganic *s*alts (GUMBOS), which have several unique applications.[21] GUMBOS are organic salts synthesized using a simple ion-exchange reaction. The variation in counter-ions results in several tunable properties, such as hydrophobicity, conductivity, and melting point, giving these materials a wide variety of applications, including selective chemotherapeutic toxicity.[22] NanoGUMBOS have several distinct advantages over conventional nanomedicines such as simple synthesis, as well as the ability to serve as the drug rather than the drug carrier. In these studies, we investigate the effect of cyclodextrin (CD) templating on the size and *in vitro* cytotoxicity of nanoGUMBOS derived from rhodamine 6G (R6G), a fluorescent lipophilic cation known to have promising anticancer properties.[23]

CDs are oligosaccharides that are typically used for drug encapsulation in order to enhance the solubility of hydrophobic drugs.[24-26] They are usually classified into three classes (α-CD, β-CD, and γ-CD) that vary in cavity sizes, with γ-CD being the largest and α-CD being the smallest. This varying cavity size allows for optimization of the interaction between the drug and the CD. For example, drugs molecules with large benzene rings are more likely to be encapsulated using β

59

or γ-CD rather than α-CD.[27] Recent studies found that the hollow, and hydrophobic cavity of cyclodextrin can also serve as a template to control size and uniformity of the nanoparticles.[28-31] Specifically, studies by Hamden et al. revealed that use of cyclodextrin to template nanoGUMBOS produced smaller and more uniform nanomaterials.[28] In contrast to conventional polymer and inorganic templates currently being employed for nanodrug fabrication, the relatively higher water solubility of CD improves therapeutic delivery.[32] Furthermore, the simple synthesis of the CD templated nanoGUMBOS using the ion-exchange technique provides a distinct advantage over other silica and polymeric based nanomaterials that rely on complex synthesis for reduction in nanoparticle size. Herein, we report the effect of templating with hydroxypropyl-alpha (HP-α-CD), hydroxypropyl-beta (HP-β-CD), and gamma (γ-CD) on the size and therapeutic properties of R6G based nanoGUMBOS.

3.2. MATERIALS AND METHODS

3.2.1. Materials

Rhodamine 6G (95%), phosphate buffered saline (10x concentrate, 0.2 uM filtered), sodium tetraphenylborate [Na][TPB], methylene chloride, dimethylsulfoxide, citric acid monohydrate, HP-α-CD, HP- β-CD, and 0.2 uM nylon filters were purchased from Sigma-Aldrich (Milwaukee, WI). γ-CD was purchased from Fluka (Germany). Sodium phosphate dibasic was purchased from Fisher Scientific (Fair Lawn, New Jersey). Lithium bis (perfluoroethylsulfonyl) imide ([Li][BETI]) was obtained from Ionic Liquid Technologies (Tuscaloosa, Al). Triply deionized water was obtained from an Aires High Purity Water System (Port Allen, LA). The MTT (3-[4, 5-Dimethylthiazol-2-yl]-2, 5-diphenyltetrazolium bromide) cell viability assay was purchased from Promega Corporation (Madison, WI). TEM grids were purchased from Ted Pella (Redding, CA).

3.2.2. Synthesis of nanoGUMBOS

A 2 mM solution of [R6G][Cl] with and without cyclodextrin (0.8 mg) was mixed with a 2 mM solution of [Li][BETI] or [Na][TPB]. An ultrasonic processor was used to probe sonicate this solution at 20% amplitude at 30 mhz. The solution was then centrifuged twice at 35,000 rpm for 30 minutes using a Beckman L8-70M Ultracentrifuge while washing the pellet in between runs to remove excess cyclodextrin, and [Li][Cl] byproduct. Finally, the product was dried by removal of water *in vacuo*. All nanoGUMBOS were resuspsended under ultrasonication for 2 h in cell media to ensure homogeneity prior to cell studies.

3.2.3. Dynamic Light Scattering and Zeta Potential

NanoGUMBOS were resuspended in 0.01 M PBS buffer to make a 100 µM solution. These nanoGUMBOS were then diluted to 5 µM for dynamic light scattering (DLS) and zeta potential measurements.

3.2.4. Cell Culture

MDA-MB-231 breast adenocarcinoma cells, Mia-Paca pancreatic carcinoma and Hs578Bst normal breast fibroblast cells were purchased from the American Tissue Culture Collection (ATCC, Manassas, VA). All cell lines were grown to 90% confluency according to the ATCC guidelines prior to plating.

3.2.5. Cytotoxicity Studies

A 96 well plate was seeded with 5000 cells/well and incubated for 24 h to allow the cells to attach. Cells were treated with a serial dilution of the nanoGUMBOS from 100 µM to 1.56 µM of nanoGUMBOS and the last row was kept as an untreated control with only cell media. An MTT assay was then performed to determine cell viability. In brief, the cells were treated with 15 µL of MTT assay and incubated for 3 hrs. Then, 100 µL of stop solution was added to solubilize the

purple formazan crystals. A microplate spectrophotometer was used to measure the absorbance at 570 nm. Cell viability was calculated as a percentage of the ratio between absorbance of treated cells and absorbance of an untreated control containing only cell media. All measurements were carried out in triplicate, and reported cell viabilities represent an average of these measurements.

3.2.6. Cellular Uptake Studies

The cellular uptake studies were performed in triplicate using 35 mM petri dishes plated with 200,000 cells/dish for 24 hrs. The cells were treated with a 5 µM nanoGUMBOS solution and incubated at 37°C for 5 hrs. The control sample was only incubated with fresh cell media without nanoGUMBOS. Following the 5 h incubation, it was assumed that some of the nanoparticles had internalized. Thus, the cell media was removed and the cells were washed with PBS buffer several times to remove excess compound that was not internalized. The cells were then treated with 3 mL of DMSO for 5 h to lyse the cells open and release any internalized drug. Subsequently, absorbance measurements of the DMSO solution were examined using the control cells treated with only cell media was used as the reference. A set of five DMSO calibration standards from 1-10 µM, were prepared in triplicate for each nanoGUMBOS, and the absorbance of each solution was recorded. The internalized concentration of nanoGUMBOS present in the DMSO of the treated cells was calculated using the linear equation generated from calibration curve of the standards.

3.3. RESULTS AND DICUSSIONS

3.3.1. Characterization of nanoGUMBOS

R6G nanoGUMBOS were synthesized via an ion-exchange reaction between [R6G][Cl] and lithium bis (perfluoroethylsulfonyl)imide [Li][BETI] or sodium tetraphenylborate [Na][TPB] to from [R6G][BETI] and [R6G][TPB] respectively. The ion-exchange reaction was performed under ultrasonication to form nanoGUMBOS directly from the ion-exchange products. This

reaction is depicted in Figure 3.1. The synthesized nanoGUMBOS were characterized using several techniques such as mass spectrometry, FTIR, and NMR. The presence of [BETI] and [TPB] counter-ion peaks in the negative mode electrospray ionization mass spectrum indicates successful ion exchange of [R6G][Cl] to form respective GUMBOS. Data for α-CD [R6G][BETI] and α -CD [R6G][TPB] are shown in Figures 3.2 and 3.3. Similar results were obtained for all three CD employed. FTIR and NMR of [R6G][BETI] and [R6G][TPB] showed no peak shift for the CD-templated nanoGUMBOS suggesting that CD was only used as a template and was washed away during synthesis. Figures 3.4 and 3.5 display the respectively the NMR and FTIR of α-CD [R6G][BETI] and [R6G][TPB]. Similar results were obtained for all employed CDs.
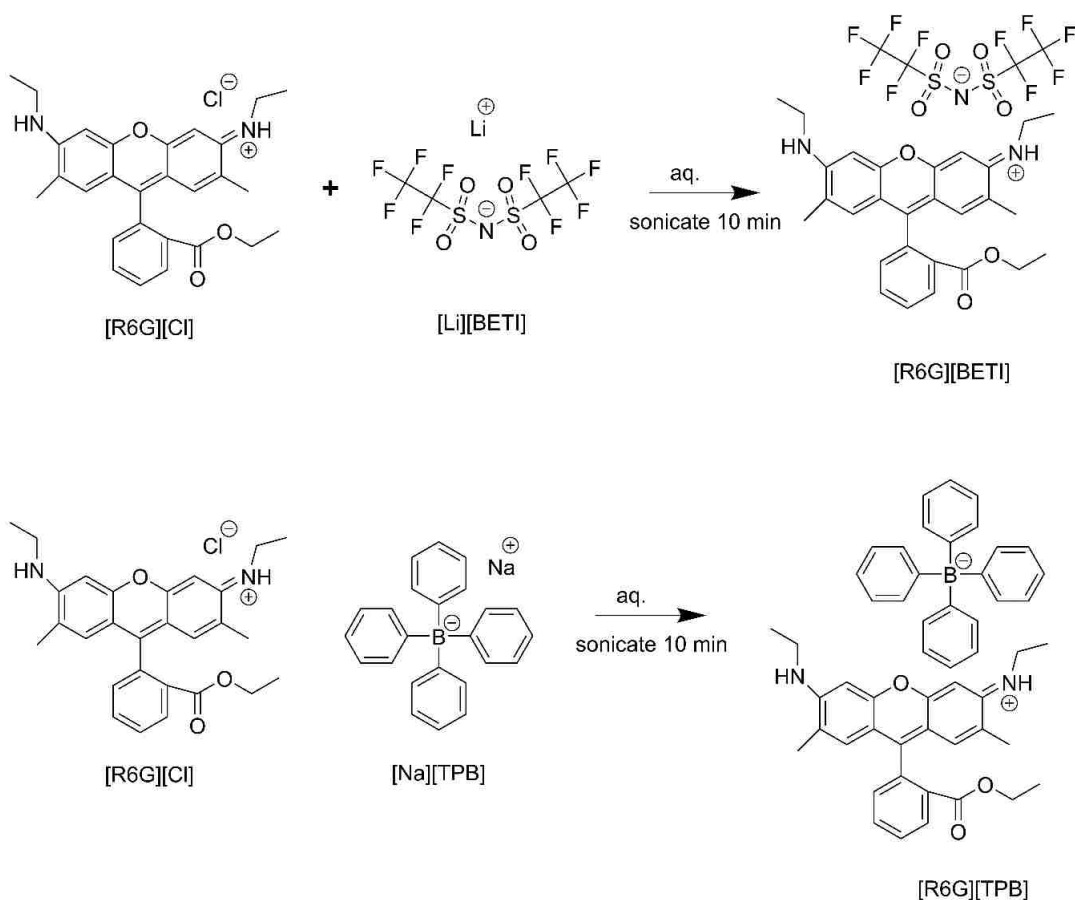
Figure 3.1. Synthesis of [R6G][BETI] and [R6G][TPB] nanoGUMBOS
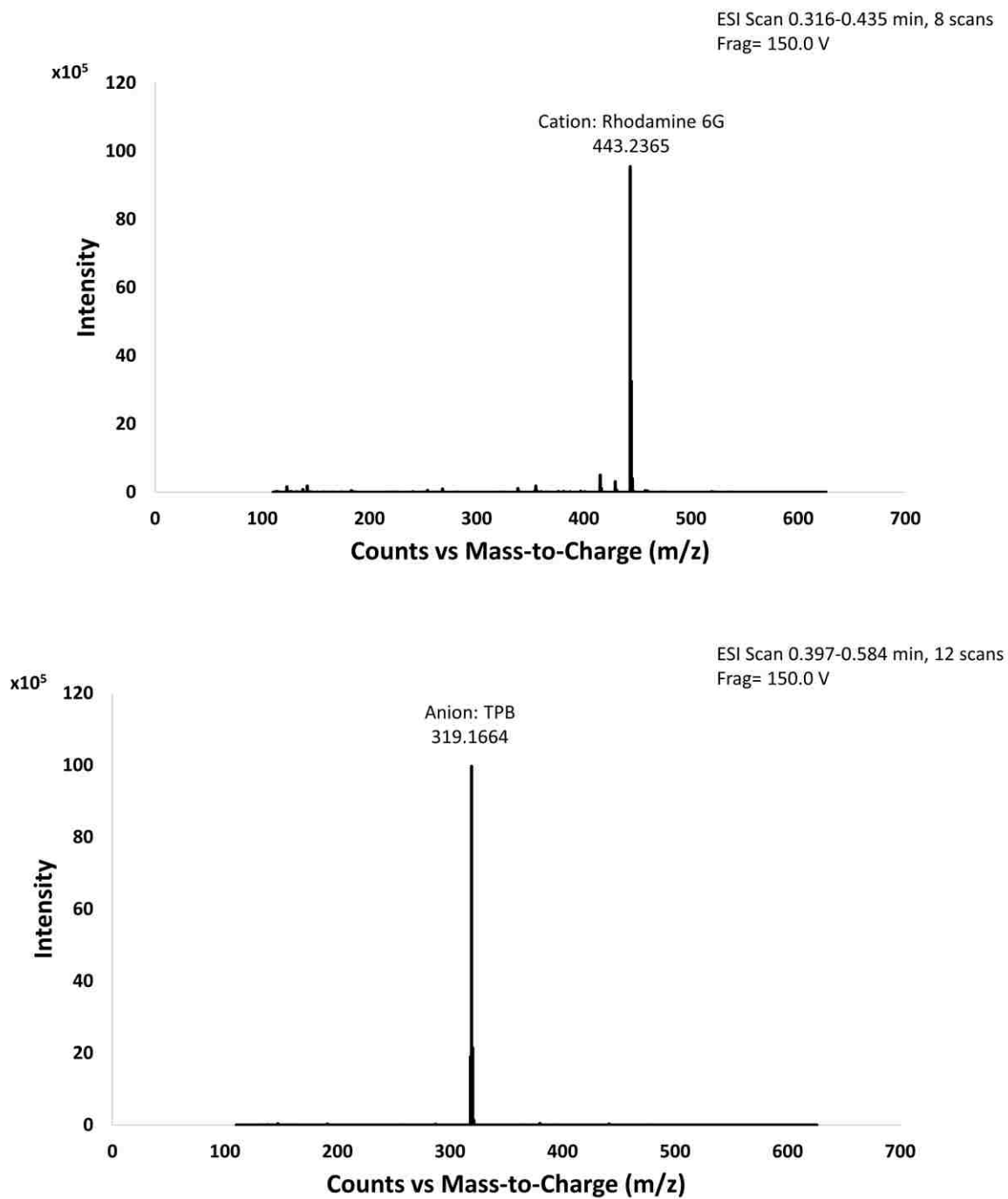
Figure 3.2. Electrospray Ionization Mass Spectrum in positive and negative mode for α-CD R6G TPB

Cation: Rhodamine 6G
443.2384

Anion: BETI
379.9127
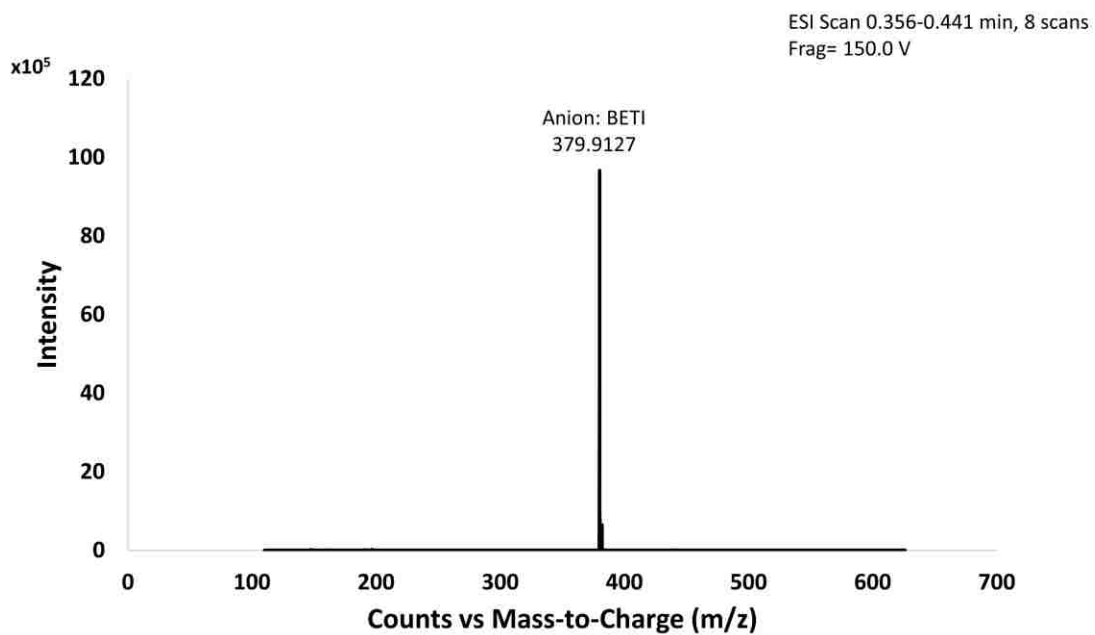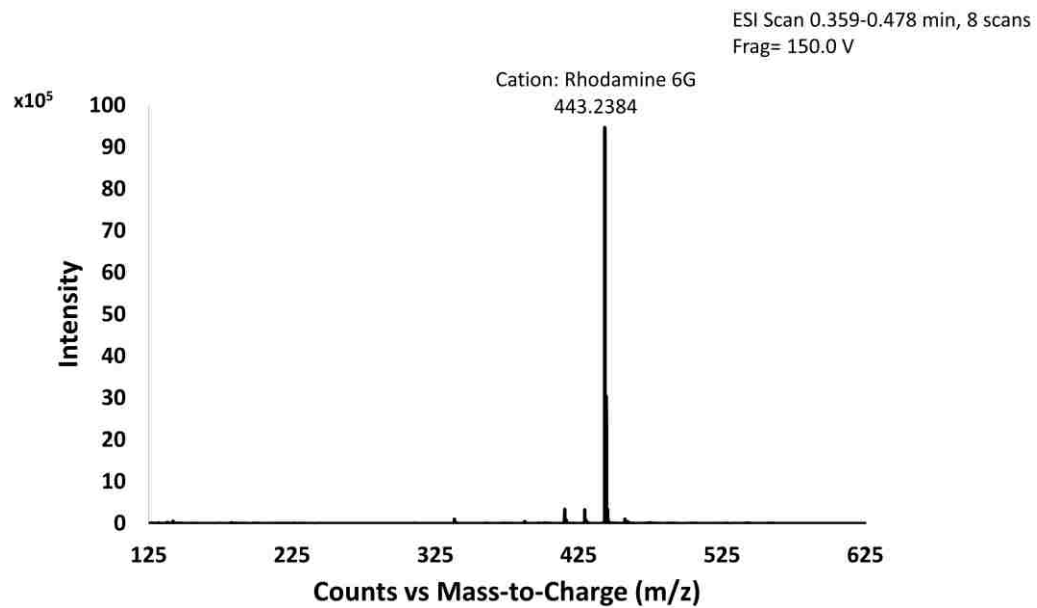
Figure 3.3**.** Electrospray Ionization Mass Spectrum in positive and negative mode for α-CD R6G BETI
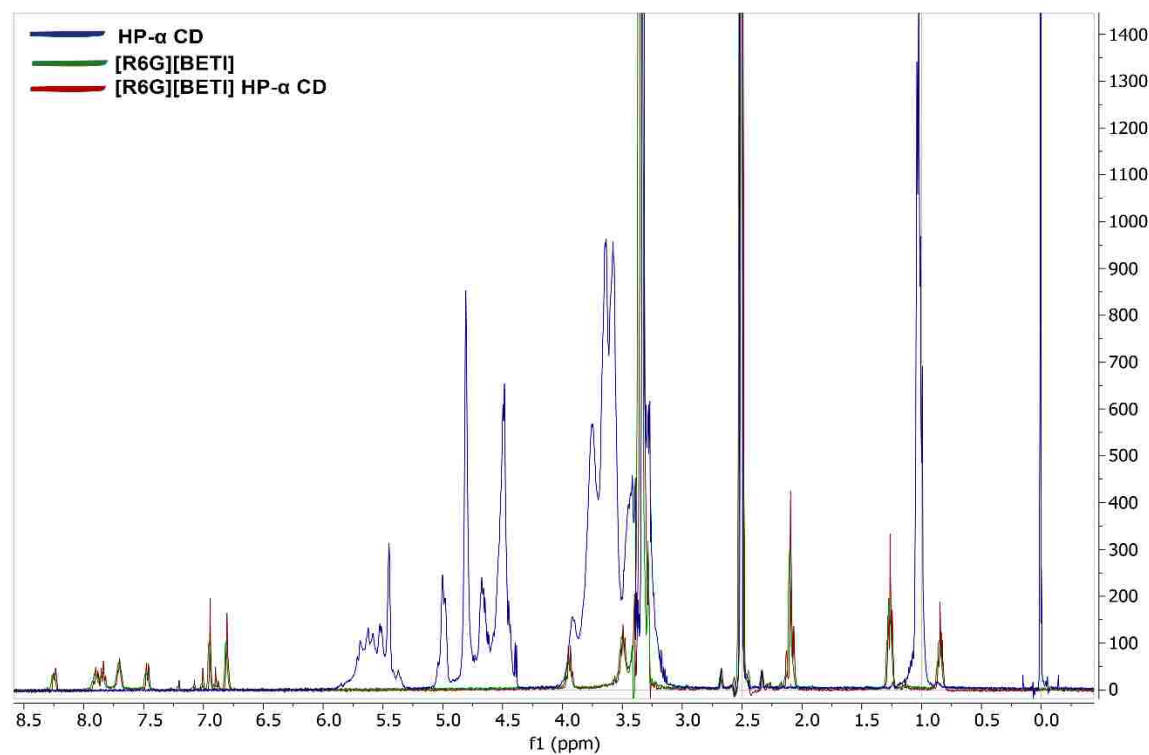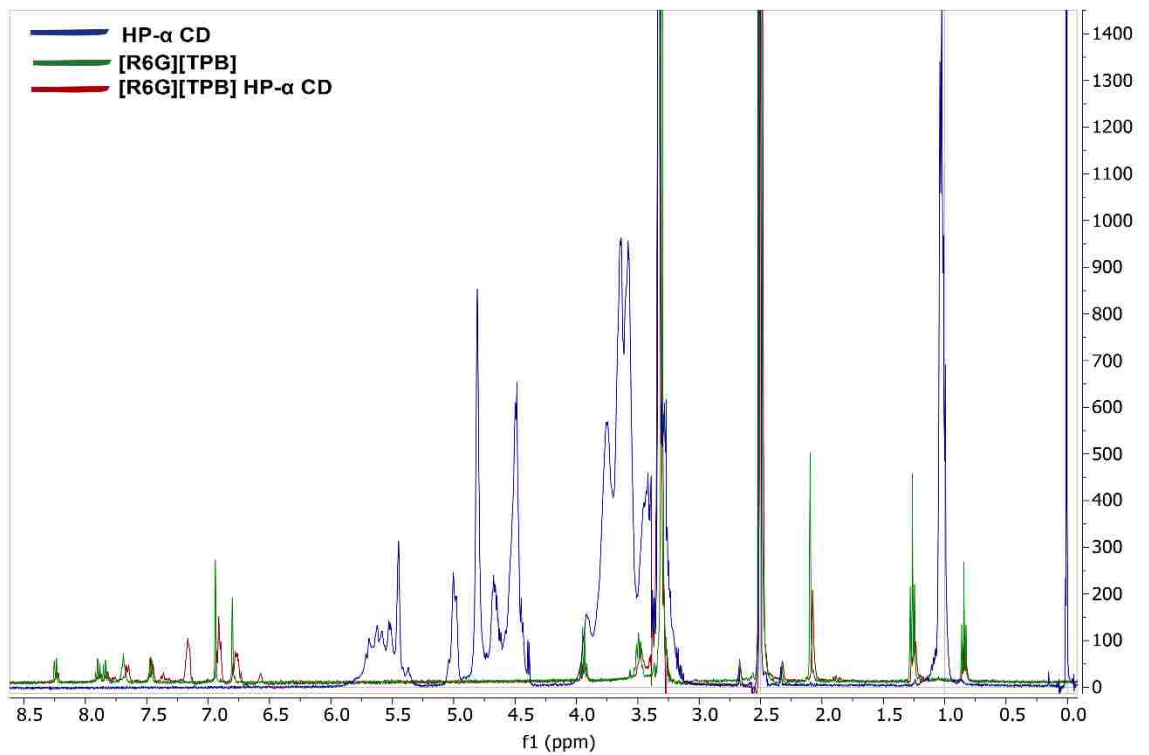
Figure 3.4. Overlay of NMR of [R6G][TPB] and [R6G][BETI] nanoGUMBOS with and without CD-templating
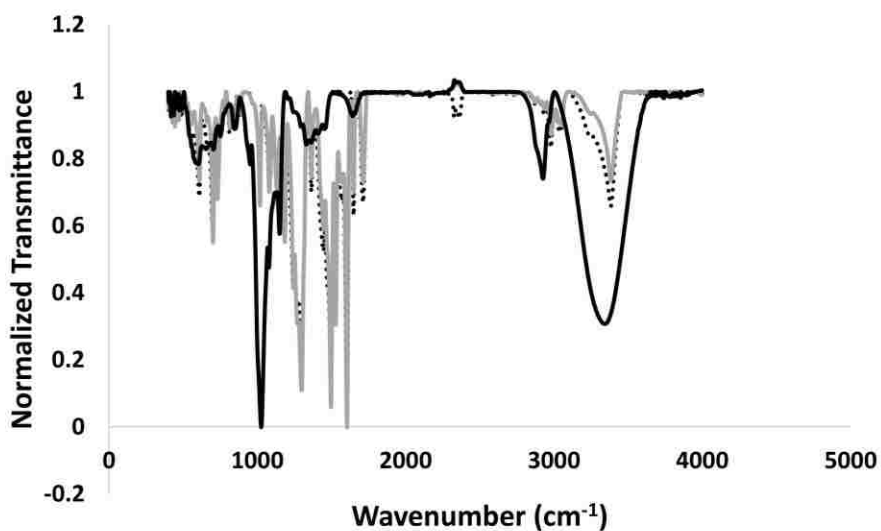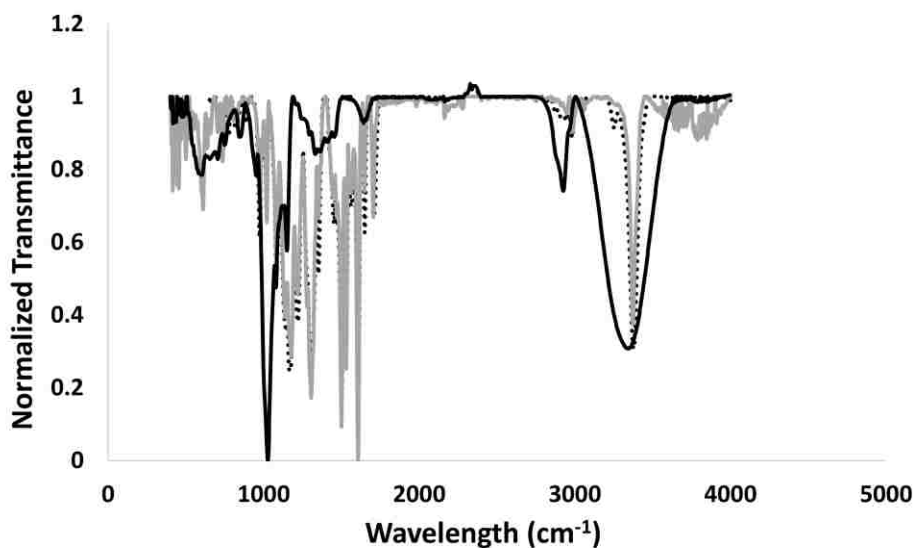
Figure 3.5. FTIR of [R6G][TPB] and [R6G][BETI] nanoGUMBOS with and without CD-templating

TEM microscopy and zeta potential of the nanoGUMBOS were then investigated to assess size and stability of the nanoparticles. Figure 3.6 and 3.7 portray TEM images of respectively [R6G][TPB] and [R6G][BETI] nanoGUMBOS with and without CD-templating. Table 3.1 summarizes sizes for both [R6G][TPB] and [R6G][BETI] nanoGUMBOS in the presence and

absence of CD. A significant reduction in size was observed in the presence of CD-templating for both [R6G][TPB] and [R6G][BETI] nanoGUMBOS. These results are consistent with findings from Hamden et al. that indicated CD-templating of nanoGUMBOS can lead to a significant reduction in nanoparticle size.[28] In addition, significantly improved polydispersity of the synthesized nanoparticles was observed due to formation within the CD cavity.[28,33]

Correlation between the sizes of the nanoparticles and the CD type suggest that size of the nanoparticle depends upon both the size of the drug and the CD cavity. Almost a 50% reduction in nanoparticle size was observed for the HP-α-CD, and HP-β-CD [R6G][TPB] nanoGUMBOS while a slightly larger size was observed for the γ-CD [R6G][TPB]. This difference in size can be attributed to the relatively smaller cavity size of the α and β-CD as compared to γ-CD.[33] In contrast, while a slight variation in size was observed, all of the [R6G][BETI] CD-templated nanoGUMBOS had relatively similar sizes around 70-80 nm. This behavior is most likely due to the bulky aromatic rings of TPB in contrast to the relatively smaller structure of BETI. In this regard, a larger cavity size is more likely to optimally fit the large aromatic ring structure of TPB, resulting in a larger variation in size.

| — 500 nm | — 500 nm | — 500 nm | —— 500 nm |
| [R6G][TPB] | [R6G][TPB] α-CD | [R6G][TPB] β-CD | [R6G][TPB] γ-CD |
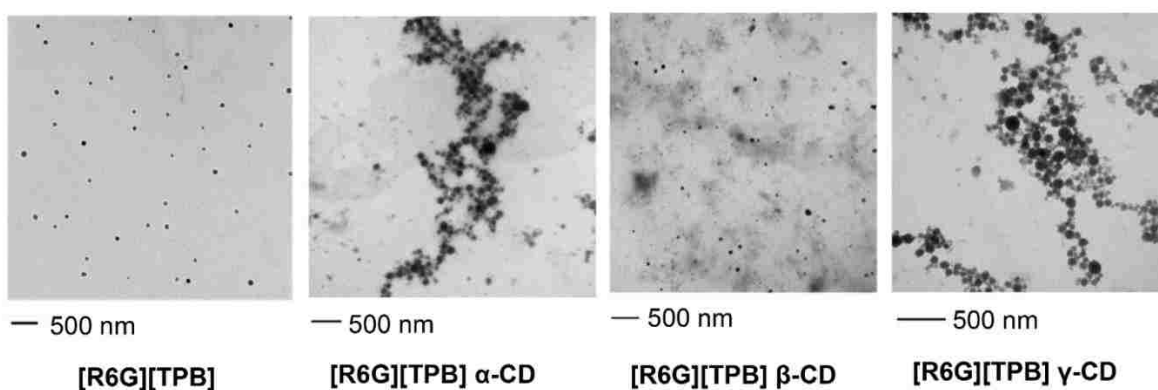
Figure 3.6. TEM images of 100 µM [R6G][TPB] nanoGUMBOS with and without CD-templating
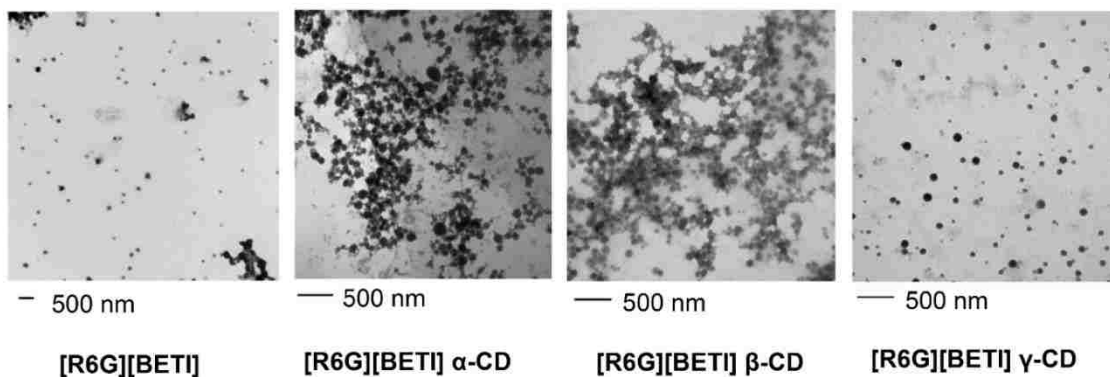
Figure 3.7. TEM images of 100 µM [R6G][BETI] nanoGUMBOS with and without CD-templating

Table 3.1. Sizes of [R6G][TPB] and [R6G]BETI] nanoGUMBOS

NanoGUMBOS	Size (nm)
[R6G][TPB] Control	99 ± 16
[R6G][TPB] HP-α-CD	55 ± 5
[R6G][TPB] HP-β-CD	44 ± 4
[R6G][TPB] γ-CD	69 ± 6
[R6G][BETI] Control	92 ± 14
[R6G]BETI] HP-α-CD	68 ± 8
[R6G][BETI] HP-β-CD	66 ± 4
[R6G][BETI] γ-CD	80 ± 7

Following TEM characterization, DLS and zeta potential measurements were performed to further understand the effect of cyclodextrin on size distribution and stability of the nanoGUMBOS respectively. DLS measurements indicated that all synthesized nanoGUMBOS displayed a polydispersity of 0.2; thus, indicating relatively monodispersed nanoparticles. Zeta potential measurements were carried out in phosphate buffered saline maintained at physiological pH (pH 7.4) to mimic the biological environment. As shown in table 3.2, while the zeta potential

measurement for [R6G][TPB] is around -23.1 ± 1.2 mV, CD-templated nanoGUMBOS displayed a zeta potential of around -28 mV, indicating formation of slightly more stable nanoparticles with CD templating. Similar results were seen for [R6G][BETI] nanoGUMBOS where the zeta potential varied from -24.3 ± 1.3 mV to -29 mV between the control and CD-templated nanoGUMBOS respectively. These results suggest that use of the CD-templating led to improved stability of the nanoGUMBOS.

Table 3.2. Zeta Potential of [R6G][TPB] and [R6G]BETI] nanoGUMBOS

NanoGUMBOS	Zeta Potential (mV)
[R6G][TPB] Control	-23.1 ± 1.2
[R6G][TPB] HP-α-CD	-27.2 ± 1.5
[R6G][TPB] HP-β-CD	-29.5 ± 1.1
[R6G][TPB] γ-CD	-28.3 ± 0.9
[R6G][BETI] Control	-24.3 ± 1.2
[R6G]BETI] HP-α-CD	-29.0 ± 1.1
[R6G][BETI] HP-β-CD	-30.1 ± 0.8
[R6G][BETI] γ-CD	-29.8 ± 1.6

3.3.2. Examination of Cell Viability

NanoGUMBOS were then employed i*n vitro* to assess the effect of this size variation on the toxicity. Figure 3.8 is a graphical representation of the cytotoxicity of [R6G][TPB] nanoGUMBOS with and without CD templating towards MDA-MB-231 breast cancer cells. The IC_{50} values, the concentration at which 50% cell death occurs, for [R6G][TPB] nanoGUMBOS are reported in Table 3.3. Interestingly, an enhanced cytotoxicity was observed for CD-templated [R6G][TPB] nanoGUMBOS as compared to the nanoGUMBOS alone. In this regard, while the [R6G][TPB] nanoGUMBOS displayed an IC_{50} value of 7.32 µg/mL in the absence of CD,

templating with α and β-CD led to a three-fold reduction in IC_{50} value to 2.64 µg/mL and 2.77 µg/mL respectively. Templating with γ-CD led to a five-fold reduction in the IC50 to 1.41 µg/mL. Statistical analysis indicated that the IC_{50} concentration of γ-CD significantly varies from that of α and β-CD at a 95% confidence level.

Toxicity of the [R6G][BETI] nanoGUMBOS with and without cyclodextrin templating is presented in Figure 3.9. Similar the [R6G][TPB] nanoGUMBOS, an enhanced cytotoxicity was observed for the CD-templated [R6G][BETI] nanoGUMBOS as compared to the nanoparticles alone. In this regard, CD-templating led to a decrease in IC_{50} concentration from 4.23 µg/mL for nanoGUMBOS alone to 2.81 µg/mL for the γ-CD templated nanoGUMBOS, suggesting almost a two-fold increase in toxicity (Table 3.4). Templating with HP-α and HP-β-CD led to an even greater reduction in IC50 concentration to 1.45 µg/mL and 1.72 µg/mL respectively. Statistical analysis, however, suggested that the variation in IC50 concentration with CD-cavity size was insignificant. This indicates that in contrast to the CD-templated [R6G][TPB] nanoGUMBOS, the toxicity of CD-templated [R6G][BETI] nanoGUMBOS was independent of CD-cavity size. In order to further understand this contrasting behavior, toxicity of the nanoGUMBOS were then assessed in Mia-Paca pancreatic cancer cells. Interestingly, similar results were seen for the Mia-Paca pancreatic cell line, corroborating the results observed with the MDA-MB-231 cancer cells. Remarkably, all synthesized nanoGUMBOS displayed less than 1 µg/mL IC_{50} values toward Mia-Paca pancreatic cancer cells (Table 3.5), suggesting their promising therapeutic potential.
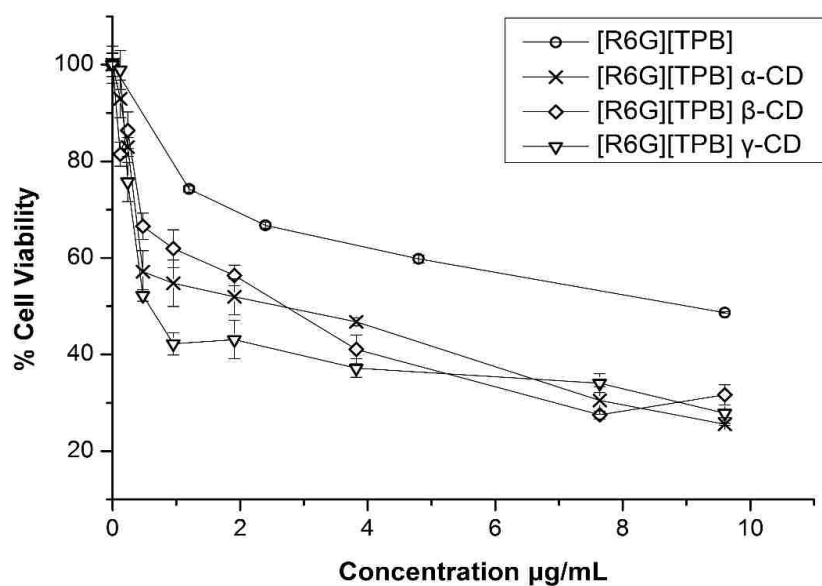
Figure 3.8. Toxicity of [R6G][TPB] nanoGUMBOS with and without CD-templating towards MDA-MB-231 breast cancer cells

Table 3.3. IC$_{50}$ Concentrations of [R6G][TPB] nanoGUMBOS towards MDA-MB-231 breast cancer cells

Compound	IC50 µg/mL
[R6G][TPB] Control	7.32 ± 1.21
[R6G][TPB] HP-α-CD	2.64 ± 0.30
[R6G][TPB] HP-β-CD	2.77 ± 0.21
[R6G][TPB] γ-CD	1.41 ± 0.24
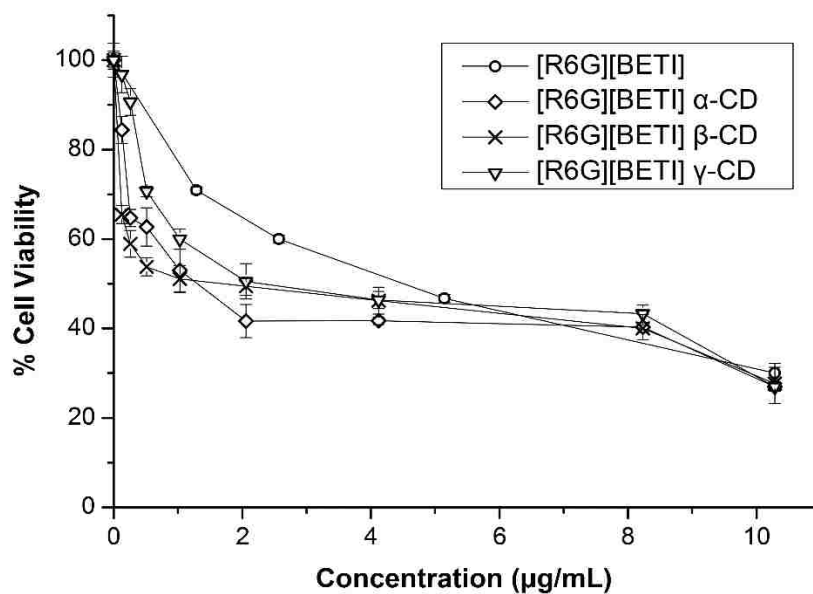
Figure 3.9. Toxicity of [R6G][BETI] nanoGUMBOS with and without cyclodextrin templating towards MDA-MB-231 cancer cells

Table 3.4: IC$_{50}$ Concentrations of [R6G][BETI] nanoGUMBOS towards MDA-MB-231 breast cancer cells

Compound	IC$_{50}$ µg/mL
[R6G][BETI] Control	4.23 ± 0.42
[R6G]BETI] HP-α-CD	1.45 ± 0.44
[R6G][BETI] HP-β-CD	1.72 ± 0.66
[R6G][BETI] γ-CD	2.81 ± 0.54

Table 3.5. IC$_{50}$ Concentrations of [R6G][TPB] and [R6G][BETI] nanoGUMBOS towards Mia-Paca Pancreatic Cancer Cells

Compound	IC$_{50}$ µg/mL
[R6G][TPB] Control	0.75 ± 0.05
[R6G][TPB] HP-α-CD	0.37 ± 0.03
[R6G][TPB] HP-β-CD	0.39 ± 0.06
[R6G][TPB] γ-CD	0.24 ± 0.04
[R6G][BETI] Control	0.45 ± 0.05
[R6G]BETI] HP-α-CD	0.21 ± 0.03
[R6G][BETI] HP-β-CD	0.25 ± 0.04
[R6G][BETI] γ-CD	0.33 ± 0.03

3.3.3 Cellular Uptake of nanoGUMBOS

In order to further understand the relationship between reduced size and enhanced toxicity of the nanoGUMBOS, cellular uptake was examined. Figures 3.10 and 3.11 display the cellular uptake (nmol) of 5 µM [R6G][TPB] and [R6G][BETI] nanoGUMBOS respectively after 5 h. As shown in figure 4a, the cellular uptake of [R6G][TPB] nanoGUMBOS in the absence of CD is significantly lower than that of the CD-templated nanoGUMBOS. Similarly, an increased cellular uptake was also observed for the CD-templated [R6G][BETI] nanoGUMBOS as compared to the control without CD-templating. HP-β-CD [R6G][TPB] nanoGUMBOS displayed a relatively lower cellular uptake as compared to nanoGUMBOS templated with HP-α-CD or γ-CD. Furthermore, in the case of the [R6G][BETI] nanoGUMBOS, all CD-templated nanoGUMBOS displayed similar cellular uptakes, which is consistent with their relatively similar IC$_{50}$ concentrations.
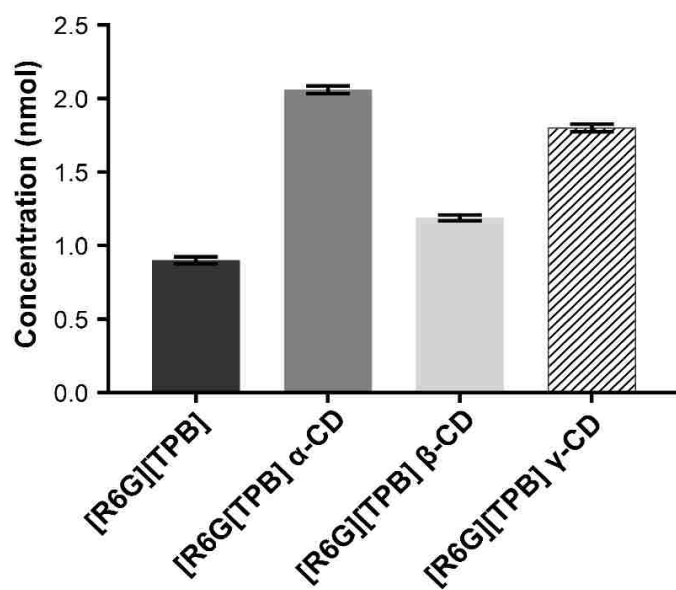
Figure 3.10. Cellular uptake of 5 µM [R6G][TPB] nanoGUMBOS with and without CD-templating in MDA-MB-231 cancer cells after 5 hrs
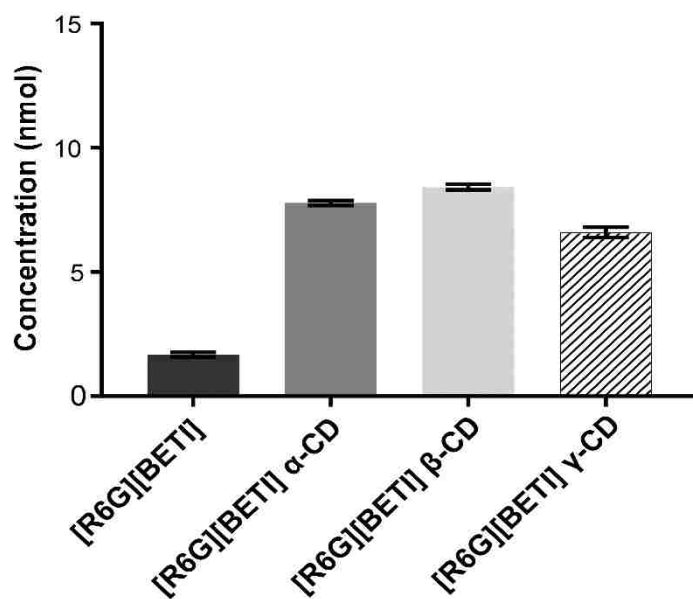
Figure 3.11. Cellular uptake of 5 µM [R6G][BETI] nanoGUMBOS with and without CD-templating in MDA-MB-231 cancer cells after 5 hrs

3.3.4. Examination of Selectivity

After detailed understanding of their behavior in cancer cells, nanoGUMBOS were employed in Hs578Bst normal breast cells to investigate the effect of cyclodextrin on the selective behavior of the nanomaterials. Figures 3.12 and 3.13 are graphical representations of the toxicity of [R6G][TPB] and [R6G][BETI] with and without cyclodextrin templating towards Hs578Bst normal breast cells. Intriguingly, the cell viability was almost 100% in normal cells for both [R6G][TPB] and [R6G][BETI] cyclodextrin templated nanoGUMBOS, similar to the respective controls without CD. This indicates that CD templating enhances the toxicity of the R6G nanoGUMBOS towards cancer cells without affecting the nontoxic nature towards normal cells under experimental conditions.
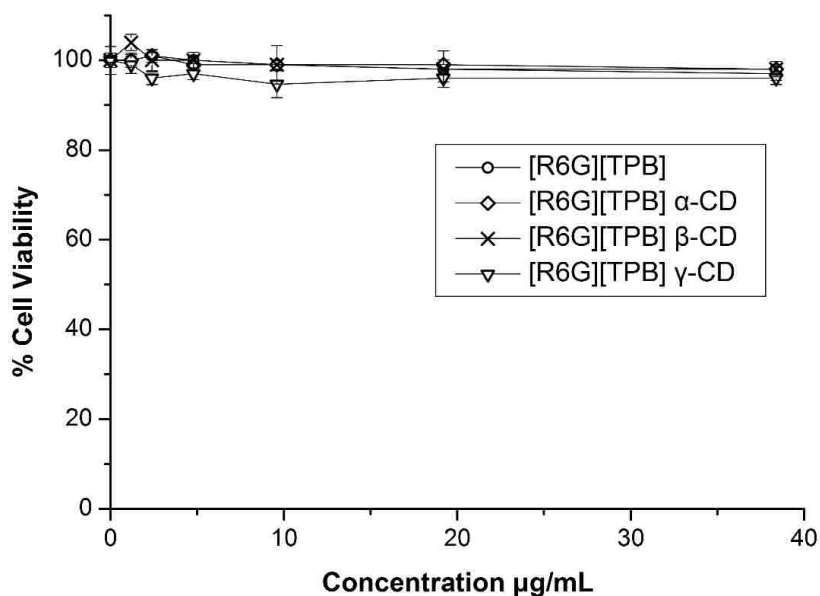
Figure 3.12. Toxicity of [R6G][TPB] nanoGUMBOS with and without CD-templating towards Hs578Bst normal breast cells
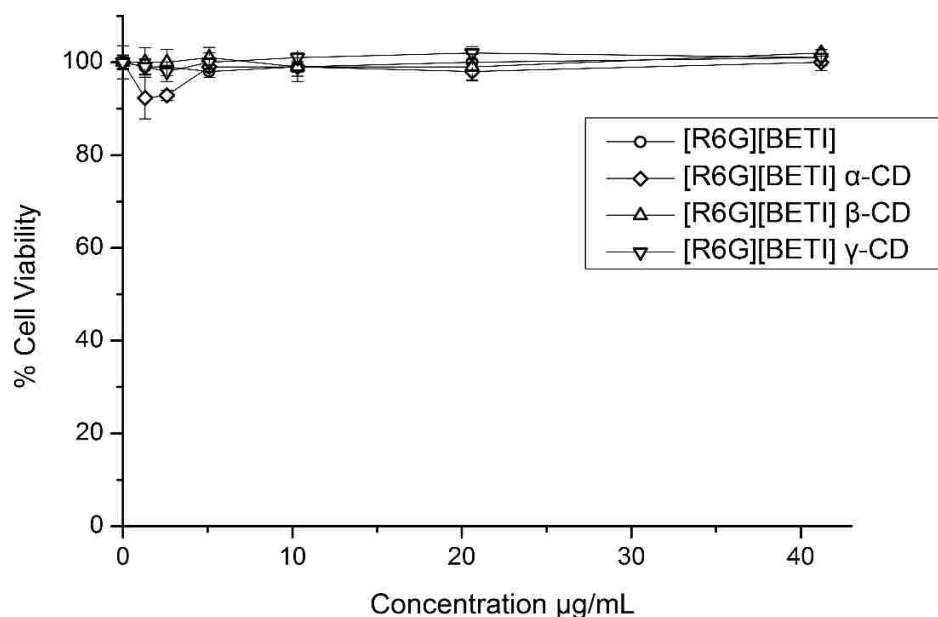
Figure 3.13. Toxicity of [R6G][BETI] nanoGUMBOS with and without CD-templating towards Hs578Bst normal breast cells.

3.3.5. Optimal Size for Toxicity

Results from our studies indicate that cyclodextrin templating led to reduced size, enhanced cellular uptake and improved cytotoxicity of the R6G nanoGUMBOS. As discussed above, a significant reduction in IC_{50} was observed with the cyclodextrin templated [R6G][TPB] nanoGUMBOS as compared to respective nanoGUMBOS without cyclodextrin. This enhanced toxicity of the CD-templated nanoGUMBOS is consistent with the cellular uptake, which demonstrated increased cellular internalization for the CD-templated [R6G][TPB] nanoGUMBOS. This observation is consistent with several studies which found that reduction in size results in increased cellular uptake due to the EPR effect and variation in internalization pathways.[34-35] Furthermore, a relatively smaller cellular uptake is observed for [R6G][TPB] nanoparticles templated with beta-CD in comparison to the γ-CD and HP-α-CD [R6G][TPB]. Correlation of the cellular uptake to the size suggests that the relatively smaller size of β-CD

templated [R6G][TPB] nanoGUMBOS allows for rapid internalization and excretion, ultimately leading to poor cellular retention.[36]

Additionally, correlation between size and cytotoxicity of both [R6G][TPB] CD-templated nanoGUMBOS indicates an optimal size was observed for enhanced toxicity. In this regard, γ-CD templated [R6G][TPB] nanoparticles have a size around 70 nm, while 2HP-β-CD and 2HP-α-CD templated [R6G][TPB] nanoparticles have sizes below 60 nm. Comparison of their IC50 values indicates that γ-CD templated nanoparticles displayed a statistically significant reduction in IC50 concentration as compared to the 2HP-β-CD and 2HP-α-CD templated nanoparticles. Moreover, this suggests that the 70 nm nanoparticles obtained from γ-CD templating led to the most optimal toxicity for the [R6G][TPB] nanoGUMBOS.

Similar to the [R6G][TPB] nanoGUMBOS, the CD templated [R6G][BETI] nanoGUMBOS displayed a reduced size as compared to a control with no templating. In contrast to the [R6G][TPB] nanoGUMBOS, however, the sizes for all the CD-templated [R6G][BETI] nanoGUMBOS were all between 70-80 nm. In this regard, the IC50 concentrations and cellular uptakes were relatively similar for the different CD-templated nanoGUMBOS. Thus, for the [R6G][BETI] nanoGUMBOS, while CD-templating led to a significant reduction in IC50 concentration, no variation in IC50 concentration was with varying CD cavity size. Furthermore, the optimal IC_{50} for the [R6G][TPB] nanoGUMBOS from the 70 nm γ-CD templated nanoGUMBOS, is relatively similar to that of all the CD-templated [R6G][BETI] nanoGUMBOS. This indicates that 70-80 nm is most likely the optimal size for improved toxicity of nanoGUMBOS developed from R6G. It is interesting to note that while the nanoGUMBOS without CD displayed lower or comparable toxicity to the previously reported toxicity of the parent dye [R6G][Cl], the CD-templated nanoGUMBOS displayed an improved toxicity.[21]

3.4. CONCLUSIONS

These results suggest a simple and rapid synthesis technique to control the size and ultimately tune the cytotoxicity of nanodrugs. These studies demonstrated that CD-templated nanoparticles display reduced size and improved stability, which can provide several benefits in biological systems. Significantly improved *in vitro* toxicity was observed for [R6G][BETI] and [R6G][TPB] CD-templated nanoGUMBOS in comparison to a control without CD. Furthermore, γ-CD templating displayed optimal toxicity for the [R6G][TPB] nanoGUMBOS. In contrast, the IC50 concentration was relatively similar among the different CD-templated nanoGUMBOS for [R6G][BETI]. Moreover, the γ-CD [R6G][TPB] nanoGUMBOS and all the R6G BETI CD-templated nanoGUMBOS displayed similar IC_{50} concentrations. Correlation of size and toxicity suggests that 70-80 nm particles displayed optimal therapeutic properties for investigated R6G nanoGUMBOS. Further examination of the nanoGUMBOS indicates no toxicity to normal breast cells under the reported conditions giving further insight to the promising therapeutic potential of these nanoGUMBOS. Moreover, these studies report the effect of reduced size on the toxicity of rhodamine 6G nanoGUMBOS and the results can provide insights for similar strategies for other chemotherapeutic nanodrugs.

3.5. REFERENCES

1.   Society, A. C. Cancer Facts and Figures 2017. www.cancer.org (accessed May 2).

2.   Miller, K. D.; Siegel, R. L.; Lin, C. C.; Mariotto, A. B.; Kramer, J. L.; Rowland, J. H.; Stein, K. D.; Alteri, R.; Jemal, A., Cancer treatment and survivorship statistics, 2016. *CA: a cancer journal for clinicians* **2016,** *66* (4), 271-289.

3.   Park, K., Facing the Truth about Nanotechnology in Drug Delivery. *ACS Nano* **2013,** *7* (9), 7442-7447.

4.   Wicki, A.; Witzigmann, D.; Balasubramanian, V.; Huwyler, J., Nanomedicine in cancer therapy: Challenges, opportunities, and clinical applications. *Journal of Controlled Release* **2015,** *200*, 138-157.

5.   Krishnamurthy, S.; Vaiyapuri, R.; Zhang, L.; Chan, J. M., Lipid-coated polymeric nanoparticles for cancer drug delivery. *Biomaterials science* **2015,** *3* (7), 923-936.

6.   Mura, S.; Nicolas, J.; Couvreur, P., Stimuli-responsive nanocarriers for drug delivery. *Nature materials* **2013,** *12* (11), 991-1003.

7.   Markman, J. L.; Rekechenetskiy, A.; Holler, E.; Ljubimova, J. Y., Nanomedicine therapeutic approaches to overcome cancer drug resistance. *Advanced Drug Delivery Reviews* **2013,** *65* (13–14), 1866-1879.

8.   Kumari, A.; Yadav, S. K.; Yadav, S. C., Biodegradable polymeric nanoparticles based drug delivery systems. *Colloids and Surfaces B: Biointerfaces* **2010,** *75* (1), 1-18.

9.   Albanese, A.; Tang, P. S.; Chan, W. C., The effect of nanoparticle size, shape, and surface chemistry on biological systems. *Annual review of biomedical engineering* **2012,** *14*, 1-16.

10.   Li, Y.; Lin, J.; Huang, Y.; Li, Y.; Yang, X.; Wu, H.; Wu, S.; Xie, L.; Dai, L.; Hou, Z., Self-Targeted, Shape-Assisted, and Controlled-Release Self-Delivery Nanodrug for Synergistic Targeting/Anticancer Effect of Cytoplasm and Nucleus of Cancer Cells. *ACS Applied Materials & Interfaces* **2015,** *7* (46), 25553-25559.

11.   Huang, P.; Wang, D.; Su, Y.; Huang, W.; Zhou, Y.; Cui, D.; Zhu, X.; Yan, D., Combination of Small Molecule Prodrug and Nanodrug Delivery: Amphiphilic Drug–Drug Conjugate for Cancer Therapy. *Journal of the American Chemical Society* **2014,** *136* (33), 11748-11756.

12.   Greish, K., Enhanced permeability and retention of macromolecular drugs in solid tumors: a royal gate for targeted anticancer nanomedicines. *Journal of drug targeting* **2007,** *15* (7-8), 457-464.

13.   Jain, R. K.; Stylianopoulos, T., Delivering nanomedicine to solid tumors. *Nature reviews. Clinical oncology* **2010,** *7* (11), 653-664.

14.   Peer, D.; Karp, J. M.; Hong, S.; Farokhzad, O. C.; Margalit, R.; Langer, R., Nanocarriers as an emerging platform for cancer therapy. *Nat Nano* **2007,** *2* (12), 751-760.

15.   Greish, K., Enhanced Permeability and Retention (EPR) Effect for Anticancer Nanomedicine Drug Targeting. In *Cancer Nanotechnology: Methods and Protocols*, Grobmyer, S. R.; Moudgil, B. M., Eds. Humana Press: Totowa, NJ, 2010; pp 25-37.

16.   Tang, L.; Yang, X.; Yin, Q.; Cai, K.; Wang, H.; Chaudhury, I.; Yao, C.; Zhou, Q.; Kwon, M.; Hartman, J. A., Investigating the optimal size of anticancer nanomedicine. *Proceedings of the National Academy of Sciences* **2014,** *111* (43), 15344-15349.

17.   Maeda, H.; Nakamura, H.; Fang, J., The EPR effect for macromolecular drug delivery to solid tumors: Improvement of tumor uptake, lowering of systemic toxicity, and distinct tumor imaging in vivo. *Advanced Drug Delivery Reviews* **2013,** *65* (1), 71-79.

18.   Blanco, E.; Shen, H.; Ferrari, M., Principles of nanoparticle design for overcoming biological barriers to drug delivery. *Nat Biotech* **2015,** *33* (9), 941-951.

19.   Torchilin, V., Tumor delivery of macromolecular drugs based on the EPR effect. *Advanced Drug Delivery Reviews* **2011,** *63* (3), 131-135.

20.   Farokhzad, O. C.; Langer, R., Nanomedicine: Developing smarter therapeutic and diagnostic modalities. *Advanced Drug Delivery Reviews* **2006,** *58* (14), 1456-1459.

21.   Magut, P. K. S.; Das, S.; Fernand, V. E.; Losso, J.; McDonough, K.; Naylor, B. M.; Aggarwal, S.; Warner, I. M., Tunable Cytotoxicity of Rhodamine 6G via Anion Variations. *Journal of the American Chemical Society* **2013,** *135* (42), 15873-15879.

22.   Warner, I. M.; El-Zahab, B.; Siraj, N., Perspectives on Moving Ionic Liquid Chemistry into the Solid Phase. *Analytical Chemistry* **2014,** *86* (15), 7184-7191.

23.   Kutushov, M.; Gorelik, O., Low concentrations of Rhodamine-6G selectively destroy tumor cells and improve survival of melanoma transplanted mice. *Neoplasma* **2013,** *60* (3), 262-73.

24.   Tiwari, G.; Tiwari, R.; Rai, A. K., Cyclodextrins in delivery systems: Applications. *Journal of Pharmacy and Bioallied Sciences* **2010,** *2* (2), 72-79.

25.   Zhang, J.; Ma, P. X., Cyclodextrin-based supramolecular systems for drug delivery: Recent progress and future perspective. *Advanced Drug Delivery Reviews* **2013,** *65* (9), 1215-1233.

26.   Brewster, M. E.; Loftsson, T., Cyclodextrins as pharmaceutical solubilizers. *Advanced Drug Delivery Reviews* **2007,** *59* (7), 645-666.

27.   Del Valle, E. M., Cyclodextrins and their uses: a review. *Process biochemistry* **2004,** *39* (9), 1033-1046.

28.   Hamdan, S.; Dumke, J. C.; El-Zahab, B.; Das, S.; Boldor, D.; Baker, G. A.; Warner, I. M., Strategies for controlled synthesis of nanoparticles derived from a group of uniform materials based on organic salts. *Journal of Colloid and Interface Science* **2015,** *446*, 163-169.

29.   Bleta, R.; Lannoy, A.; Machut, C.; Monflier, E.; Ponchel, A., Understanding the Role of Cyclodextrins in the Self-Assembly, Crystallinity, and Porosity of Titania Nanostructures. *Langmuir* **2014,** *30* (39), 11812-11822.

30.   Chung, J. W.; Guo, Y.; Kwak, S.-Y.; Priestley, R. D., Understanding and controlling gold nanoparticle formation from a robust self-assembled cyclodextrin solid template. *Journal of Materials Chemistry* **2012,** *22* (13), 6017-6026.

31.   Ganguly, B. N.; Verma, V.; Chatterjee, D.; Satpati, B.; Debnath, S.; Saha, P., Study of Gallium Oxide Nanoparticles Conjugated with β-Cyclodextrin: An Application To Combat Cancer. *ACS Applied Materials & Interfaces* **2016,** *8* (27), 17127-17137.

32.   Davis, M. E.; Brewster, M. E., Cyclodextrin-based pharmaceutics: past, present and future. *Nature Reviews Drug Discovery* **2004,** *3* (12), 1023-1035.

33.   van de Manakker, F.; Vermonden, T.; van Nostrum, C. F.; Hennink, W. E., Cyclodextrin-Based Polymeric Materials: Synthesis, Properties, and Pharmaceutical/Biomedical Applications. *Biomacromolecules* **2009,** *10* (12), 3157-3175.

34.   Acharya, S.; Sahoo, S. K., PLGA nanoparticles containing various anticancer agents and tumour delivery by EPR effect. *Advanced Drug Delivery Reviews* **2011,** *63* (3), 170-183.

35.   Svenson, S.; Prud'homme, R. K., *Multifunctional nanoparticles for drug delivery applications: imaging, targeting, and delivery*. Springer Science & Business Media: 2012.

36.   Li, S.-D.; Huang, L., Pharmacokinetics and biodistribution of nanoparticles. *Molecular pharmaceutics* **2008,** *5* (4), 496-504.

CHAPTER 4
SELECTIVE CHEMOTHERAPEUTIC APPLICATIONS OF ESTER DERIVATIVES OF RHODAMINE (R123 AND SNAFR-5) BASED NANOGUMBOS

4.1. INTRODUCTION

Lipophilic cationic structures such as rhodamine derivatives have been widely investigated for chemotherapeutic applications due to their hydrophobic structure and cationic properties.[1-3] As discussed in first Chapter, several studies have found that the mitochondrial membrane in cancer cells is relatively more negative as compared to the mitochondrial membrane in normal cells.[4-5] In this regard, lipophilic cations have found to have a significantly greater accumulation in cancer cells in contrast to normal cells, ultimately resulting in partially selective toxicity.[3, 5-6] Further studies have shown that in addition to ionic nature, hydrophobicity also plays a major role in the mitochondrial accumulation.[7-8] Intriguingly, the hydrophobicity of rhodamine 123 is found to be optimal for this partially selective behavior in contrast to other triarylmethane dyes such as ethyl violet.[2, 8-10]

In this regard, several studies have shown that R123 demonstrates promising *in vitro* and *in vivo* therapeutic efficacy.[11-14] R123 displayed a significant *in vitro* toxicity towards several pancreatic and breast cancer cell lines with no toxicity towards normal cells at low concentrations (10 µg/mL), suggesting its partially selective behvaior.[12-13] *In vivo* studies of R123 revealed a significant reduction in tumor volume, suggesting its great therapeutic efficacy.[15-16] Interestingly, R123 was also employed in clinical trials for prostate cancer due to its high retention in prostate tissue; however, a poor therapeutic efficacy was observed for the dye. Studies revealed that while the R123 was able to inhibit doubling time for prostate-specific antigen, these results were not statistically significant against a control that measured the doubling time in the absence of R123.[17]

Moreover, these results indicate that while R123 has shown promising properties in-vitro and in-vivo, clinical applications of the dye did not corroborate these results.

Nanomaterials have been widely investigated for enhanced selectivity as well as enhanced retention in tumor tissue.[18-20] Furthermore, due to their interaction with the phospholipid bilayer, nanomaterials typically internalize via active transport pathways such as endocytosis in contrast to free dye internalization through passive diffusion.[21] In regards to the poor clinical toxicity of the R123 moiety, formation of nanomaterials can possibly lead to enhanced toxicity due to this varied internalization. In addition, synthesis of nanomaterials can lead to a more targeted therapy for minimized systemic toxicity of the drug.

Our research group has developed nanomaterials, nanoGUMBOS, based on rhodamine 6G (R6G) for selective chemotherapeutic applications.[22] These nanoGUMBOS are a nanoparticle assembly of the drug itself; thus, they can be synthesized without any matrix.[23] As indicated in Magut et al., synthesis of GUMBOS from R6G led to tunable hydrophobicity, and toxicity.[22] The tunable hydrophobicity can enhance the hydrophobic interaction with the cell membrane for dyes such as R123. In contrast to the studies investigated by Belostotsky et al. that suggested the major role of hydrophobicity plays in the selective accumulation, GUMBOS provide a rapid interface to tune the hydrophobicity of a single cation rather than examine several cations.[8, 22-23]

In the studies presented, GUMBOS derived from two rhodamine derivatives, R123 and Seminapthofluorone-5 (SNAFR-5), containing an ester structure similar to that of R6G were examined for selective chemotherapeutic behavior that was observed with the R6G nanoGUMBOS. Relative hydrophobicity of the GUMBOS was characterized using octanol-water partition coefficients. Subsequently, the nanoGUMBOS were employed in-vitro in MDA-MB-231 cancer cells to examine their cellular uptake and therapeutic potential. Lastly, the nanoGUMBOS

were employed in Hs578Bst normal cells to examine if these GUMBOS also displayed the selective chemotherapeutic behavior observed with the R6G nanoGUMBOS. These studies provide further insight to an approach for rapid synthesis of selective nanomaterials from cationic drugs in order to minimize their systemic toxicity.

4.2. MATERIALS AND METHODS

4.2.1. Materials

Rhodamine 123, phosphate buffered saline (10x concentrate, 0.2 uM filtered), sodium tetraphenylborate [Na][TPB], dicholromethane (DCM), dimethylsulfoxide (DMSO), and 1-octanol were purchased from Sigma-Aldrich (Milwaukee, WI). Lithium bis (perfluoroethylsulfonyl) imide [Li][BETI] was obtained from Ionic Liquid Technologies (Tuscaloosa, Al). SNAFR-5 was obtained from Dr. Robert Strongin (Portland, OR). Triply deionized water was obtained from an Aires High Purity Water System (Port Allen, LA). The cell viability MTT (3-[4, 5-Dimethylthiazol-2-yl]-2, 5-diphenyltetrazolium bromide) assay was purchased from Promega Corporation (Madison, WI). TEM (copper) grids were purchased from Ted Pella (Redding, CA).

4.2.2. Synthesis of Rhodamine-based GUMBOS

The rhodamine-based GUMBOS were synthesized using a biphasic ion-exchange reaction. Briefly, a DCM solution of [R123][Cl] was mixed with aqueous [Li][BETI] or [Na][TPB] at a 1:1.2 molar ratio. This biphasic mixture was allowed to stir for 48 h at room temperature. Subsequently, the water layer was removed, and the DCM layer was washed with deionized water to remove any traces amount of [Li][Cl] or [Na][Cl]. The DCM layer was then evaporated and the product was dried *in vacuo* for 24 h to obtain the final product. The synthesized GUMBOS were

characterized using electrospray ionization (ESI) mass spectrometry. A similar protocol was employed for synthesis of the SNAFR-5 based GUMBOS as well.

4.2.3. Synthesis of Rhodamine-based nanoGUMBOS

The rhodamine-based nanoGUMBOS were synthesized using a reprecipitation method. Briefly, the GUMBOS were dissolved in a small amount of DMSO and a small amount of this solution was rapidly injected in cell media under ultrasonication for five minutes to make a 1 mM solution of nanoGUMBOS. Subsequently the nanoparticles were allowed to grow for 30 minutes. The obtained nanoparticles were further diluted to the working concentration for characterization and cell studies.

4.2.4. Characterization of the nanoGUMBOS

The nanoGUMBOS were characterized using TEM, DLS and zeta potential measurements. For the TEM, the 5 µL of a 100 µM solution was spotted on a TEM grid and allowed to dry overnight. For DLS and Zeta potential measurements, the 1 mM solution of nanoGUMBOS was centrifuged, and then dried *in-vacuo*. The resulting pellet was then resuspended in phosphate buffered saline to make a 12 µM solution of nanoGUMBOS.

4.2.5. Octanol-Water Partition Coefficients

A 1:1 volume ratio of octanol and water was stirred overnight. The water and octanol layer were then separated. The octanol layer was then used to generate a calibration curve from the absorbance of the compound at various concentrations. A known concentration (C_i) was chosen from the calibration curve and an equivalent volume of water was then added to the octanol layer and this mixture was stirred for 24 h. The absorbance of the octanol layer was determined. The calibration curve generated in octanol was then used to calculate the compound in octanol (C_o).

The concentration of dye in the water (C_w) was then calculated using the formula $C_i - C_o = C_w$. The octanol water partition coefficient (K_{ow}) was then calculated using the formula $K_{ow} = C_f/C_w$

4.2.6. Cell Culture

Hormone independent human breast adenocarinoma (MDA-MB-231) and normal human breast fibroblast (Hs578Bst) were all purchased from the American Tissue Culture Collection (ATCC, Manassas, VA). Cell lines were cultured to 90% confluence according to ATCC protocol prior to experimentation.

4.2.7. Cytotoxicity Measurements

A 96 well plate was incubated with 5000 cells/well for 24 h. Subsequently, a 1 mM solution of the nanoGUMBOS was synthesized and diluted to 100 µM. The cells were then treated with 0–100 µM of the nanoGUMBOS and incubated for another 48 h. Each compound was tested in triplicates to obtain a standard deviation. Following the 48 h incubation, an MTT assay was performed to determine cytotoxicity. First, 15 µL of the MTT dye was incubated into the cells for 3 h. Then, the cells were treated with 100 µL of the stop solution and incubated for another 1 h. The absorbance of the 96 well plate was measured at 570 nm using a microplate spectrophotometer. The cell viability is reported as a percentage of the ratio of experimental cells to an untreated control normalized to 100% cell viability. All plates were performed in triplets to obtain a standard deviation, and reported cell viabilities represent the average of these measurements.

4.2.8. Cellular Uptake Studies

For the cellular uptake studies 35 mM petri dishes were seeded with 20,000 cells per petri dish for 24 h. Following the 24 h. incubation, the cells were then treated with a 50 µM solution of nanoGUMBOS and incubated for 1 h. to allow the nanoGUMBOS to internalize. One petri dish

was only treated with cell media and served as a control. After 1 h, the cell media was removed and any nanoGUMBOS not internalized by the cell were washed away using PBS buffer. Subsequently, 3 mL of DMSO was incubated for 5 h. to lyse the cells open. The absorbance of the DMSO solution was then measured using the untreated control cells as the reference cell. Calibration curves for each of the nanoGUMBOS was made by taking the absorbance of at 1, 2, 4, 6, and 10 µM in DMSO. The calibration curve was then used to calculate the concentration nanoGUMBOS in the DMSO used to treat the cells, this concentration was recorded as internalized concentration. The cellular uptake of the compound was calculated in nanomoles of compound internalized. All measurements were carried out in triplicate to obtain standard error.

4.3. RESULTS AND DISCUSSIONS

4.3.1. Characterization of GUMBOS and nanoGUMBOS

Four GUMBOS ([R123][BETI], [R123][TPB], [SNAFR][BETI], and [SNAFR][TPB]) were synthesized using a simple metathesis reaction depicted in Figure 4.1. GUMBOS were characterized using electrospray mass spectrometry to confirm the presence of the desired counter-ion (Table 4.1). Following synthesis of the GUMBOS, hydrophobicity was examined using octanol water partition coefficients (K_{ow}). The GUMBOS showed varied hydrophobicity based on cation variation. Table 4.2 presents the log K_{ow} for the parent dyes as well as the GUMBOS. Examination of the log K_{ow} for the parent dyes indicates that, for a constant cation and varying anions, the hydrophobicity trend beginning with the most hydrophobic compound is [R123][BETI] > [R123][TPB] > [R123][Cl]. A similar trend was observed with the SNAFR based GUMBOS as well. Furthermore, for both of the GUMBOS, the BETI anion remained the most hydrophobic. These results suggest that counter-ion variation of the R123 salts led to varying hydrophobicity of the resulting GUMBOS.
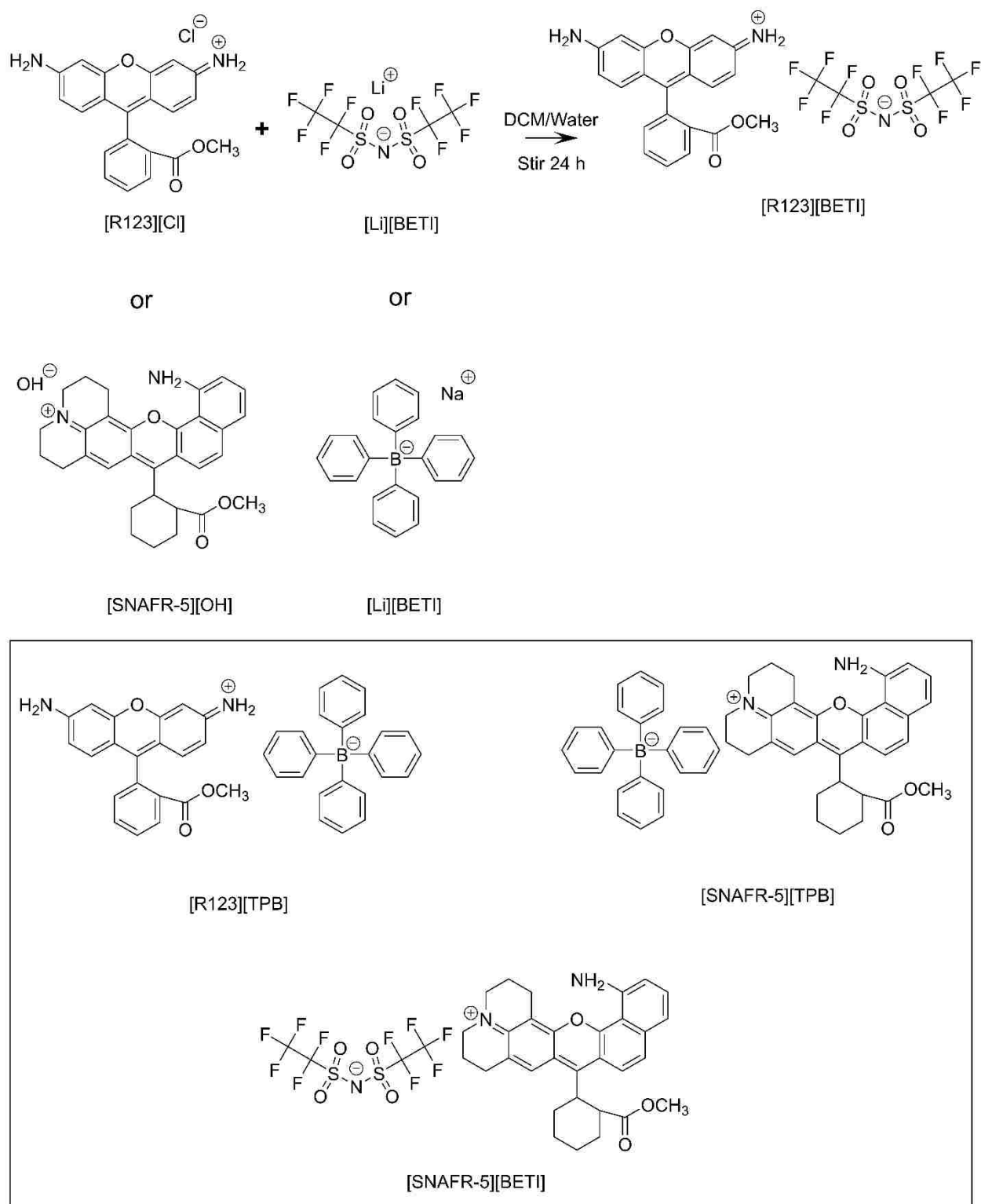
Figure 4.1. Synthesis of R123 and SNAFR-5 GUMBOS

Table 4.1. Results from ESI mass spectrometry characterization of GUMBOS

Compound	Positive Mode		Negative Mode	
	Theoretical Mass	Actual Mass	Theoretical Mass	Actual Mass
[R123][BETI]	345.4	345.6	381.1	381.4
[R123][TPB]	345.4	345.5	319.3	319.2
[SNAFR-5][BETI]	458.3	458.2	381.1	381.2
[SNAFR-5][TPB]	458.3	458.2	319.3	319.1

Table 4.2. Relative hydrophobicity of R123 and SNAFR-5 based GUMBOS

Compound	Log K_{ow}
[R123][BETI]	1.10 ± 0.22
[R123][TPB]	0.80 ± 0.28
[R123][Cl]	0.25 ± 0.05
[SNAFR-5][BETI]	1.40 ± 0.25
[SNAFR-5][TPB]	1.20 ± 0.16
[SNAFR-5][OH]	0.28 ± 0.04

Following examination of the hydrophobicity of the GUMBOS, nanoGUMBOS were synthesized using a simple reprecipitaiton method described in the experimental section. TEM images in Figure 4.2 display spherical nanoparticles with a size around 100 nm for both R123 and SNAFR based nanoGUMBOS. Table 4.3 presents the zeta potential of the R123 and SNAFR GUMBOS at physiological pH (7.4). As shown in table 4.3, zeta potentials for the R123 and SNAFR nanoGUMBOS are around –17 mV which suggests formation of relatively stable nanomaterials. Nanoparticles displayed a polydispersity below 0.2 when subjected to dynamic light scattering (DLS), indicating formation of relatively monodispersed nanoparticles.

Table 4.3. Zeta potential of R123 and SNAFR-5 nanoGUMBOS

NanoGUMBOS	Zeta Potential (mV)
[R123][BETI]	-16.8 ± 1.1
[R123][TPB]	-16.5 ± 1.4
[SNAFR-5][BETI]	-17.4 ± 0.8
[SNAFR-5][TPB]	-16.9 ± 1.3
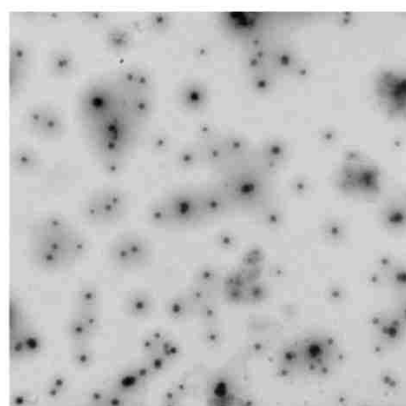
— 500 nm

[R123][BETI]
92 ± 17 nm
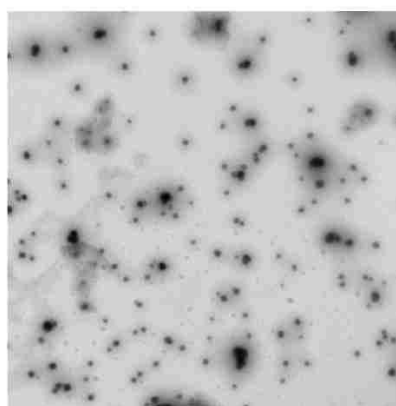
— 500 nm

[R123][TPB]
95 ± 21 nm

— 500 nm

[SNAFR-5][BETI]
96 ± 14 nm
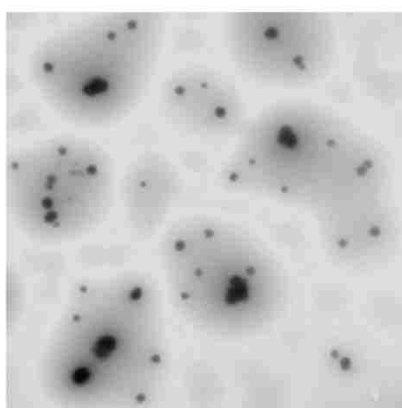
— 500 nm

[SNAFR-5][TPB]
105 ± 19 nm

Figure 4.2. TEM images of R123 and SNAFR-5 nanoGUMBOS

4.3.2. Spectroscopic Studies

Following synthesis and characterization of GUMBOS and nanoGUMBOS, spectroscopic studies were performed to examine the optical behavior of the new materials. As indicated in Figure 4.3, no shift in absorbance and fluorescence e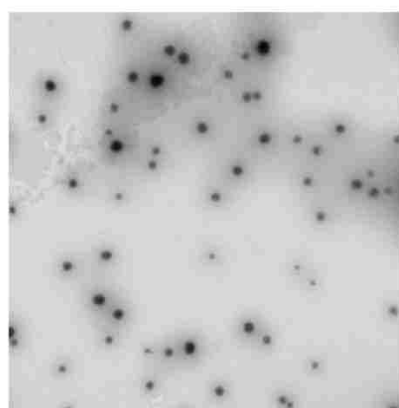mission peak maxima were observed for between the R123 GUMBOS and the parent dye [R123][Cl]. Formation of R123 nanoGUMBOS in water led to a slight 10 nm blue shift; however, no peak shift was observed between the nanoGUMBOS and the parent dye in water (Figure 4.4). Examination of the absorbance and fluorescence emission of the SNAFR-5 based GUMBOS presented in Figure 4.5 indicates no peak shift following formation of the GUMBOS, similar to the R123 based GUMBOS described earlier. Interestingly, a significant peak shift was observed between [SNAFR][TPB] nanoGUMBOS and the parent dye, while no peak shift was observed for the [SNAFR][BETI] nanoGUMBOS. In this regard, the absorbance of [SNAFR][BETI] nanoGUMBOS and [SNAFR][OH] parent dye displayed blue shifting in water as compared to their absorbance in DMSO. In contrast, the absorbance of [SNAFR][TPB] nanoGUMBOS was further red shifted in water in comparison to its absorbance in DMSO. Examination of the fluorescence emission presented in Figure 4.6 suggests a significantly diminished fluorescence intensity for [SNAFR][TPB] in comparison to [SNAFR][BETI] and [SNAFR][OH]. This could possibly be due to J-aggregation of [R6G][TPB] nanoGUMBOS as indicated by the red-shifted absorbance.[24] In addition, the longer wavelength of the [SNAFR][TPB] nanoGUMBOS in contrast to typical rhodamines suggests that these nanoparticles have suitable properties to act as a photosensitizer dye for photodynamic therapy applications.[25]
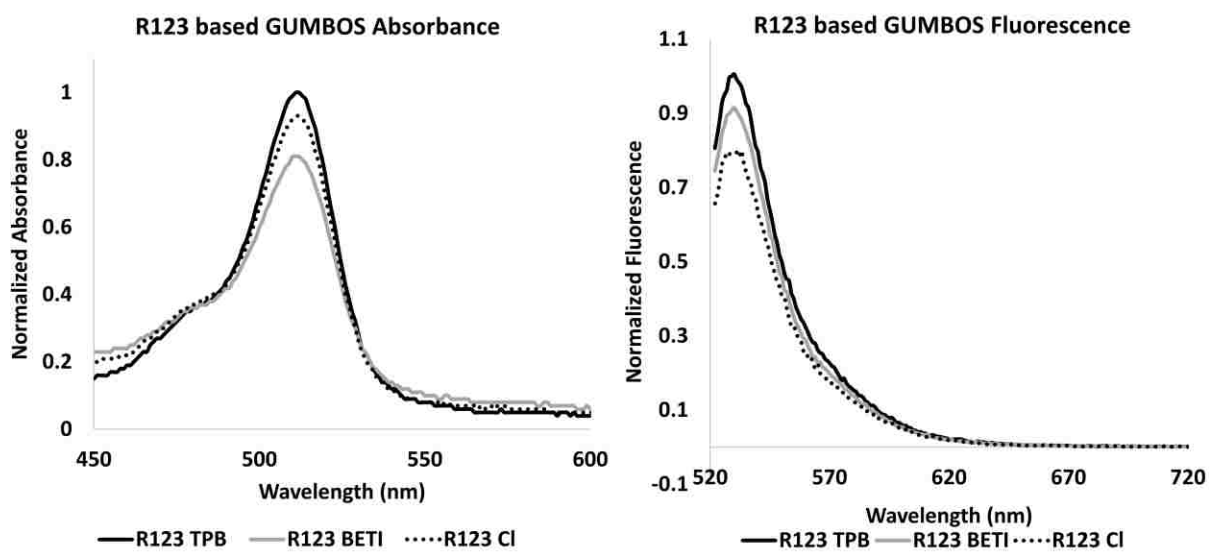
Figure 4.3. Absorbance and fluorescence of R123 based GUMBOS in DMSO
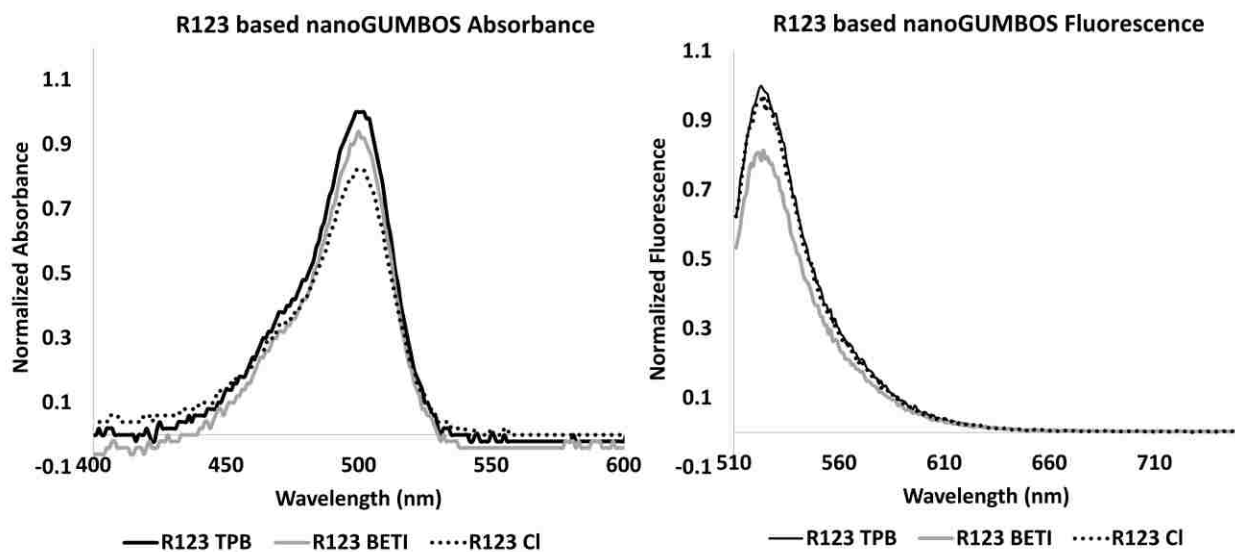
Figure 4.4. Absorbance and fluorescence of R123 based nanoGUMBOS in water
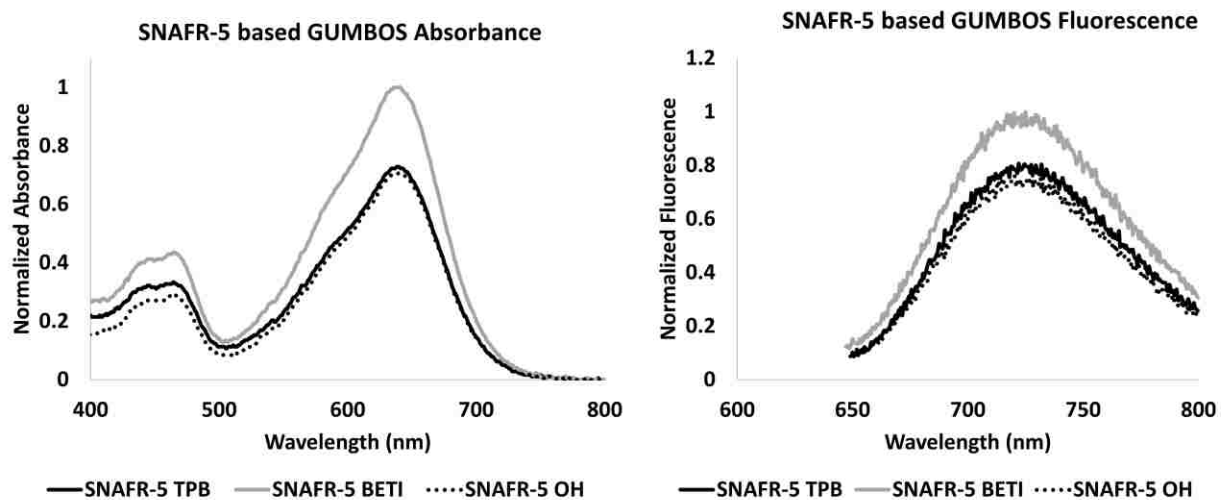
Figure 4.5. Absorbance and fluorescence of SNAFR-5 based GUMBOS in DMSO
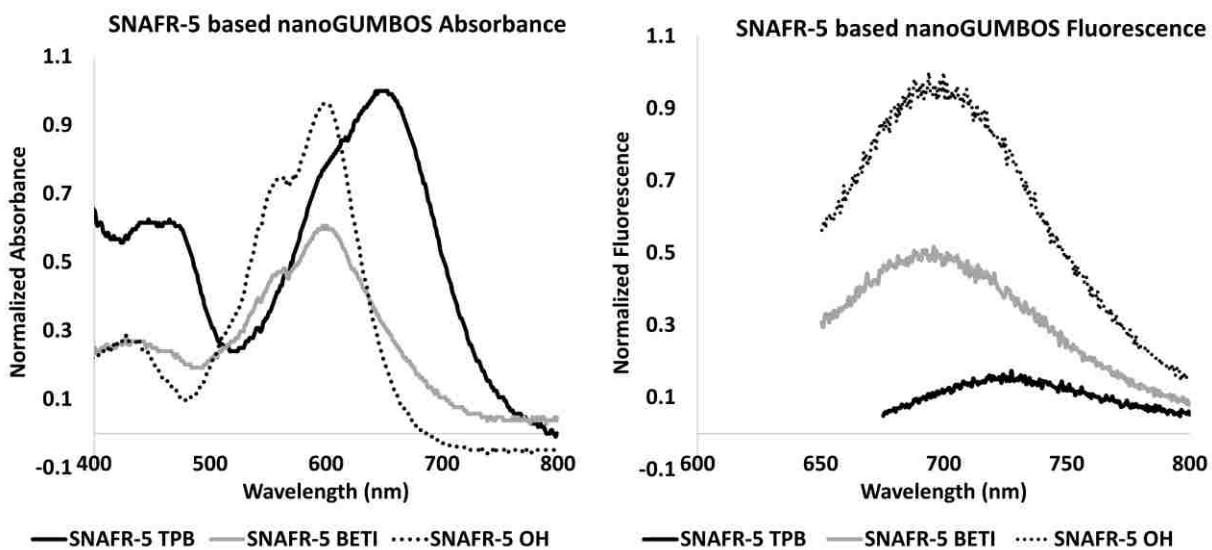
Figure 4.6. Absorbance and fluorescence of SNAFR-5 based nanoGUMBOS in PBS buffer

4.3.3. Examination of Toxicity

These compounds were then employed in MDA-MB-231 breast cancer cells to examine their chemotherapeutic properties. Figures 4.7 and 4.8 are graphical representation of the toxicity of the R123 and SNAFR-5 based nanoGUMBOS towards MDA-MB-231 breast cancer cells

94

respectively. R123 nanoGUMBOS display similar toxicity to that of the parent dye [R123][Cl] as shown in Figure 4.7. [R123][TPB] and [R123][BETI] displayed IC_{50} concentrations of 17.41 and 20.62 µM, which are relatively similar to the IC_{50} concentration of [R123][Cl], 24.32 µM. While the IC_{50} values for the R123 nanoGUMBOS are slightly lower than that of parent dye, statistical analysis indicate no significant difference between the concentrations. [SNAFR-5][BETI] and [SNAFR-5][TPB] displayed IC_{50} concentrations of 8.75 µM and 12.22 µM respectively, while the parent dye [SNAFR-5][OH] displayed an IC_{50} concentration of 1.31 µM. These results indicate that formation of SNAFR based nanoGUMBOS led to decreased toxicity in comparison with the parent dye.
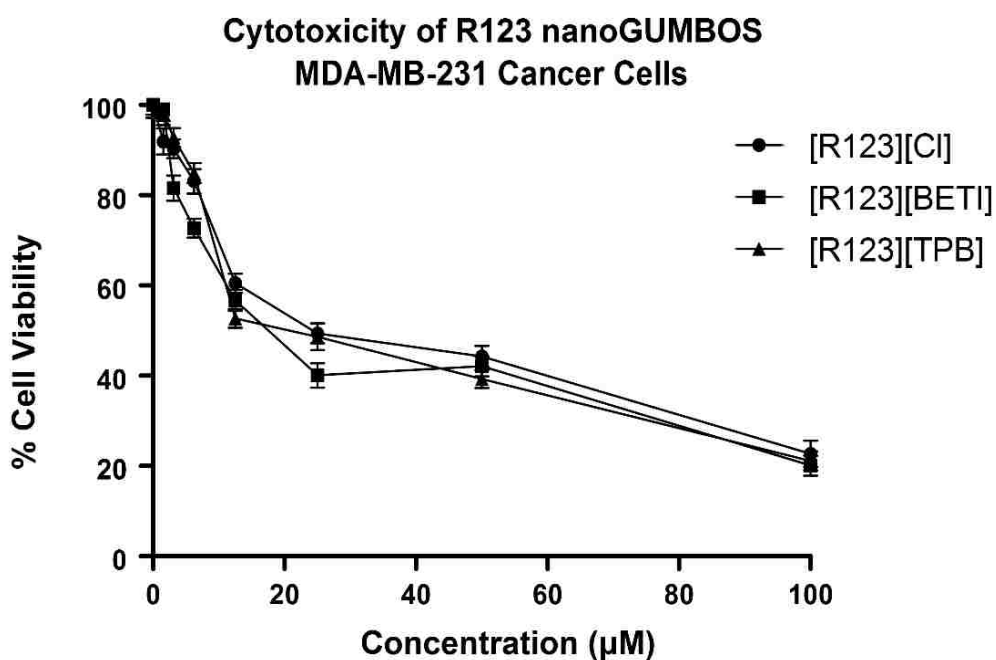
Figure 4.7. Toxicity of R123 nanoGUMBOS towards MDA-MB-231 cancer cells
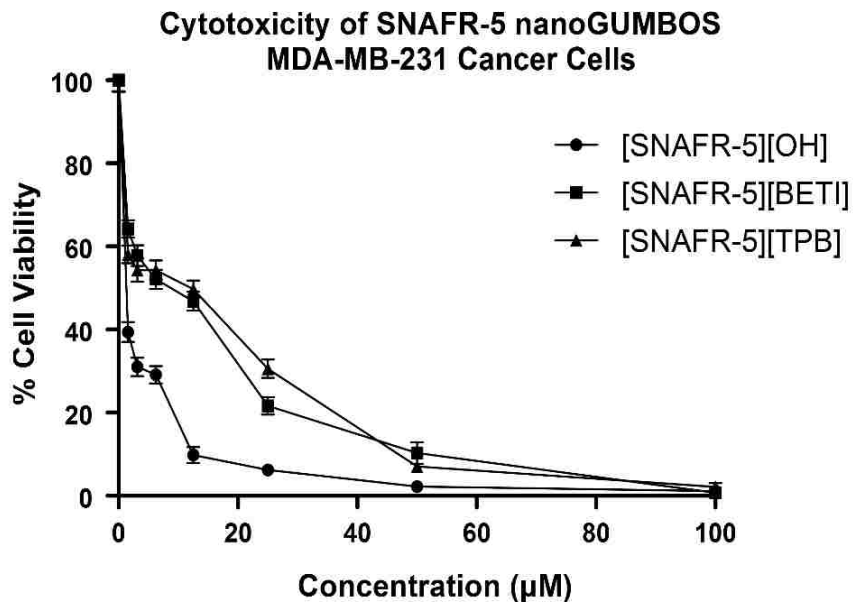
Figure 4.8. Toxicity of SNAFR-5 nanoGUMBOS towards MDA-MB-231 cancer cells

Figure 4.9 presents the cellular uptake of the R123 and SNAFR nanoGUMBOS in MDA-MB-231 breast cancer cells after 5 h. incubation. The R123-based nanoGUMBOS displayed cellular uptake comparable to that of the parent dye [R123][Cl]. This is consistent with the toxicity results that showed similar IC50 concentrations between the R123 nanoGUMBOS and the parent dye. In contrast, SNAFR-5 based nanoGUMBOS displayed a significantly lower than that of the parent dye. This further corroborates the decreased toxicity for the nanoGUMBOS in comparison with the parent dyes.
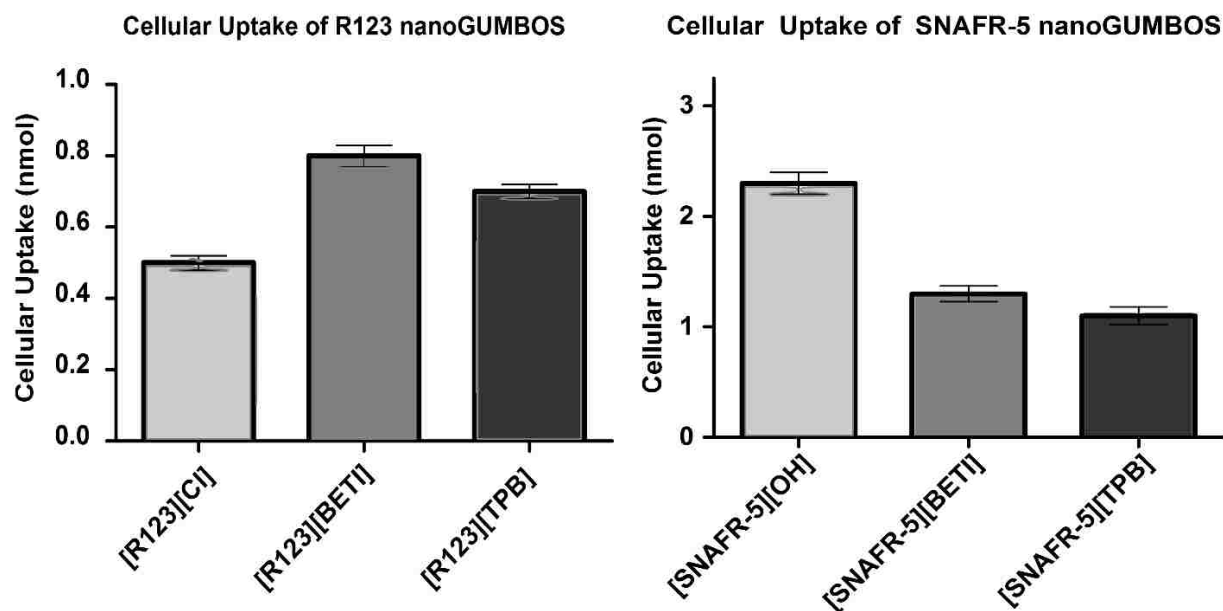
Figure 4.9. Cellular Uptake of R123 and SNAFR-5 nanoGUMBOS

Toxicity of the GUMBOS towards MCF7 breast cancer and MiaPaca pancreatic cancer cells was also evaluated. Table 4.4 compares the IC_{50} of R123 and SNAFR-5 based nanoGUMBOS towards MDA-MB-231, MCF7 and Mia-Paca cancer cell lines. While the R123 compounds displayed IC_{50} concentrations of 17-25 µM and 1-3 µM for the MDA-MB-231 and MiaPaca cell lines respectively, they displayed an IC_{50} above 100 µM for the MCF7 cancer cells. These examinations indicated that that the toxicity of the nanoGUMBOS is greater towards the more aggressive MDA-MB-231 and Mia Paca cancer cells in contrast to the less aggressive MCF7 cancer cell line. Similar results were seen for the SNAFR-5 based nanoGUMBOS as well. However, in contrast to the R123 compounds, the overall toxicity of the SNAFR-5 was found to be greater. It is interesting to note that the SNAFR-5 based nanoGUMBOS displayed less than 1 µM IC_{50} concentrations towards MiaPaca cancer cells, suggesting their great therapeutic potential.

Table 4.4. IC$_{50}$ values for R123 and SNAFR-5 based nanoGUMBOS towards MDA-MB-231, MiaPaca and MCF7 cancer cell lines

	MDA-MB-231 IC$_{50}$ (μM)	MiaPaca IC$_{50}$ (μM)	MCF7 IC$_{50}$ (μM)
[R123][BETI]	17.41 ± 3.73	1.61 ± 0.72	>100
[R123][TPB]	20.62 ± 3.51	2.52 ± 0.94	>100
[R123][Cl]	24.32 ± 2.24	3.15 ± 1.12	>100
[SNAFR-5][BETI]	8.75 ± 1.86	0.66 ± 0.03	32.50 ± 1.12
[SNAFR-5][TPB]	12.22 ± 2.90	0.72 ± 0.02	26.75 ± 2.26
[SNAFR-5]	1.31 ± 0.52	0.13 ± 0.02	3.71 ± 0.71

Following application in cancer cell lines, these nanoGUMBOS were also employed in Hs578Bst normal breast cells. Figures 4.10 and 4.11 display the toxicity of the R123 and SNAFR-5 based nanoGUMBOS, respectively towards Hs578Bst normal breast cells. Intriguingly, while both of the parent dyes [R123][Cl] and [SNAFR-5][OH] displayed slight toxicity towards normal cells, formation of the nanoGUMBOS led to completely selective behavior under investigated conditions. Furthermore, both the parent dyes displayed a higher IC$_{50}$ for normal cells as compared to cancer cells. This partially selective behavior is consistent with findings from Belostotsky et al. that lipophilic rhodamine cations have enhanced cellular uptake in cancer cells as compared to normal cells due to their electrostatic interaction with the negative cell membrane.[8] Furthermore, the selective behavior of the nanoGUMBOS most likely resulted from use of energy dependent pathways in contrast to diffusion. While both SNAFR and R123 are relatively soluble in water and can use diffusion to internalize, the nanoGUMBOS most likely use active transport for internalization; thus, this variation in internalization pathway, similar to that observed in Chapter 2 of this dissertation, is a possible explanation for the selective chemotherapeutic behavior of the SNAFR and R123 nanoGUMBOS.
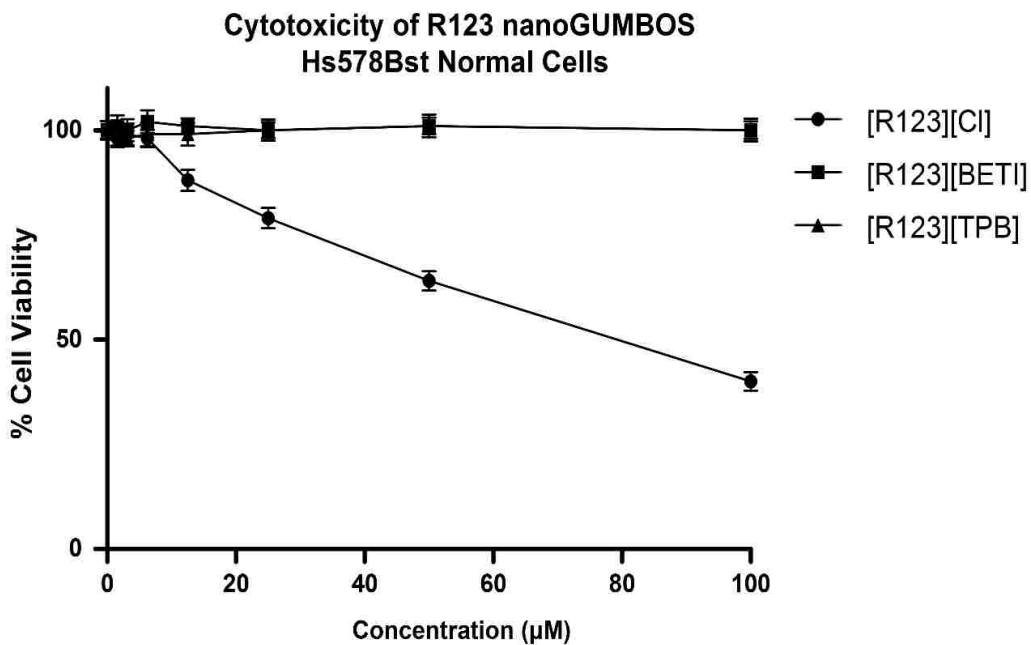
Figure 4.10. Toxicity of R123 nanoGUMBOS towards Hs578Bst normal cells
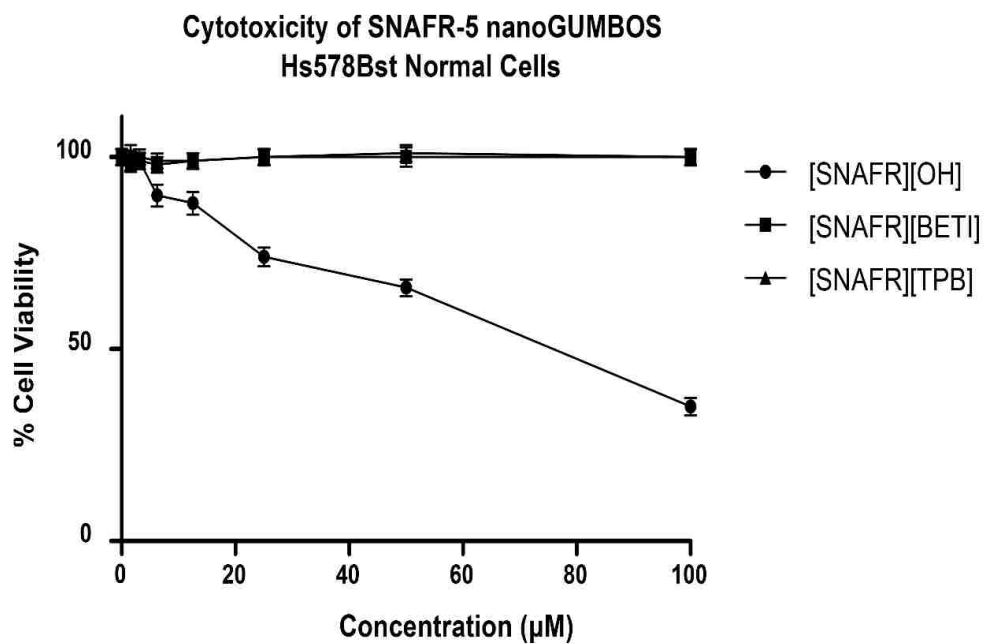
Figure 4.11. Toxicity of SNAFR-5 nanoGUMBOS towards Hs578Bst normal cells

4.4. CONCLUSIONS

These results present an approach to develop tunable nanomaterials that display selective toxicity towards cancer cells with minimal effect to normal cells. Synthesis of GUMBOS led to enhanced hydrophobicity in comparison to the respective parent dyes. This increased hydrophobicity led to nanoparticle formation in aqueous medium. These nanoGUMBOS demonstrated promising *in vitro* toxicity towards both breast and pancreatic cancer cells. Remarkably, no toxicity towards normal cells under experimental conditions were observed. This selective behavior is of great interest to reduce the numerous side-effects of current chemotherapeutics. Interestingly, evaluation of the nanoGUMBOS toxicity towards multiple cell lines suggested greater efficacy towards the more aggressive cell lines. Evaluation of the optical properties of these nanoGUMBOS indicates that in addition to employment as chemotherapeutics, the synthesized nanoGUMBOS also display strong cellular imaging potential. Moreover, these results give further insight to rapid development of selective chemotherapeutic nanomaterials for chemotherapy and tumor imaging applications.

4.5. REFERENCES

1.   He, H.; Li, D.-W.; Yang, L.-Y.; Fu, L.; Zhu, X.-J.; Wong, W.-K.; Jiang, F.-L.; Liu, Y., A novel bifunctional mitochondria-targeted anticancer agent with high selectivity for cancer cells. *Scientific reports* **2015,** *5*.

2.   Modica-Napolitano, J. S.; Aprille, J. R., Delocalized lipophilic cations selectively target the mitochondria of carcinoma cells. *Advanced drug delivery reviews* **2001,** *49* (1), 63-70.

3.   Ross, M.; Kelso, G.; Blaikie, F.; James, A.; Cocheme, H.; Filipovska, A.; Da Ros, T.; Hurd, T.; Smith, R.; Murphy, M., Lipophilic triphenylphosphonium cations as tools in mitochondrial bioenergetics and free radical biology. *Biochemistry (Moscow)* **2005,** *70* (2), 222-230.

4.   Bonnet, S.; Archer, S. L.; Allalunis-Turner, J.; Haromy, A.; Beaulieu, C.; Thompson, R.; Lee, C. T.; Lopaschuk, G. D.; Puttagunta, L.; Bonnet, S., A mitochondria-K+ channel axis is suppressed in cancer and its normalization promotes apoptosis and inhibits cancer growth. *Cancer cell* **2007,** *11* (1), 37-51.

5.   Trapp, S.; Horobin, R. W., A predictive model for the selective accumulation of chemicals in tumor cells. *European Biophysics Journal* **2005,** *34* (7), 959-966.

6.   Murphy, M. P., Selective targeting of bioactive compounds to mitochondria. *Trends in biotechnology* **1997,** *15* (8), 326-330.

7.   McKeage, M. J.; Berners-Price, S. J.; Galettis, P.; Bowen, R. J.; Brouwer, W.; Ding, L.; Zhuang, L.; Baguley, B. C., Role of lipophilicity in determining cellular uptake and antitumour activity of gold phosphine complexes. *Cancer chemotherapy and pharmacology* **2000,** *46* (5), 343-350.

8.   Belostotsky, I.; Da Silva, S.; Paez, M.; Indig, G., Mitochondrial targeting for photochemotherapy. Can selective tumor cell killing be predicted based on n-octanol/water distribution coefficients? *Biotechnic & Histochemistry* **2011,** *86* (5), 302-314.

9.   Modica-Napolitano, J. S.; Aprille, J. R., Basis for the selective cytotoxicity of rhodamine 123. *Cancer research* **1987,** *47* (16), 4361-4365.

10.   Summerhayes, I. C.; Lampidis, T. J.; Bernal, S. D.; Nadakavukaren, J. J.; Nadakavukaren, K. K.; Shepherd, E. L.; Chen, L. B., Unusual retention of rhodamine 123 by mitochondria in muscle and carcinoma cells. *Proceedings of the National Academy of Sciences* **1982,** *79* (17), 5292-5296.

11.   Lampidis, T. J.; Castello, C.; Del Giglio, A.; Pressman, B. C.; Viallet, P.; Trevorrow, K. W.; Valet, G. K.; Tapiero, H.; Savaraj, N., Relevance of the chemical charge of rhodamine dyes to multiple drug resistance. *Biochemical pharmacology* **1989,** *38* (23), 4267-4271.

12.   Bernal, S.; Lampidis, T. J.; Summerhayes, I. a.; Chen, L., Rhodamine-123 selectively reduces clonal growth of carcinoma cells in vitro. *Science* **1982,** *218* (4577), 1117-1119.

13.   Lampidis, T. J.; Bernal, S. D.; Summerhayes, I. C.; Chen, L. B., Selective toxicity of rhodamine 123 in carcinoma cells in vitro. *Cancer research* **1983,** *43* (2), 716-720.

14.   Nadakavukaren, K. K.; Nadakavukaren, J. J.; Chen, L. B., Increased rhodamine 123 uptake by carcinoma cells. *Cancer research* **1985,** *45* (12 Part 1), 6093-6099.

15.   Goffney, W. H.; Wong, J. H.; Kern, D. H.; Chase, D.; Krag, D. N.; Storm, F. K., In–Vitro and in–Vivo Cytotoxicity of Rhodamine 123 Combined with Hyperthermia. *Cancer Research* **1990,** *50* (3), 459-463.

16.   You, J.; Hau, D.; Lin, I.; Huang, H.; Chen, K.; Chiou, Y., Subcutaneous tumors of mice treated with rhodamine-123 and laser irradiation. *Changgeng yi xue za zhi* **1999,** *22* (3), 362-369.

17.   Jones, L.; Narayan, K.; Shapiro, C. a.; Sweatman, T., Rhodamine-123: therapy for hormone refractory prostate cancer, a phase I clinical trial. *Journal of chemotherapy* **2005,** *17* (4), 435-440.

18.   Mattheolabakis, G.; Rigas, B.; Constantinides, P. P., Nanodelivery strategies in cancer chemotherapy: biological rationale and pharmaceutical perspectives. *Nanomedicine* **2012,** *7* (10), 1577-1590.

19.   Chidambaram, M.; Manavalan, R.; Kathiresan, K., Nanotherapeutics to overcome conventional cancer chemotherapy limitations. *Journal of pharmacy & pharmaceutical sciences* **2011,** *14* (1), 67-77.

20.   Greish, K., Enhanced permeability and retention (EPR) effect for anticancer nanomedicine drug targeting. *Cancer Nanotechnology: Methods and Protocols* **2010**, 25-37.

21.   Sahay, G.; Alakhova, D. Y.; Kabanov, A. V., Endocytosis of nanomedicines. *Journal of controlled release* **2010,** *145* (3), 182-195.

22.   Magut, P. K.; Das, S.; Fernand, V. E.; Losso, J.; McDonough, K.; Naylor, B. M.; Aggarwal, S.; Warner, I. M., Tunable cytotoxicity of rhodamine 6G via anion variations. *Journal of the American Chemical Society* **2013,** *135* (42), 15873-15879.

23.   Warner, I. M.; El-Zahab, B.; Siraj, N., Perspectives on moving ionic liquid chemistry into the solid phase. *Analytical chemistry* **2014,** *86* (15), 7184-7191.

24.   Deng, Y.; Yuan, W.; Jia, Z.; Liu, G., H- and J-Aggregation of Fluorene-Based Chromophores. *The Journal of Physical Chemistry B* **2014,** *118* (49), 14536-14545.

25.   Fabian, J.; Nakazumi, H.; Matsuoka, M., Near-infrared absorbing dyes. *Chemical Reviews* **1992,** *92* (6), 1197-1226.

CHAPTER 5
CHEMOTHERAPEUTIC APPLICATIONS OF CARBOXYLIC ACID BEARING RHODAMINE BASED GUMBOS AND NANOGUMBOS

5.1 INTRODUCTION

In addition to the R123 dye discussed in Chapter 4, rhodamine 110 (R110) and rhodamine B (RB) have also been investigated for chemotherapeutic and in-vitro imaging applications.[1-3] Several studies have compared the in-vitro imaging of the zwitterion R110 and the cation R123 in order to understand the relevance of structure and charge on cellular uptake. Interestingly, while R110 suffers from poor cellular uptake, R123 exhibits promising *in vitro* chemotherapeutic imaging properties.[4-5] In this regard, the cationic charge of R123 enables a strong electrostatic interaction with the negative cell membrane, while the zwitterion structures of RB and R110 hinder this interaction. This hindered interaction between these zwitterion dyes with the cell membrane ultimately leads to reduced internalization, limiting their biomedical applications.[5]

Further studies have demonstrated cellular internalization of R110 and RB in their protonated acid form; however, the acid-base properties of the carboxylic acid functional group limit their therapeutic and imaging potential. As discussed in Chapter 1, rhodamine dyes preferentially accumulate in the mitochondria and block ATP production, causing cellular apoptosis. However, the carboxylic acid functional group of RB and R110 causes a reduction in mitochondrial pH, leading to minimal mitochondrial accumulation and decreased therapeutic potential.[2, 6] Thus, while cationic dyes such as R123 serve as strong imaging agents for the mitochondria, the zwitterion structure of RB and R110 deters their imaging applications.

Nanocarrier systems such as liposomes, polymers and micelles have been investigated as intracellular delivery systems to enhance the internalization of hydrophobic drugs.[7-10] This increased cellular uptake is typically due to the nanoscale size of the nanoparticle that allows for

rapid permeation into the cell.[11-12] Additionally, several studies have also demonstrated that endocytic internalization of nanoparticles can be exploited for selective toxicity towards cancer cells with minimal toxicity towards normal cells.[13-15] Our research group has developed nanoGUMBOS, i.e. nanomaterials derived from a *group* of *uniform materials based on organic salts* (GUMBOS), that displayed selective chemotherapeutic properites.[16] As discussed in Chapter 1, synthesis of nanoGUMBOS from rhodamine 6G, a lipophilic cation with known anticancer properties, led to selective chemotherapeutic toxicity of the resulting nanomaterials under examined conditions.[17] In contrast to the existing nanocarrier systems that typically consist of liposomes and polymers, nanoGUMBOS give distinct advantages such as ease of synthesis, as well as tunable toxicity. Intriguingly, nanoGUMBOS serve as the drug themselves eliminating the need for detailed characterization of drug loading and release profiles.[18-20] However, since the nanoGUMBOS is developed from the dye itself, the zwitterion structure of the RB and R110 may affect the surface charge of the nanomaterials, ultimately affecting their therapeutic properties.[21]

In this regard, the tunable nature of GUMBOS allows for modification of several properties through counter-ion variation.[16, 22] Typical GUMBOS consist of cation and anion moieties, but the zwitterion structure of RB and R110 dyes allows for addition of a secondary cation at physiological pH resulting in a triple GUMBOS structure. This allows for a simple synthetic route to modify the overall charge of the resulting compounds. Furthermore, if the secondary cation chosen has anticancer properties then the developed nanodrug possesses dual therapeutic properties. Moreover, this allows for innovative combinations of multiple anticancer compounds into a novel nanoparticle.

Herein, we report the *in vitro* therapeutic properties of the GUMBOS derived from RB and R110. GUMBOS were synthesized through counter-ion variation using the tetraphenylborate

(TPB) and lithium bis(perfluoroethylsulfonyl)imide (BETI) anions investigated in the previous chapters. Addition of a secondary cation to the zwitterion structure of these dyes was also explored to synthesize a triple nanoGUMBOS. The effect of counter-ion variation on the hydrophobicity was examined using octanol-water partition coefficients. Subsequently, toxicity and cellular uptake of the nanoGUMBOS was examined in MDA-MB-231 cancer cells to assess their therapeutic potential. Lastly, toxicity of the nanoGUMBOS was examined in Hs578Bst normal breast cells to study the effect of counter-ion variation and modification of the carboxylic acid structure on the selective behavior of the nanoGUMBOS. Furthermore, these results give further insight to a method to improve the cytotoxic behavior and imaging properties of zwitterion dyes.

5.2. MATERIALS AND METHODS

5.2.1. Materials

Rhodamine B chloride, rhodamine 110 chloride, phosphate buffered saline (10x concentrate, 0.2 µM filtered), sodium tetraphenylborate [Na][TPB], dichloromethane (DCM), dimethylsulfoxide (DMSO), 1-octanol, sodium hydroxide (NaOH), citric acid monohydrate, and sodium phosphate dibasic were purchased from Sigma-Aldrich (Milwaukee, WI). Lithium bis(perfluoroethylsulfonyl)imide ([Li][BETI]) was obtained from Ionic Liquid Technologies (Tuscaloosa, Al). Triply deionized water was obtained from an Aires High Purity Water System (Port Allen, LA). The MTT (3-[4, 5-Dimethylthiazol-2-yl]-2, 5-diphenyltetrazolium bromide) cell viability assay was purchased from Promega Corporation (Madison, WI). TEM grids were purchased from Ted Pella (Redding, CA).

5.2.2. Synthesis of GUMBOS

All GUMBOS were synthesized via a one phase reaction scheme. Briefly, the rhodamine dye and the desired counter ion, either [Li][BETI] or [Na][TPB], were dissolved in a pH 3 citric

acid phosphate buffer, and the solution was stirred for 15 minutes. Subsequently, the pink precipitate was centrifuged multiple times while washing the in between with citric acid phosphate buffer to remove any byproduct. The product was then dried *in vacuo*.

5.2.3. Synthesis of Triple GUMBOS

Triple GUMBOS were synthesized via a biphasic metathesis reaction modified from literature.[23] Firstly, [R110][Cl] or [RB][Cl] was dissolved in water with an equimolar concentration of sodium hydroxide (NaOH). Subsequently, this aqueous solution was mixed with a DCM solution containing either [R6G][Cl] or [P4444][Br], and this biphasic mixture was allowed to stir for 24 h. Completion of the ion exchange was indicated by a transfer of the rhodamine pink color from the aqueous layer to the DCM organic layer. The clear aqueous layer was then removed and an aqueous solution containing [Na][TPB] was then added to the organic layer, and this biphasic mixture was stirred for 48 h. The aqueous layer was separated from DCM layer and washed with water several times to remove any byproduct. The DCM was then evaporated and the product was dried *in vacuo* to obtain a pink powder.

5.2.4. Synthesis of nanoGUMBOS

NanoGUMBOS were synthesized using a reprecipitation method. A DMSO solution containing GUMBOS was rapidly injected into cell media under ultrasonication at a 2% volume ratio between DMSO and cell media. NanoGUMBOS were allowed to grow for 30 minutes, and then the solution was diluted to 100 µM for TEM characterization and cell studies.

5.2.5. Octanol Buffer Partition Coefficients

In 20 ml vial, 1-Octanol is mixed with a pH 7.4 phosphate-citric acid buffer and stirred overnight. The two layers were separated and then a calibration curve is generated for each compound in 1-octanol at various concentrations. The phosphate-citric acid buffer is then added to

one of the concentrations (C_i) and this mixture is stirred for 48 h. Subsequently, the absorbance in the octanol layer was measured and the concentration (C_o) was calculated using the calibration curves. Later, the equation ($C_i - C_o = C_w$) was used to calculate the concentration in water (C_w). The octanol water partition coefficient was then calculated using the equation $K_{ow} = C_f/C_w$.

5.2.6. Solubility Studies

Approximately fifty milliliters of water was added to three milligrams of GUMBOS. Absorbance measurements were then taken over time until the absorbance reached a plateau. A calibration curve in water was then generated for the GUMBOS at a soluble concentration, and the generated equation was used to calculate the solubility concentration. The solubility constant (K_{sp}) is then calculated from the solubility concentration.

5.2.7. Spectroscopic Studies

Spectroscopic studies for all GUMBOS were preformed using a 5 µM solution of GUMBOS in either DMSO or PBS Buffer. A reprecipitaiton method was used to synthesize the triple nanoGUMBOS for these studies. Briefly, a 1 mM solution of the triple GUMBOS in DMSO was reprecipitated under ultrasonication in phosphate buffered saline (2% DMSO/buffer ratio) for five minutes and aged for another 30 minutes to synthesize a 5 µM of nanoGUMBOS. All nanoGUMBOS were sonicated for 1 minute before analysis to ensure a homogenous mixture.

5.2.8. Cell Culture

Hormone independent breast adenocarcinoma (MDA-MB-231), hormone dependent breast adenocarcinoma (MCF7), human pancreatic carcinoma (Mia-Paca), and normal human fibroblast cell lines were purchased from the American Tissue Culture Collection (ATCC, Manassas, VA). Cell lines were cultured to 90% confluence using the ATTC guidelines for cell culture prior to experimentation.

5.2.9. Cell Viability Studies

A 96 well plate was seeded with 5000 cells/well and incubated for 24 h to allow them to attach. A serial dilution from 100 µM to 0 µM was performed for each compound. The compounds were then incubated into the cells for 48 h and subsequently an MTT assay was performed to determine the cell viability. Firstly, 15 µL of the MTT dye solution wa incubated in the cells for 3 h. This MTT dye reacts with NADPH present in live cells to form an insoluble purple formazan product. Subsequently, 100 µL of the stop solution was added to solubilize this product, ending the enzymatic reaction between the NADPH and the MTT dye. The cells were incubated with the stop solution for 1 h. Subsequently, the absorbance of the formazan is then measured at 570 nm using a microplate spectrophotometer. Cell viability is reported as the percentage of the ratio between experimental groups and a control normalized to 100%. All measurements were performed in triplicate measurements to obtain standard error, and the reported cell viability is the average of these measurements.

5.2.10. Cellular Uptake

For the cellular uptake studies, 200,000 cells were seeded in a 35 mm petri dish and the cells were incubated at 37 °C overnight. The cells were then incubated with a 12.5 µM solution of nanoGUMBOS for 5 h. An untreated control containing no drug was used as a reference. Subsequently, the nanoGUMBOS solution was removed and the cells were incubated with 3 mL of DMSO for 5 h. until no cells were visually present under the microscope. The absorbance of the DMSO solution was then measured using the untreated control as a reference. A calibration curve was generated from a set of standards for each GUMBOS ranging from 1-10 µM. The cellular uptake was then calculated as the nmoles of compound internalized.

5.2.11. Microscopy

Briefly, 10,000 MDA-MB-231 cancer cells were seeded onto a 35 mm glass bottom petri dish and incubated overnight at 37 °C. Then, 20 nM of mitotracker was incubated into the cells for 30 minutes. Subsequently, a 25 nM nanoGUMBOS solution was incubated in the cells for 30 minutes. Finally, the cells were washed several times with buffer and were imaged using a 40X dipping objective on a Leica Brightfield Microscope. A FITC filter was used to measure the fluorescence of the mitotracker green and the TRITC filter was used to measure fluorescence of the nanoGUMBOS.

5.3. RESULTS AND DISCUSSIONS

5.3.1 Synthesis and characterization GUMBOS

RB and R110 based GUMBOS were synthesized using a one phase reaction scheme depicted in Figure 5.1. Characterization of the GUMBOS using electrospray mass spectrometry confirmed the presence of the desired counter-ion, indicating successful ion exchange has occurred (Table 5.1). Hydrophobicity of all the synthesized GUMBOS were characterized using octanol-water partition coefficients (K_{ow}), and data is presented in Table 5.2 The hydrophobicity trend for the RB GUMBOS from most hydrophobic to most hydrophillic is [RB][TPB] > [RB][BETI] > [RB][Cl]. Interestingly, a similar hydrophobicity trend is seen for R110 based GUMBOS as well. These results demonstrate that these GUMBOS display tunable hydrophobicity through counter-ion variation, similar to the results presented in Magut et al. and Chapter 4 of this dissertation.[17]

As discussed in previous chapters, GUMBOS are typically insoluble in water and enable the formation of a nanoGUMBOS suspension in aqueous medium. However, contrastingly from the R123 and SNAFR-5 GUMBOS investigated in Chapter 4, no distinct nanoparticles were observed for the RB and R110 GUMBOS. Thus, in order to further understand the lack of

nanoparticle formation, the water solubility of RB and R110 GUMBOS was examined at physiological pH. As shown in Table 5.3, the water solubility of GUMBOS is significantly lower than that of the parent dyes. This is consistent with the increase in hydrophobicity observed for the GUMBOS with respect to the parent dyes. However, RB and R110 GUMBOS displayed a significantly higher water solubility than that of the [R6G][BETI] and [R6G][TPB] GUMBOS which were found to make nanoGUMBOS in Magut et al.[17] Rather, the water solubility for these zwitterion GUMBOS is relatively similar to the reported more hydrophilic GUMBOS.[17] In this regard, Magut et al. reported that nanoparticles were fabricated only from the more hydrophobic [R6G][BETI] and [R6G][TPB] GUMBOS. Thus, lack of nanoparticle formation can be attributed to the relatively high water solubility of GUMBOS.
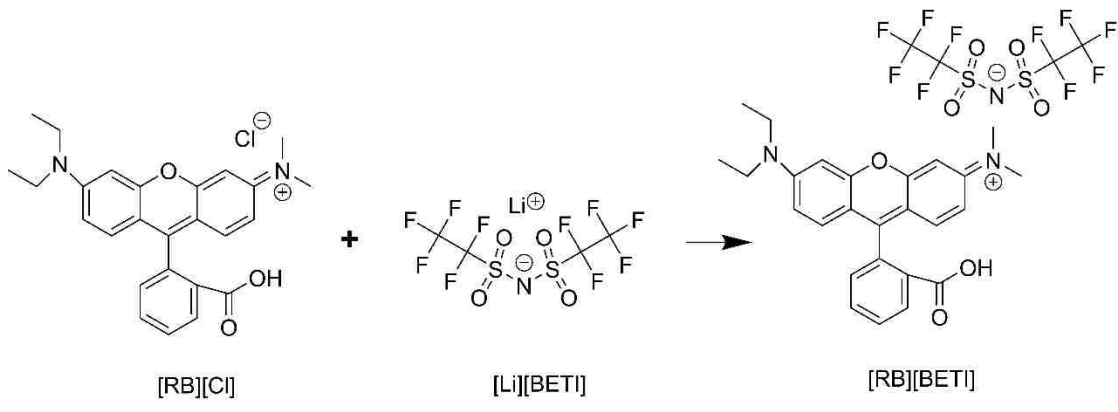
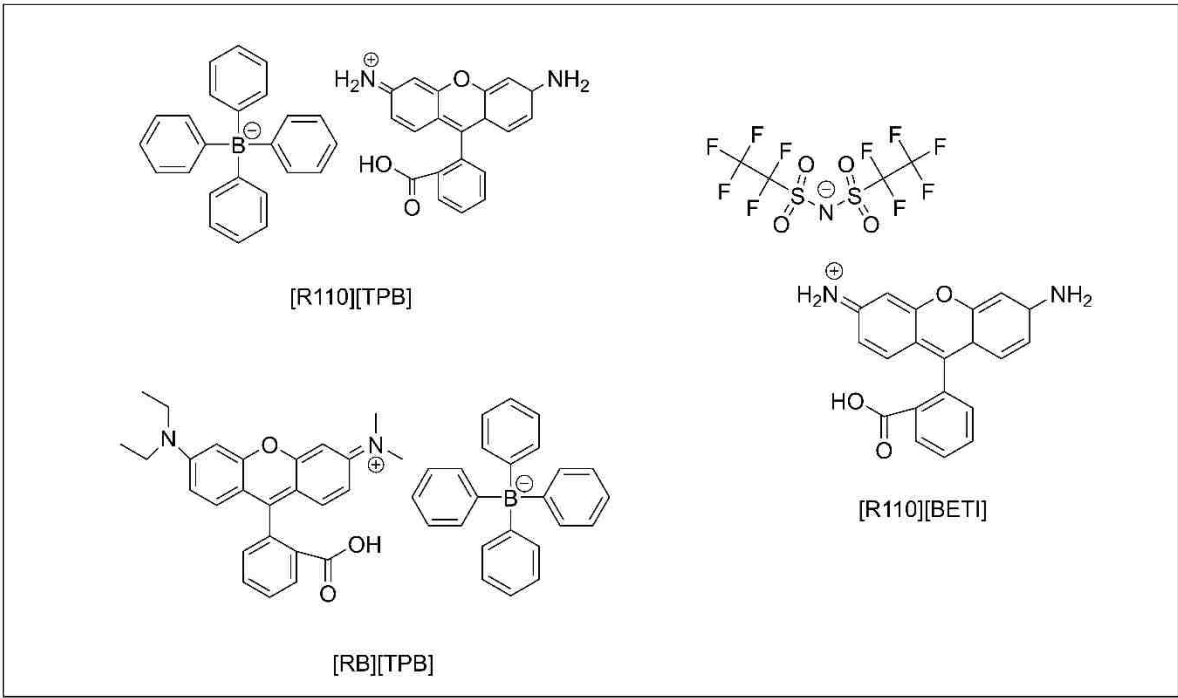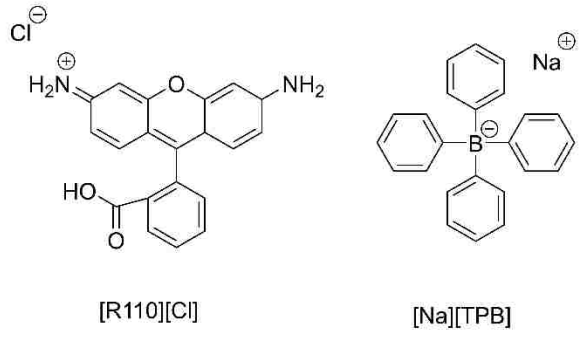Figure 5.1. Synthesis of RB and R110 GUMBOS

Table 5.1. ESI characterization of RB and R110 GUMBOS

Compound	Positive Mode		Negative Mode	
	Theoretical Mass (m/z)	Actual Mass (m/z)	Theoretical Mass (m/z)	Actual Mass (m/z)
[RB][TPB]	444.2	444.4	319.3	319.5
[RB][BETI]	444.2	44.43	381.1	381.3
[R110][TPB]	331.8	331.9	319.3	319.4
[R110][BETI]	331.8	331.7	381.1	381.4

Table 5.2. Relative hydrophobicity of RB and R110 GUMBOS

Compound	Log K_{ow}
[RB][BETI]	1.40 ± 0.14
[RB][TPB]	1.25 ± 0.21
[RB][Cl]	1.10 ± 0.18
[R110][BETI]	0.30 ± 0.04
[R110][TPB]	0.32 ± 0.03
[R110][Cl]	0.22 ± 0.04

Table 5.3. Water solubility of RB and R110 GUMBOS

Compound	Solubility (mol/L)	Dissociation Constant (mol^2/L^2)
[RB][BETI]	1.7×10^{-5}	1.7×10^{-10}
[RB][TPB]	1.3×10^{-5}	2.9×10^{-10}
[RB][Cl]	3.1×10^{-2}	9.8×10^{-4}
[R110][BETI]	4.1×10^{-5}	7.8×10^{-10}
[R110][TPB]	2.8×10^{-5}	1.7×10^{-10}
[R110][Cl]	$> 7.0 \times 10^{-4}$	$> 4.6 \times 10^{-7}$

5.3.2. Spectroscopic Studies of RB and R110 based GUMBOS

Absorbance and fluorescence behavior of the GUMBOS was then investigated to assess any variation in photophysical properties. Absorbance and fluorescence spectra of GUMBOS in DMSO displayed no apparent shift in absorbance or fluorescence emission maxima as compared to the parent dyes (Figures 5.2 and 5.3). RB GUMBOS displayed a peak absorbance at 540 nm and peak emission at 570 nm in DMSO, which corresponds to the peaks for [RB][Cl]. Similarly, R110 GUMBOS displayed a peak absorbance at 510 nm and peak emission at 538 nm, corresponding to the peaks for [R110][Cl]. The fluorescence emission intensity of [RB][TPB] and [RB][BETI] both are comparable to the parent dye [RB][Cl]. However, a decrease in fluorescence intensity was observed for R110 based GUMBOS with respect to the parent dye. These results suggest that in addition to the hydrophobicity and solubility, optical properties of the GUMBOS can also be tuned via counter-ion variation.

After examination of GUMBOS in DMSO, the optical behavior of nanoGUMBOS in PBS buffer was also investigated to mimic the biological environment. As shown in Figures 5.4 and 5.5, a 5 nm blue shift was observed for the R110 compounds in water, whereas a 10 nm red shift was observed for the RB compounds. Absorbance peak maxima for all the GUMBOS in water were consistent with respective parent dyes suggesting that the shift is due to solvent polarity. Furthermore, both RB and R110 GUMBOS displayed substantial fluorescence emission, indicating their possible use as probes for fluorescence guided surgery in addition to their chemotherapeutic application. In this regard, these dyes can aid in tumor imaging while also eradicating any unresected tumor tissue.
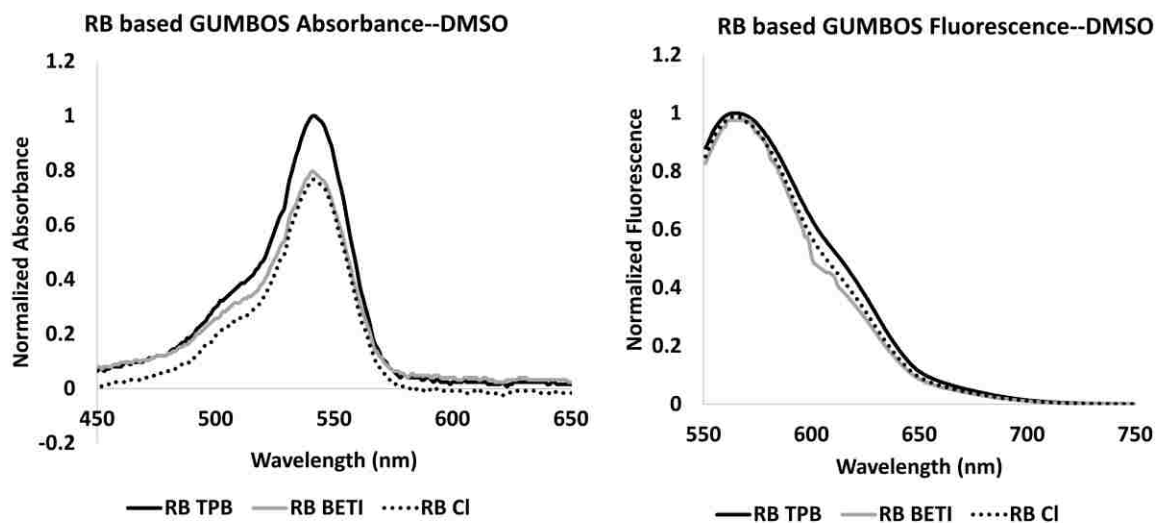
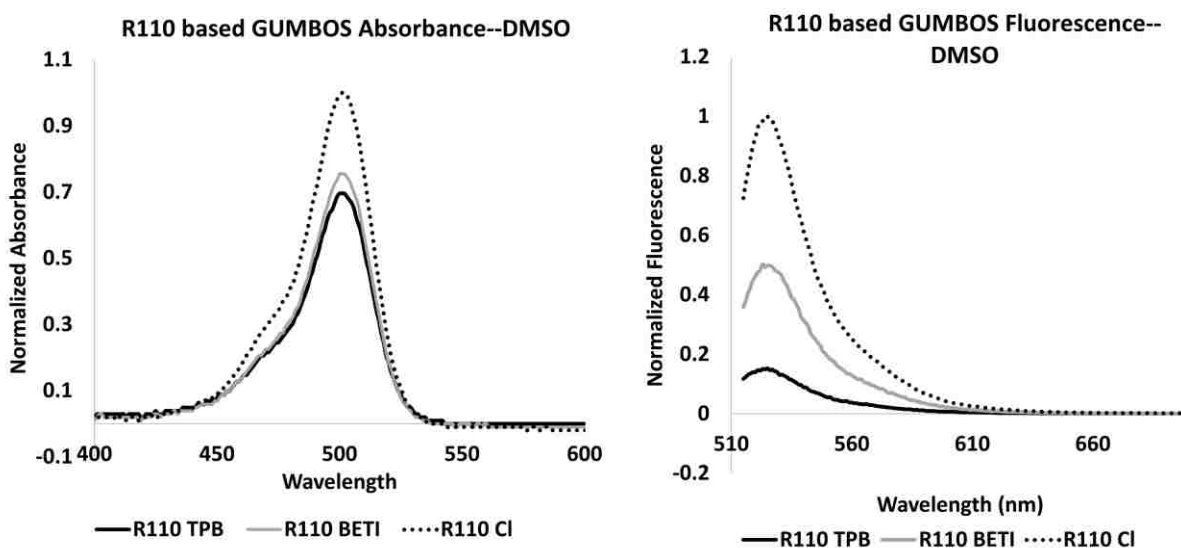Figure 5.2. Absorbance and Fluorescence of RB GUMBOS in DMSO

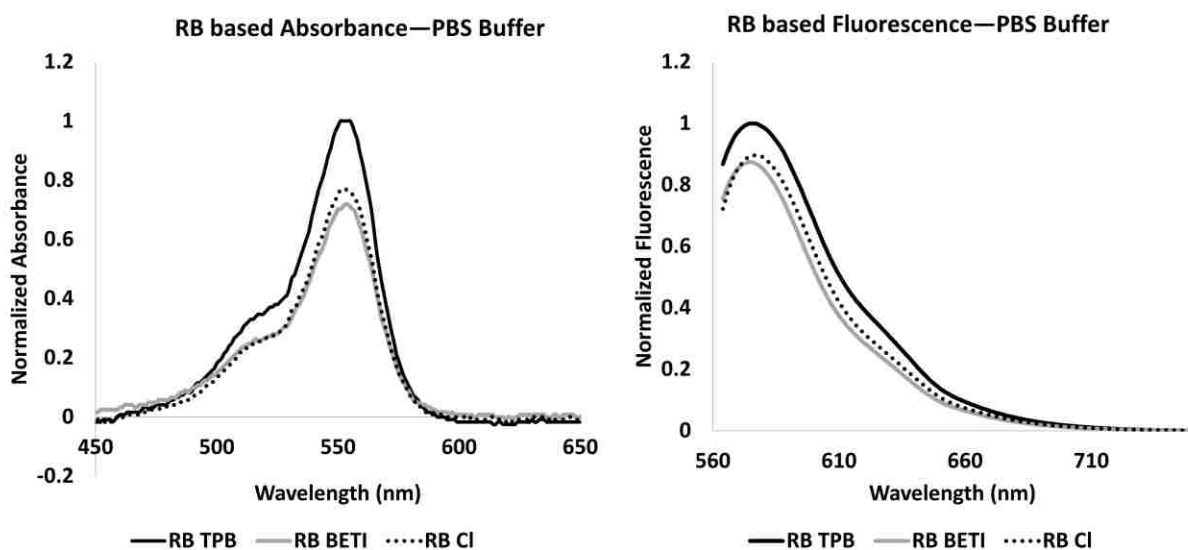Figure 5.3. Absorbance and Fluorescence of R110 GUMBOS in DMSO

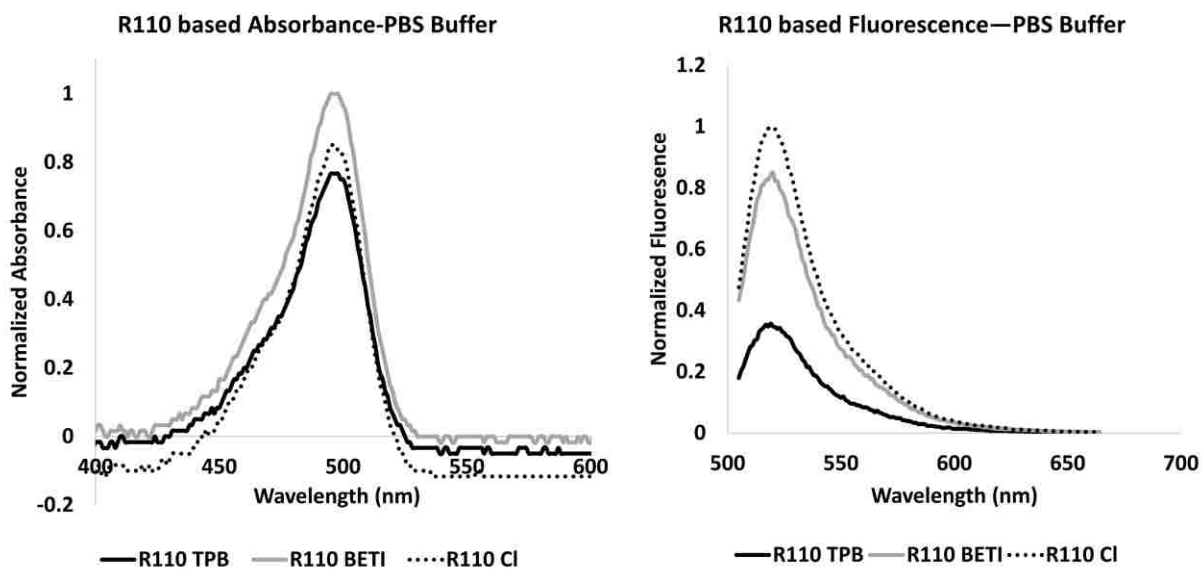Figure 5.4. Absorbance and Fluorescence of RB GUMBOS in PBS Buffer

Figure 5.5. Absorbance and Fluorescence of R110 GUMBOS in PBS Buffer

5.3.3. Examination of the Cytotoxicity

After detailed characterization, these compounds were then employed *in vitro* to evaluate their chemotherapeutic properties. Figures 5.6 and 5.7 are graphical representations of toxicity studies of RB and R110 based GUMBOS, respectively towards MDA-MB-231 cancer cells.

Intriguingly, a significant enhancement in toxicity for the GUMBOS was observed as compared to the parent dye. As shown in the graphs, the respective parent dyes remained relatively non-toxic until about 200 µM but GUMBOS displayed higher toxicity even at low concentrations. In this regard, the IC_{50} values for the parent dyes [RB][Cl] and [R110][Cl] were 291.07 and 791.29 µM respectively, while RB and R110 based GUMBOS displayed a reduced IC_{50} of 80–90 and 100–200 µM respectively. In order to further understand these variations in IC_{50}, cellular uptake of these compounds were then examined. As depicted in Figure 5.8, RB and R110 GUMBOS displayed enhanced cellular uptake as compared to the respective parent dye. This improved cellular uptake is most likely due to improved hydrophobic interactions of the dye with the phospholipid bilayer of the cell membrane. These results are consistent with the results from Belostotsky et al., which demonstrated that variation in hydrophobicity can tune the interaction of the drug with the cell membrane.[6] Furthermore, the nontoxic behavior of [RB][Cl] and [R110][Cl] at lower concentrations is most likely due to minimal cellular uptake.
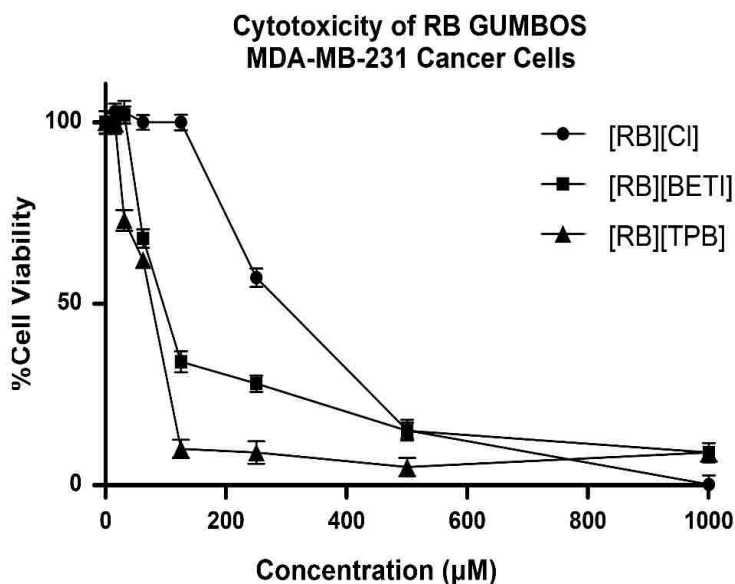

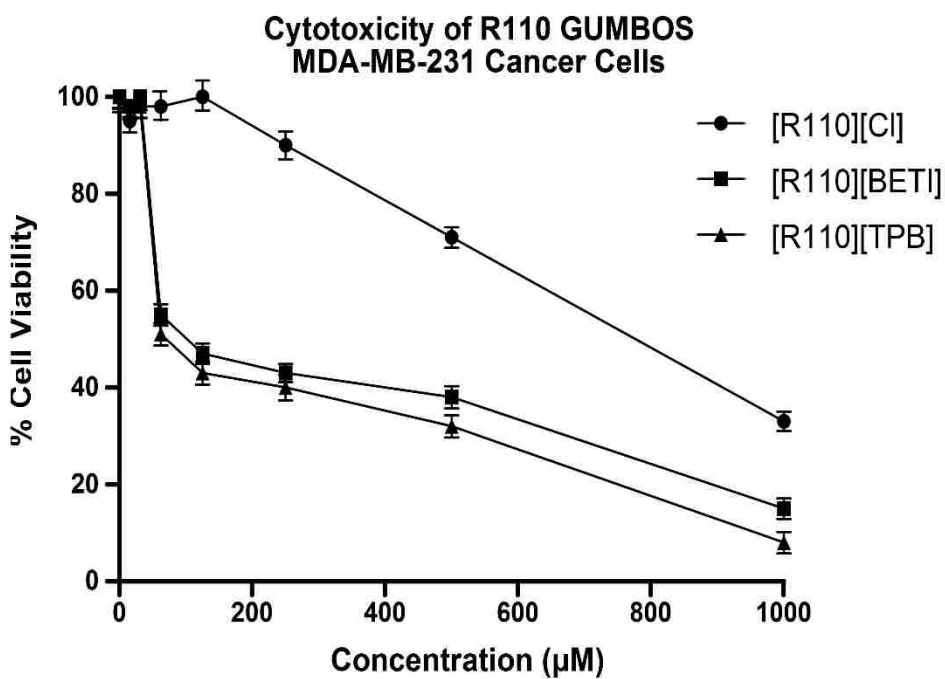Figure 5.6. Toxicity of RB GUMBOS towards MDA-MB-231 cancer cells

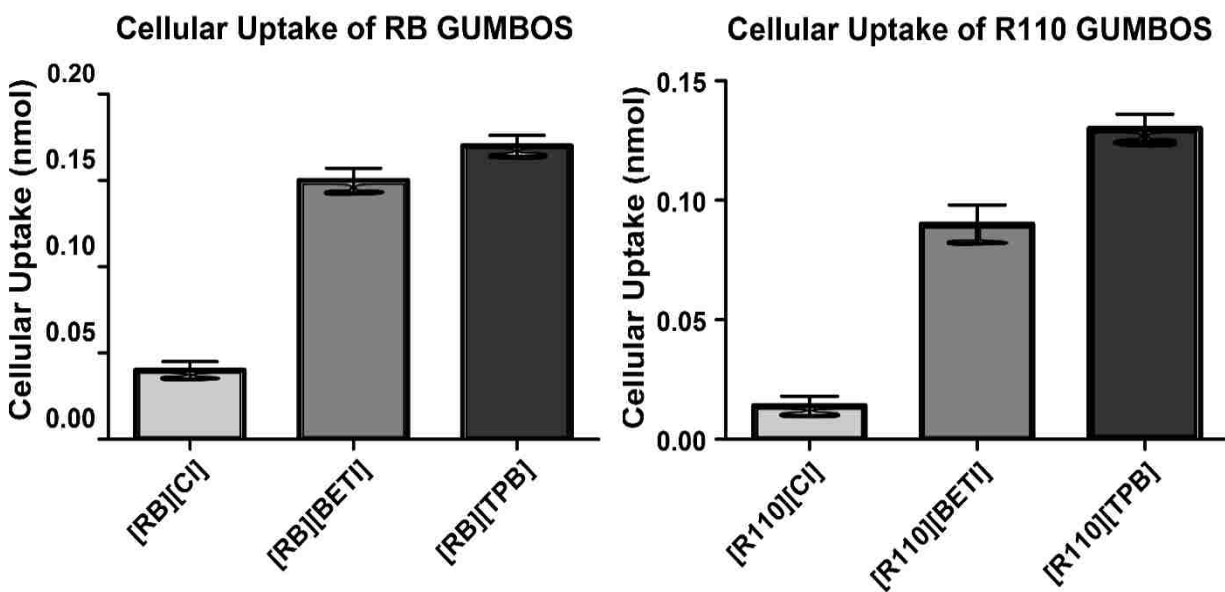Figure 5.7. Toxicity of R110 GUMBOS towards MDA-MB-231 cancer cells

Figure 5.8. Cellular uptake of RB and R110 GUMBOS

Since the GUMBOS displayed enhanced therapeutic toxicity towards cancer cells, their toxicity towards Hs578Bst normal breast cells was also evaluated to further understand their therapeutic potential. As shown in figure 5.9, R110 and RB GUMBOS displayed slightly toxic behavior towards normal cells (Figure 5.9). Interestingly, the GUMBOS displayed a significantly higher IC_{50} towards cancer cells as compared to normal cells, suggesting partially selective behavior (Table 5.4). This contradicts the behavior of nanoGUMBOS derived from ester derivatives reported in Chapter 4 of this dissertation, which displayed completely selective behavior. In this regard, while the ester derivative GUMBOS formed nanoGUMBOS in aqueous medium, the RB and R110 GUMBOS are water soluble and do not form nanoGUMBOS. As indicated earlier, the water solubility of RB and R110 GUMBOS were similar to that of the more hydrophilic GUMBOS reported in Magut et al.[17] Intriguingly, these hydrophilic GUMBOS displayed toxicity towards normal cells, suggesting that the selective behavior observed for the nanoGUMBOS derived from the ester rhodamine derivatives is most likely due to nanoparticle formation.[17] This is consistent with the results discussed in Chapter 2 of this dissertation, that the selectivity of R6G nanoGUMBOS investigated in Magut et al. was dependent upon nanoparticle formation.
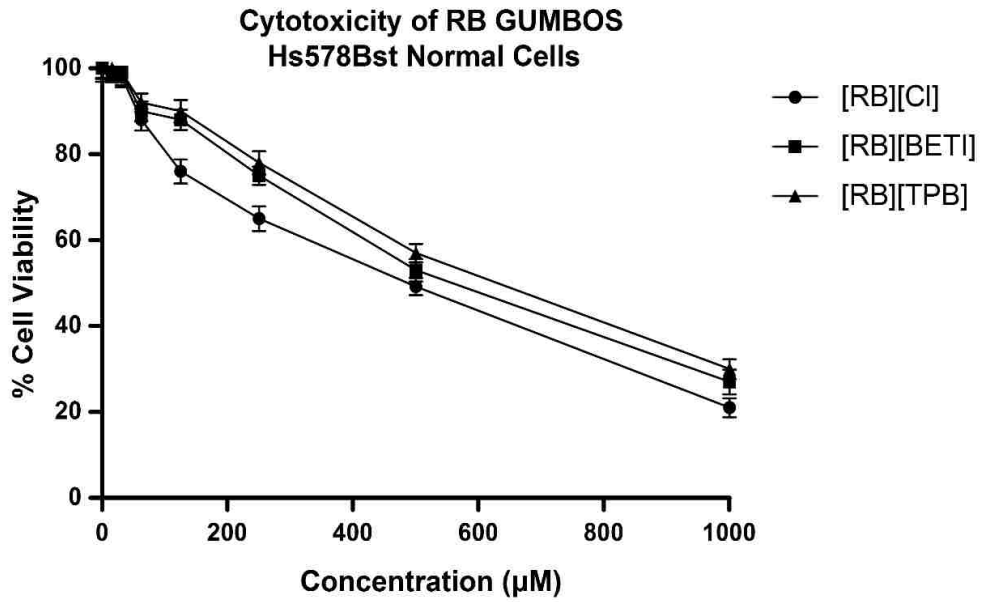
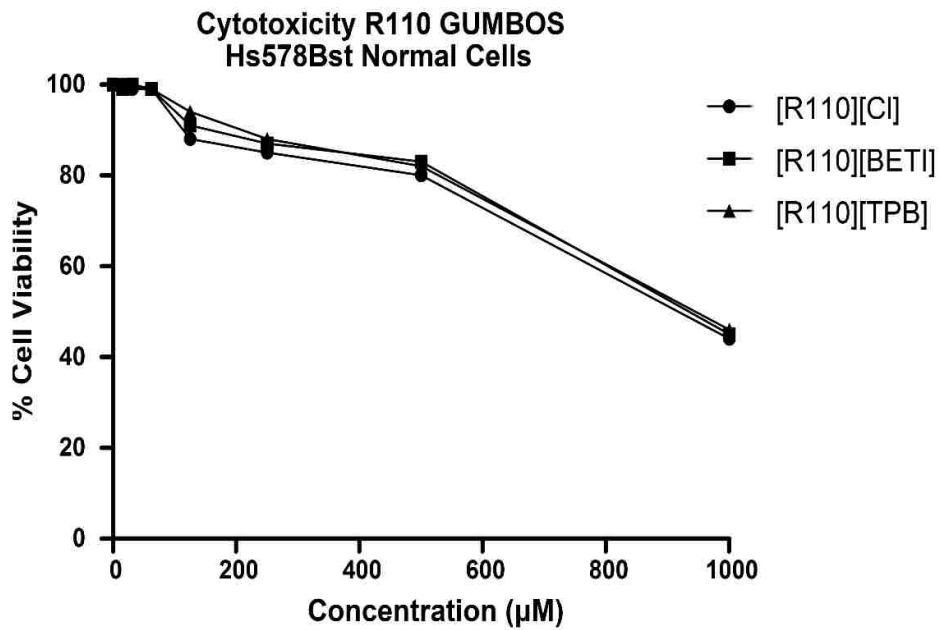Figure 5.9. Toxicity of RB GUMBOS toward Hs578Bst normal breast cells

Figure 5.10. Toxicity of R110 GUMBOS toward Hs578Bst normal breast cells

Table 5.4. IC$_{50}$ concentrations of RB and R110 GUMBOS towards MDA-MB-231 cancer and Hs578Bst normal cells

Compound	MDA-MB-231 IC$_{50}$ (µM)	Hs578Bst IC$_{50}$ (µM)
[RB][BETI]	89.56 ± 3.45	540.32 ± 6.29
[RB][TPB]	77.54 ± 5.71	533.77 ± 3.36
[RB][Cl]	291.07 ± 1.23	500.24 ± 5.21
[R110][BETI]	159.51 ± 1.18	843.84 ± 4.93
[R110][TPB]	105.52 ± 3.16	850.22 ± 3.73
[R110][Cl]	791.29 ± 2.79	836.11 ± 5.38

5.3.4. Synthesis and Characterization of Triple GUMBOS

In order to further improve the selective behavior of these hydrophilic GUMBOS, a secondary cation was added to interact with the carboxylic acid functional group. Since the pKa of the carboxylic acid group on the rhodamines is around 4, at physiological pH the carboxylic acid functional group exists in the deprotonated (COO$^-$) form.[4, 24] Thus, a secondary cation can be added to the RB and R110 GUMBOS bearing this carboxylic functional group to enhance hydrophobicity. Furthermore, this enhanced hydrophobicity could possibly lead to insolubility in water, enabling nanoGUMBOS formation. This modification of the carboxylic acid structure may also aid in elimination of poor mitochondrial localization observed for [RB][Cl] and [R110][Cl] that results from the acid-base properties of the carboxylic acid. Moreover, this modification in the carboxylic acid structure will ultimately aid in improved toxicity of the GUMBOS, while the enhanced hydrophobicity may aid in improving the selectivity.

Here, rhodamine 6G chloride and tetrabutylphosphonium bromide were employed as secondary cations on the [RB][TPB] and [R110][TPB] GUMBOS, and the therapeutic properties of the new triple GUMBOS were assessed. Rhodamine 6G is a lipophilic cation with known

anticancer properties; thus, in addition to enhancing the hydrophobicity, it will also aid in improving the anticancer properties.[25] Tetrabutylphosphonium bromide, [P4444][Br], was chosen due to its minimal systemic toxicity in contrast to other phosphonium compounds.[26] [R6G][Cl] consists of bulky aromatic rings while [P4444][Br] contains aliphatic chains; thus, the effect of the secondary cation structure on the overall toxicity of the GUMBOS can also be examined. The formation of triple GUMBOS is presented in the reaction scheme depicted in Figure 5.11. NMR was then used to confirm addition of the secondary cation (Figure 5.12 and 5.13).

Subsequently, octanol-water partition coefficients were performed for all the triple GUMBOS to assess their relative hydrophobicity. As shown in table 5.5, the [RB][R6G][TPB] GUMBOS displayed a greater hydrophobicity than the [RB][P4444][TPB] GUMBOS. A similar trend was also observed for the R110 based triple GUMBOS such that the [R110][R6G][TPB] was relatively more hydrophobic than [R110][P4444][TPB]. This behavior can be explained by the aromatic structure of R6G as compared to the aliphatic structure of P4444. Furthermore, the hydrophobicity of these triple GUMBOS are substantially increased as compared to that of [R110][TPB] and [RB][TPB]. In this regard, the triple GUMBOS were found to be insoluble in water.

Since the GUMBOS displayed insolubility in water, nanoGUMBOS were synthesized through a reprecipitation method described in the experimental section. Figures 5.14 and 5.15 display the TEM images for all the investigated nanoGUMBOS. Interestingly, fairly spherical nanoparticles with a size of approximately 100 nm was observed for all the nanoGUMBOS. This size is similar to the sizes observed in both the R6G based nanoGUMBOS in Magut et al. and the R123 and SNAFR nanoGUMBOS presented in Chapter 4 of this dissertation.[17]
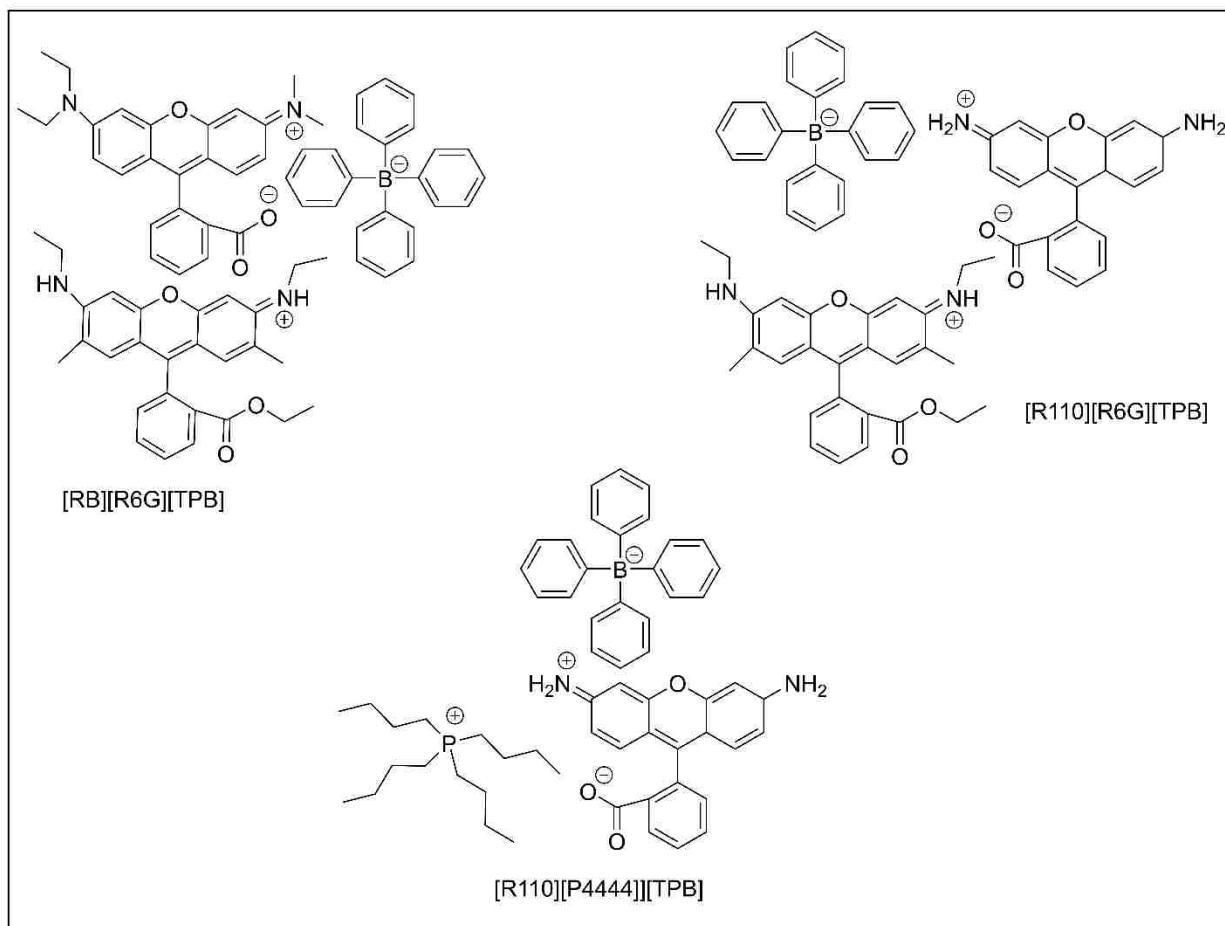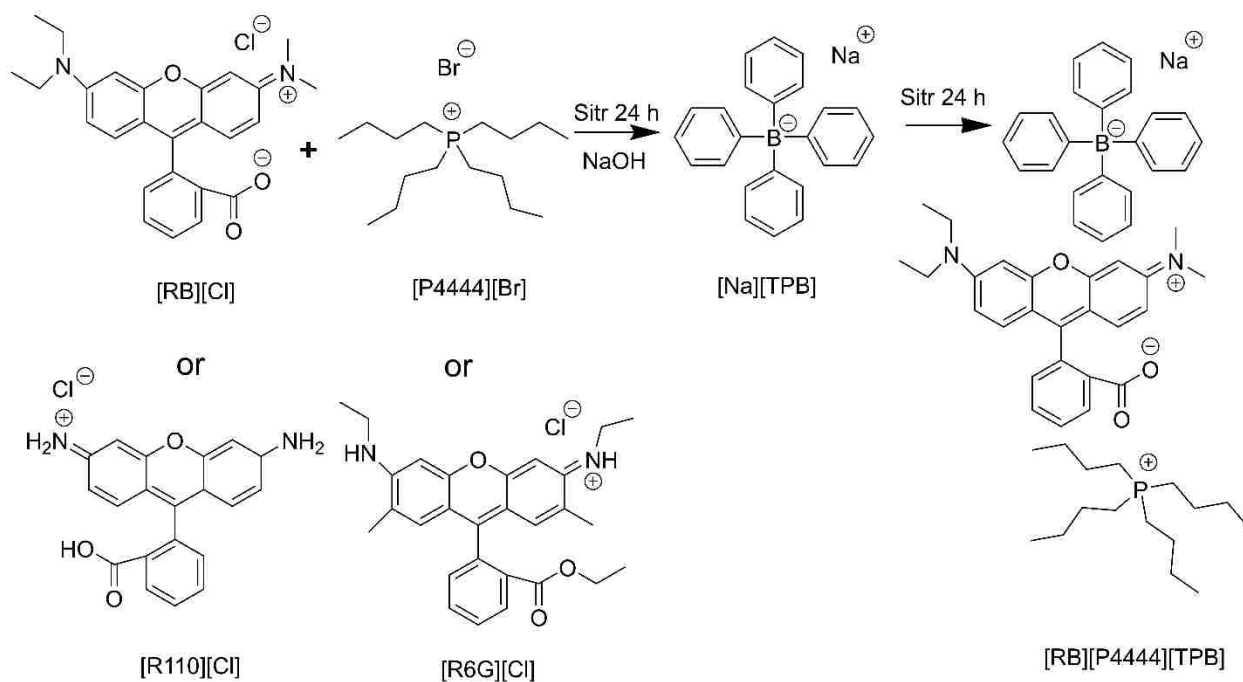
Figure 5.11. Synthesis of rhodamine based triple GUMBOS
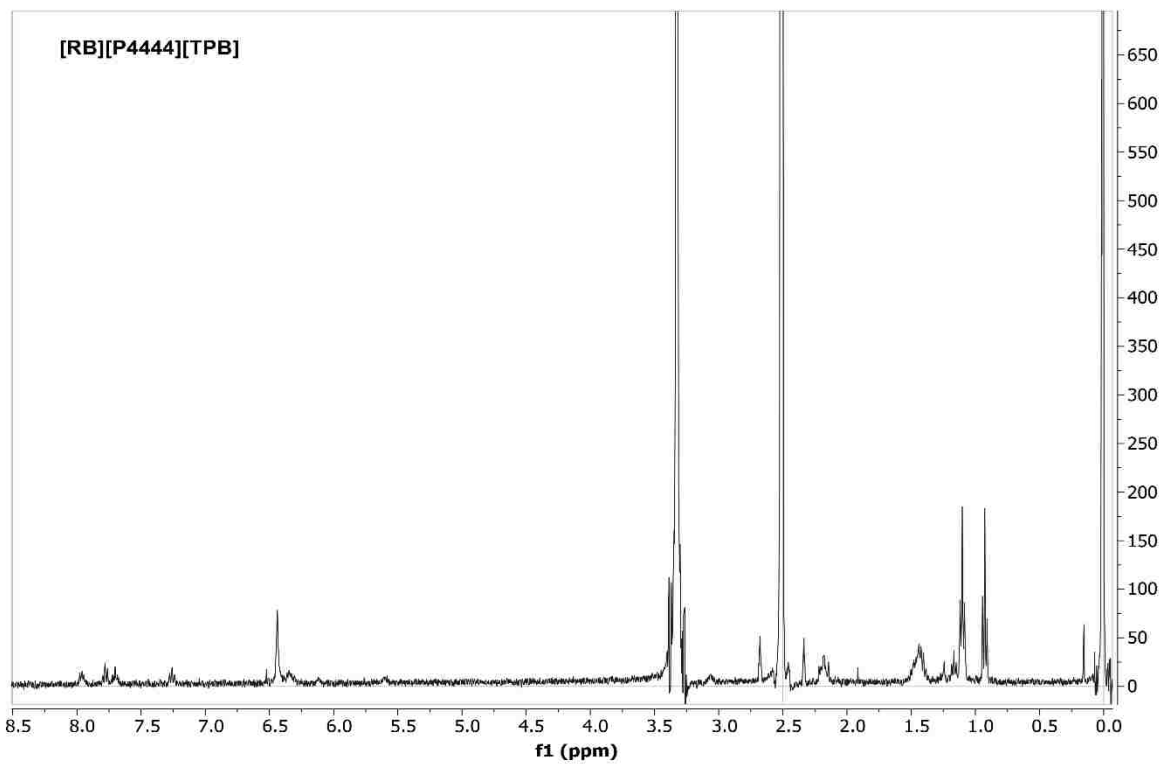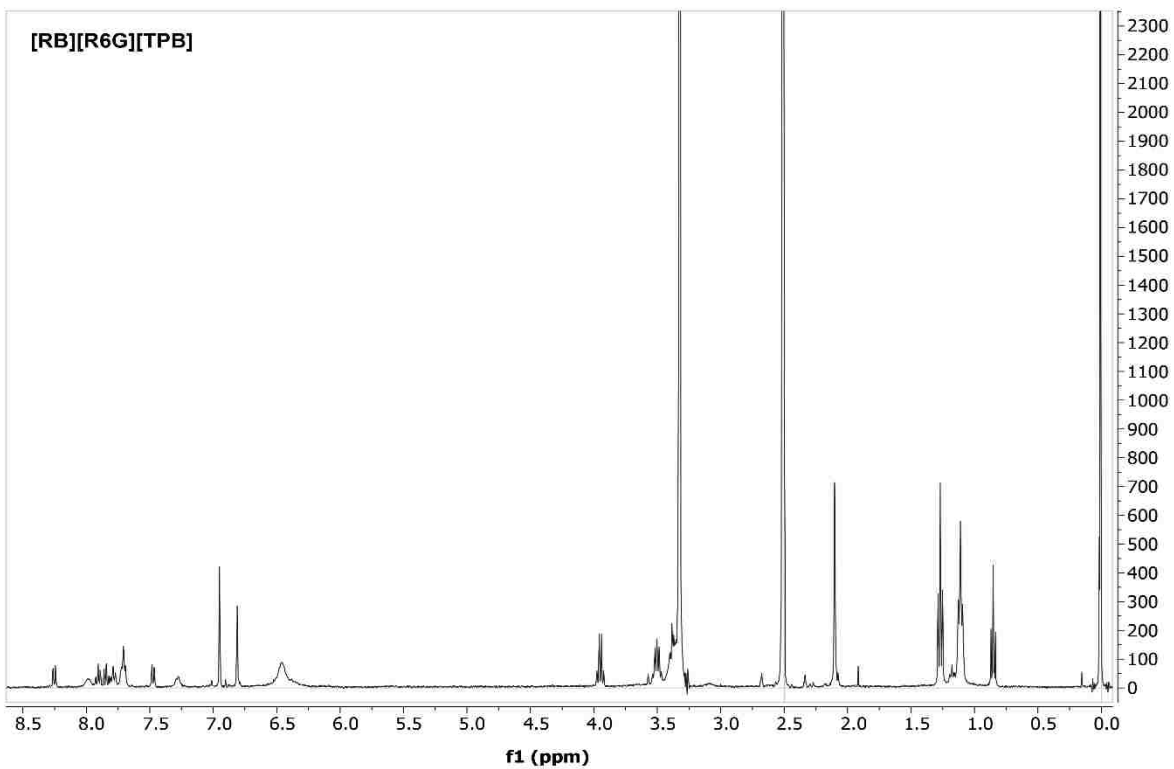
Figure 5.12. NMR spectra of RB0based triple GUMBOS
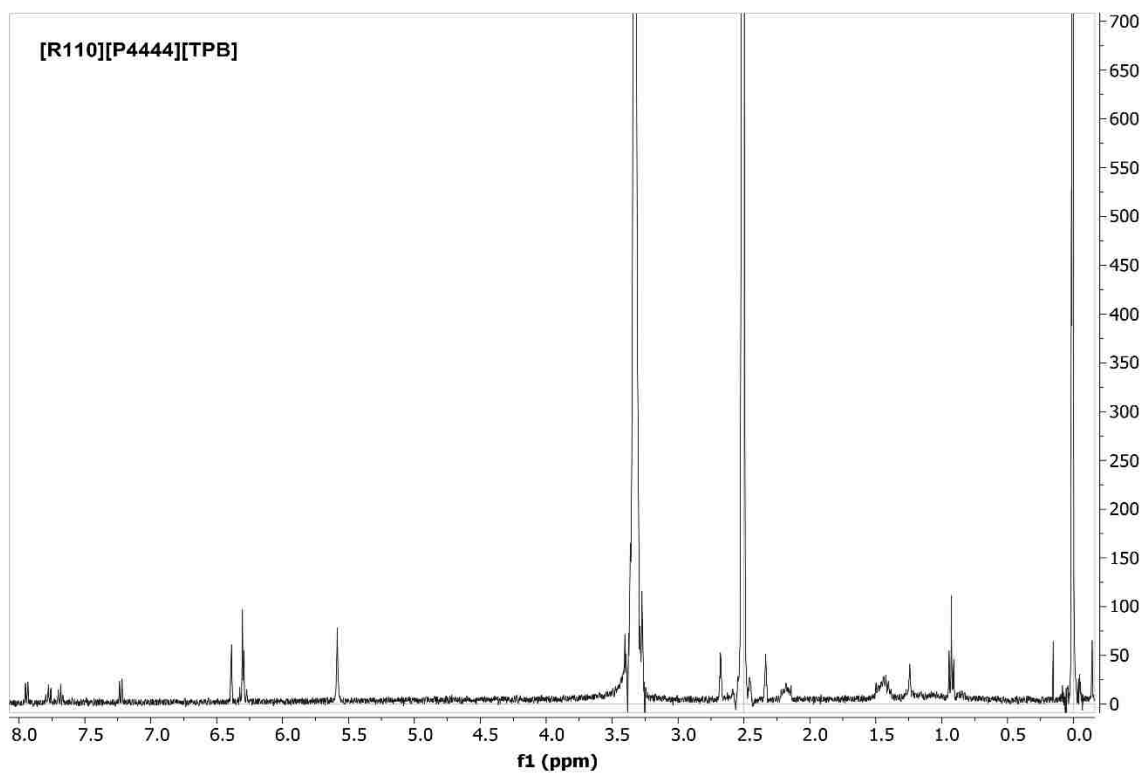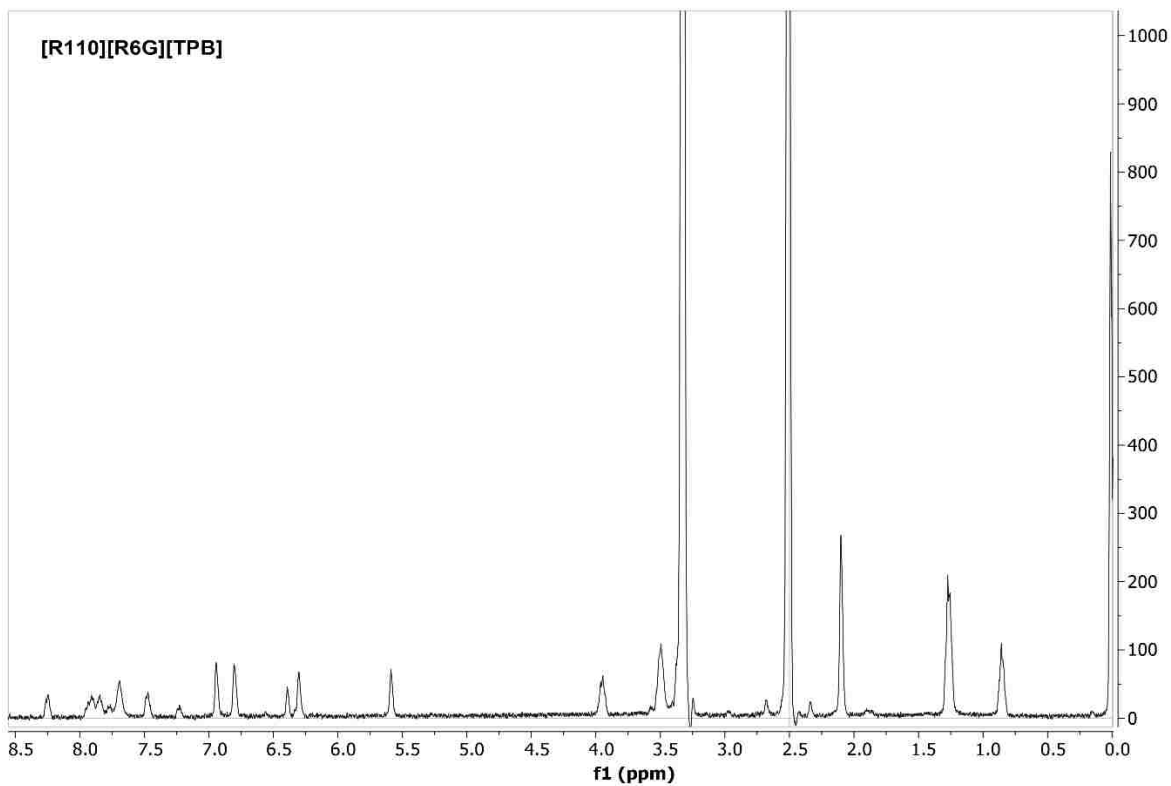
Figure 5.13. NMR spectra of R110-based triple GUMBOS

Table 5.5. Hydrophobicity of RB and R110-based triple GUMBOS

Compound	Log K_{ow}
[RB][R6G][TPB]	1.95 ± 0.11
[R110][R6G][TPB]	1.34 ± 0.24
[RB][P4444][TPB]	1.73 ± 0.29
[R110][P4444][TPB]	1.12 ± 0.15

— 500 nm

[RB][R6G][TPB]
105 ± 20 nm

— 500 nm

[RB][P4444][TPB]
110 ± 16 nm
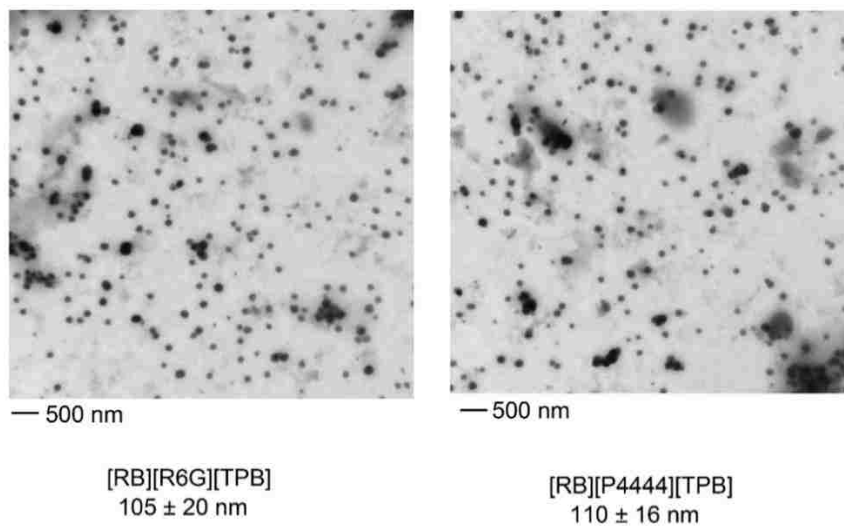
Figure 5.14. TEM images of RB-based triple GUMBOS

— 500 nm

[R110][[R6G][TPB]
108 ± 14 nm

— 500 nm

[R110][P4444][TPB]
115 ± 19

Figure 5.15. TEM images of R110-based triple GUMBOS

5.3.5. Spectroscopic studies of RB and R110 triple GUMBOS

Absorbance and fluorescence measurements were conducted for all the synthesized GUMBOS and nanoGUMBOS to examine the effect of the secondary cation on the spectral properties. Figure 5.16 displays the absorbance and fluorescence spectrum of RB and R110 triple GUMBOS and their respective parent dyes in DMSO. Interestingly, both the [RB][R6G][TPB] and [R110][R6G][TPB] displayed absorbance and emission peak maxima respectively at 537 and 575 nm, which is identical to that of [R6G][Cl]. In contrast, [RB][P4444][TPB] and [R110][P44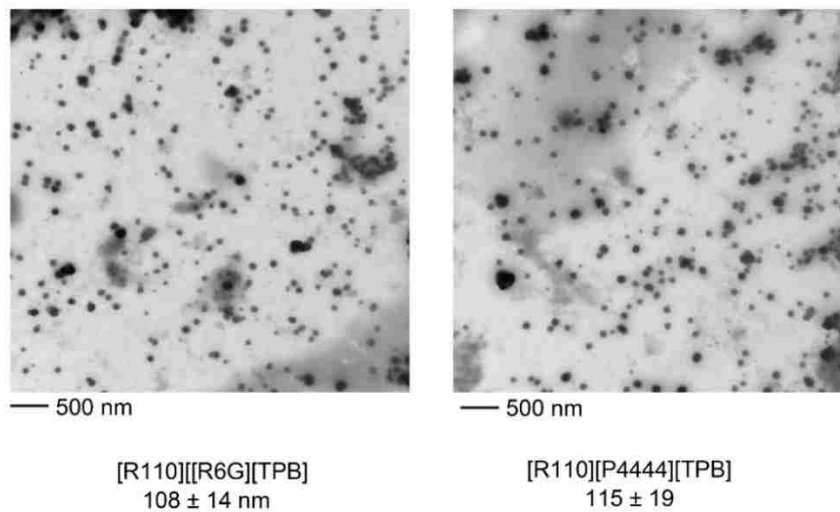44][TPB] showed absorbance and emission peaks similar to that of [R110][Cl] and [RB][Cl] respectively. In this regard, [RB][P4444][TPB] displayed an absorbance and emission of 549 and 571 nm, respectively. [R110][P4444][TPB] displayed an absorbance and emission at 510 and 538 nm, respectively.

Subsequently, fluorescence and absorbance of the nanoGUMBOS in PBS buffer was also investigated to better understand the optical behavior in a biological environment (Figures 5.17). In contrast to the absorbance measured in DMSO, the absorbance of [R110][P4444][TPB] nanoGUMBOS in water was 5 nm blue shifted to 496 nm while the absorbance of [RB][P4444][TPB] nanoGUMBOS remained at 548 nm. Interestingly, the absorbance shift for [R110][P4444][TPB] is consistent with [R110][Cl], whereas [RB][P4444][TPB] is 5 nm blue shifted in comparison to [RB][Cl]. Fluorescence emission of [R110][P4444][TPB] and [RB][P4444][TPB] in water are observed at 518 nm and 575 nm, respectively, which is consistent with their respective parent dyes. In contrast to these P4444 triple GUMBOS, a significant change in peak shape was observed for the [RB][R6G][TPB] and [R110][R6G][TPB] as compared to their parent dyes. In the case of [RB][R6G][TPB], the absorbance and emission maxima was broadened to an absorbance maxima of 534 nm and an emission maxima of 557 nm. In this regard, while the

absorbance maxima was relatively similar to that of [R6G][Cl], the peak was broadened to span the peak wavelength of both [RB][Cl] and [R6G][Cl]. Similarly, for the [R110][R6G][TPB] nanoGUMBOS, while the characteristic R110 peak at 496 nm was still observed, a shoulder peak corresponding to the [R6G][Cl] wavelength at 527 nm was also displayed. Substantial fluorescence emission is observed from both peaks, indicating that the [R110][R6G][TPB] nanoGUMBOS displayed spectral properties of both [R110][Cl] and [R6G][Cl]. These results suggest that addition of the secondary cation can be used to shift the peak wavelength of the GUMBOS.
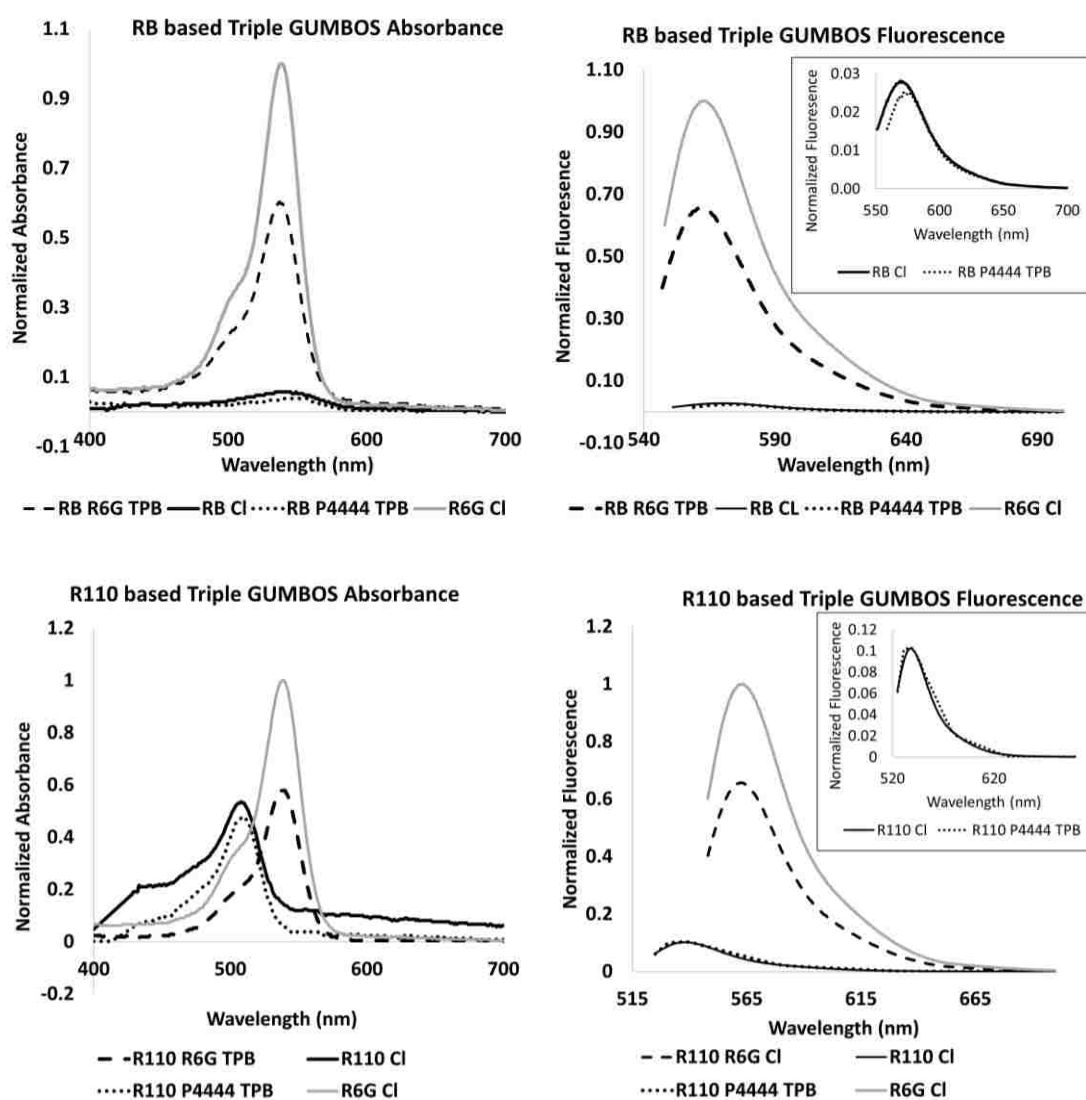
Figure 5.16. UV-Vis and fluorescence characterization of RB and R110-based triple GUMBOS in DMSO
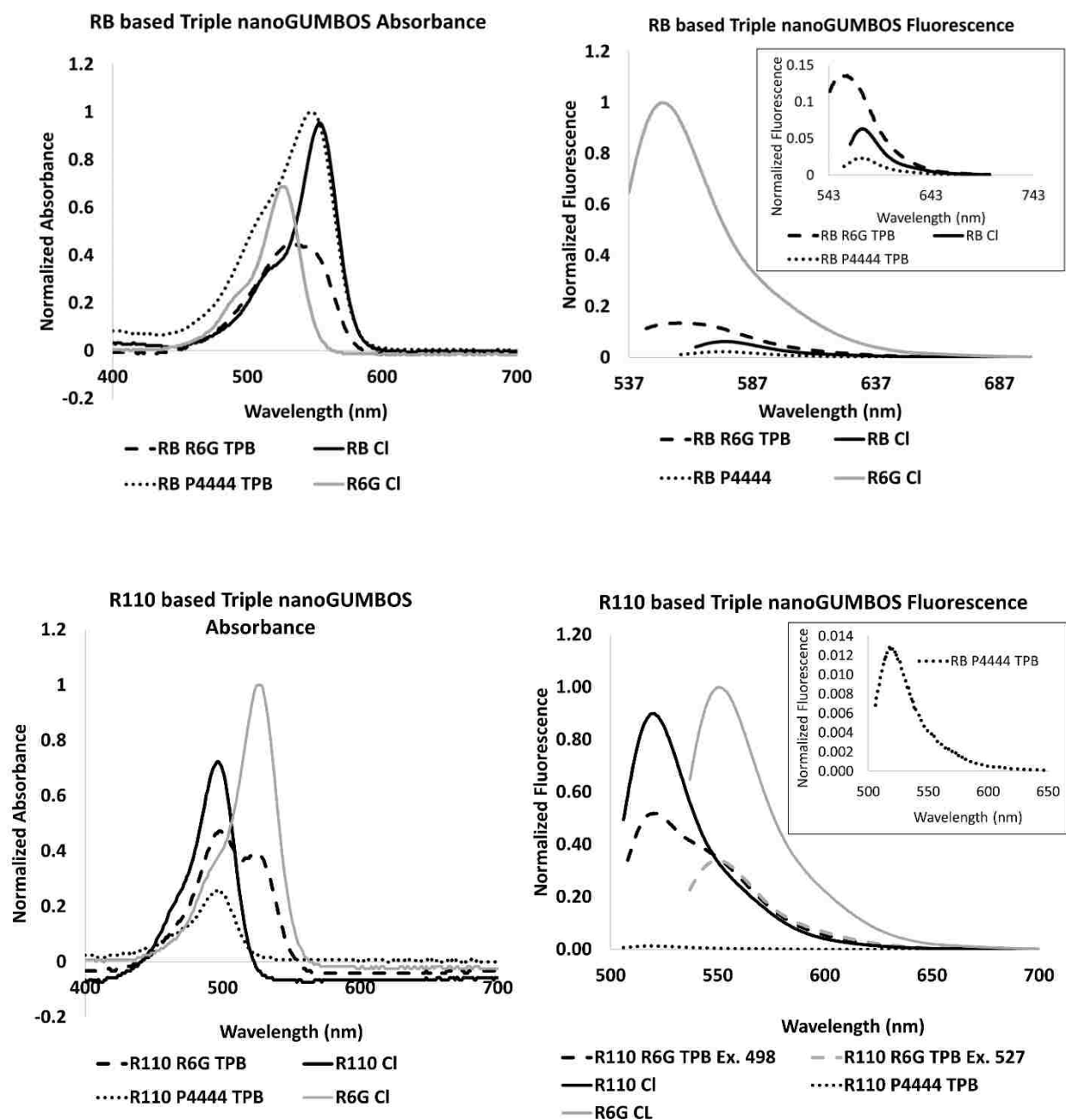
Figure 5.17. UV-Vis and fluorescence characterization of RB and R110-based triple nanoGUMBOS in water

5.3.6. Examination of selective chemotherapeutic applications of Triple GUMBOS

NanoGUMBOS were then tested *in vitro* on MDA-MB-231 cancer cells to evaluate their therapeutic efficacy. Figure 5.18 shows the toxicity of the R110 and RB based nanoGUMBOS,

respectively and IC$_{50}$ values are reported in Table 5.6. As seen in Figure 5.18, [RB][R6G][TPB] nanoGUMBOS displayed higher toxicity than that of the [RB][P4444][TPB] nanoGUMBOS. In this regard, [RB][P4444][TPB] displayed an IC$_{50}$ of 25 μM while [RB][R6G][TPB] nanoGUMBOS displayed an IC$_{50}$ around 3 μM, indicating almost a 10 fold enhancement in toxicity for the [R6G][R6G][TPB] nnanoGUMBOS. This improved toxicity can be attributed to the anticancer properties of the R6G cation.[25, 27] As shown in Table 5.6, the IC$_{50}$ value of [P4444][Br] was larger than 100 μM, indicating minimal to no toxicity towards breast cancer cells. In contrast, [R6G][Cl] has a IC$_{50}$ value around 5 μM, thus giving the R6G based triple GUMBOS a dual anticancer structure from both the RB and R6G cations. A similar trend was also observed for the R110 based triple nanoGUMBOS. Comparison of the toxicity of these triple GUMBOS to the respective parent dyes suggests a significant enhancement in toxicity for the triple GUMBOS. Furthermore, toxicity of the triple nanoGUMBOS was also improved as compared to the [RB][TPB] and [R110][TPB] GUMBOS.
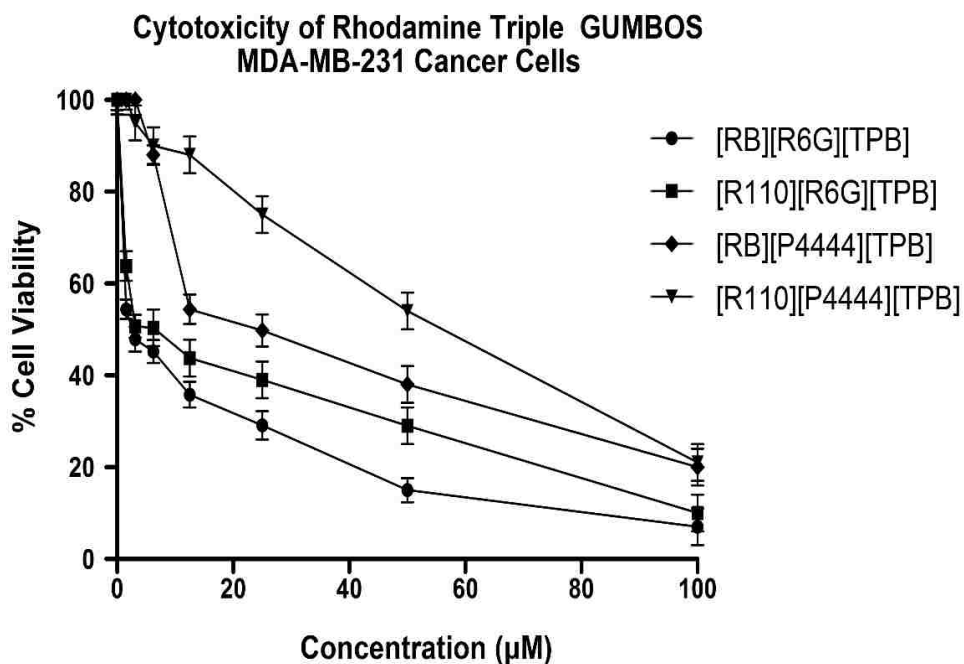

Figure 5.18. Toxicity of triple GUMBOS towards MDA-MB-231 cancer cells

Table 5.6. IC$_{50}$ concentrations of triple GUMBOS towards MDA-MB-231 cancer cells

Compound	MDA-MB-231 IC$_{50}$ (μM)
[RB][R6G][TPB]	2.54 ± 0.73
[R110][R6G][TPB]	7.12 ± 0.84
[RB][P4444][TPB]	24.46 ± 1.14
[R110][P4444][TPB]	57.22 ± 1.37
[P4444][Br]	≥ 100
[R6G][Cl]	5.27 ± 0.88

Cellular uptake studies were then performed for all the synthesized triple nanoGUMBOS. Figure 5.19 is a graphical representation of cellular uptake of all the compounds presented in picomoles internalized after 5 h. incubation of a 12.5 μM nanoGUMBOS solution. [RB][R6G][TPB] and [R110][R6G][TPB] nanoGUMBOS displayed significantly greater uptake as compared to [RB][P4444][TPB] and [R110][P4444][TPB]. This further corroborates the enhanced toxicity observed for the [RB][R6G][TPB] and [R110][R6G][TPB]. Furthermore, all triple nanoGUMBOS displayed an improved cellular uptake and toxicity as compared to the respective GUMBOS and parent dyes. This enhanced cellular uptake is most likely attributed to the modification of the zwitterion structure and formation of nanoGUMBOS. Thus, the electrostatic repulsion observed between the zwitterion structure of the dye and cell membrane is minimized.

In order to further corroborate this enhanced toxicity and cellular uptake, fluorescence microscopy was then employed to examine mitochondrial localization of the dye. Intriguingly, the triple GUMBOS displayed a substantially improved localization as compared to the parent dye. Figure 5.20 is a graphical representation of an overlay of fluorescence from mitotracker green

(green fluorescence) and the compound (red fluorescence). Almost 100% colocalization between the triple nanoGUMBOS and mitotracker was observed, indicating good mitochondrial accumulation. In contrast, the parent dye [RB][Cl] only had a 60% colocalization with the mitotracker, indicating only partial mitochondrial accumulation. These results indicate that in addition to increased cellular internalization, the improved mitochondrial colocalization also aided in the improved therapeutic efficacy.
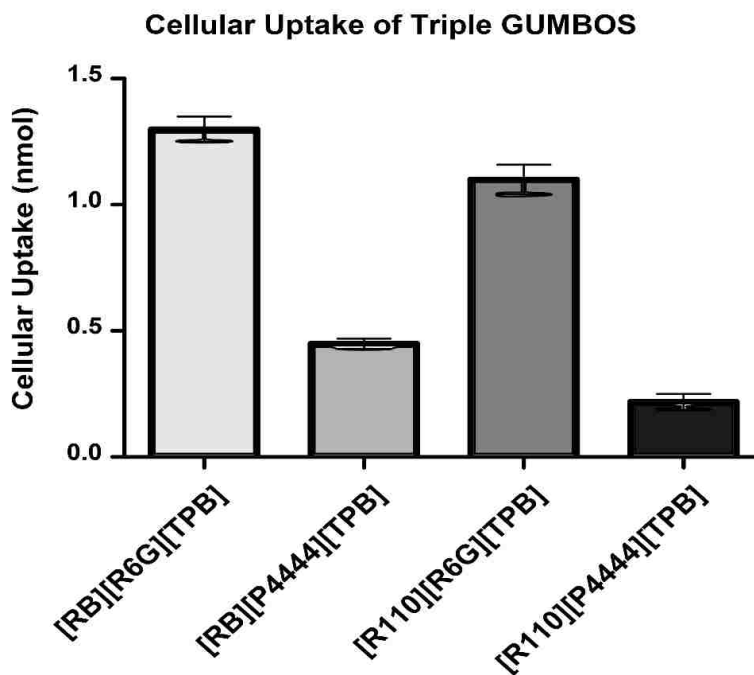
Figure 5.19. Cellular uptake of triple GUMBOS reported as nanomoles internalized

[RB][R6G][TPB]   **[RB][P4444][TPB]**   **[RB][Cl]**
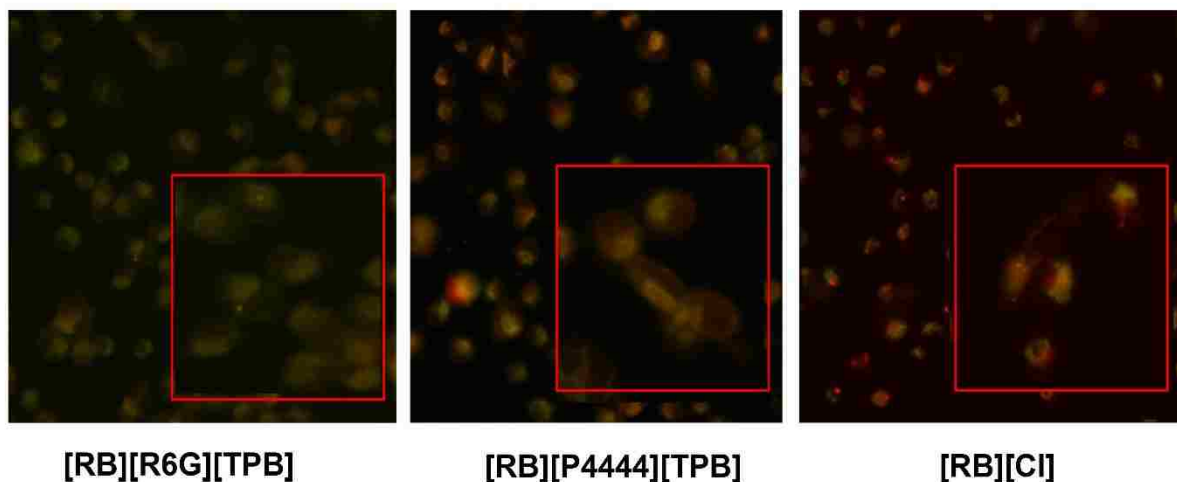
Figure 5.20. Microscopy image of RB compounds incubated in MDA-MB-231 cancer cells displaying the merged overlay between the RB dye and mitotracker.

Since the triple nanoGUMBOS displayed improved chemotherapeutic toxicity, it is essential to investigate their toxicity in breast normal cells to evaluate their selective behavior. Figure 5.21 displayed the toxicity of RB and R110 based triple nanoGUMBOS in Hs578Bst normal breast cells. Intriguingly, no toxicity was observed for the nanomaterials under examined conditions. This suggests that formation of the nanoGUMBOS led to selective toxicity towards cancer cells with no toxicity towards normal cell under examined conditions, which is similar behavior to that of previously investigated R6G nanoGUMBOS.
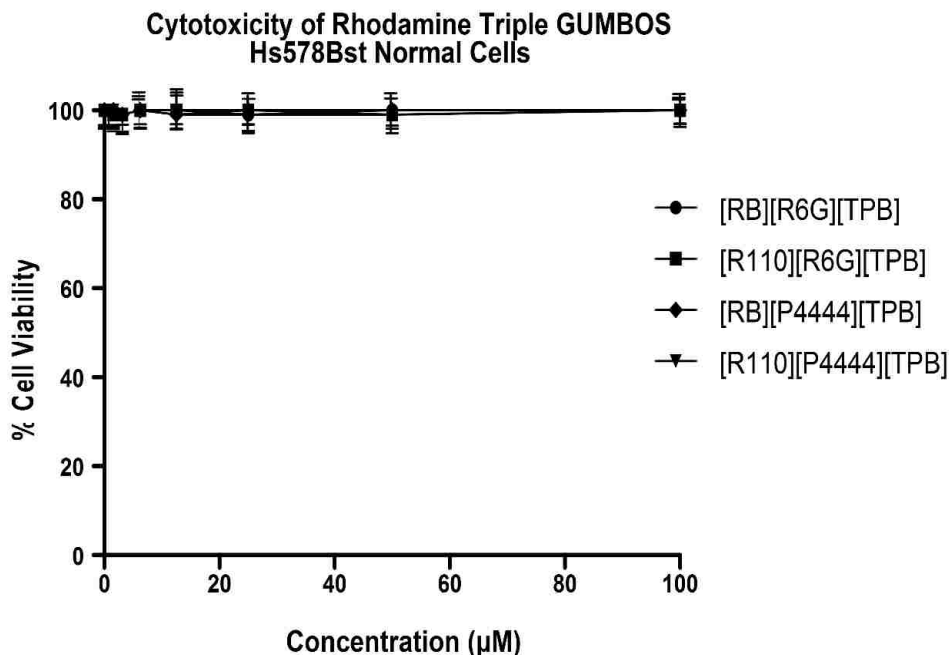
Figure 5.21. Toxicity of triple GUMBOS towards Hs578Bst normal cells

5.4. CONCLUSIONS

The results reported here demonstrate tunable hydrophobicity, solubility, and photo-physical properties of the GUMBOS through counter-ion variation. In this regard, the carboxylic acid functional groups of the R110 and RB compounds led to the formation of GUMBOS that were partly water soluble, ultimately resulting in lack of nanoparticle formation. *In vitro* evaluation of these compounds suggested that these carboxylic acid derivative rhodamine GUMBOS displayed non-selective behavior. This is consistent with the non-selective behavior of the more hydrophilic R6G nanoGUMBOS investigated in Magut et al.[17] Intriguingly, addition of a secondary cation on the carboxylic acid structure led to formation of triple nanoGUMBS that were found to have selective chemotherapeutic toxicity under examined conditions. This indicates that the selective chemotherapeutic behavior is most likely dependent upon nanoparticle formation, similar to the findings reported in Chapter 2 of this dissertation. Furthermore, these triple

GUMBOS displayed a significantly improved toxicity towards cancer cells in contrast to the respective GUMBOS and parent dyes, suggesting their great therapeutic potential. Moreover, these findings indicate that the nanoGUMBOS concept can be used for various cationic dyes to generate an array of selective chemotherapeutics to combat the problem of systemic toxicity of current chemotherapeutics.

5.5. REFERENCES

1.   Shibata, A.; Furukawa, K.; Abe, H.; Tsuneda, S.; Ito, Y., Rhodamine-based fluorogenic probe for imaging biological thiol. *Bioorganic & Medicinal Chemistry Letters* **2008,** *18* (7), 2246-2249.

2.   Jeannot, V.; Salmon, J.-M.; Deumié, M.; Viallet, P., Intracellular accumulation of rhodamine 110 in single living cells. *Journal of Histochemistry & Cytochemistry* **1997,** *45* (3), 403-412.

3.   Alford, R.; Simpson, H. M.; Duberman, J.; Hill, G. C.; Ogawa, M.; Regino, C.; Kobayashi, H.; Choyke, P. L., Toxicity of organic fluorophores used in molecular imaging: literature review. *Molecular imaging* **2009,** *8* (6), 7290.2009. 00031.

4.   Johnson, L. V.; Walsh, M. L.; Chen, L. B., Localization of mitochondria in living cells with rhodamine 123. *Proceedings of the National Academy of Sciences* **1980,** *77* (2), 990-994.

5.   Lampidis, T. J.; Castello, C.; Del Giglio, A.; Pressman, B. C.; Viallet, P.; Trevorrow, K. W.; Valet, G. K.; Tapiero, H.; Savaraj, N., Relevance of the chemical charge of rhodamine dyes to multiple drug resistance. *Biochemical pharmacology* **1989,** *38* (23), 4267-4271.

6.   Belostotsky, I.; Da Silva, S.; Paez, M.; Indig, G., Mitochondrial targeting for photochemotherapy. Can selective tumor cell killing be predicted based on n-octanol/water distribution coefficients? *Biotechnic & Histochemistry* **2011,** *86* (5), 302-314.

7.   Heo, D. N.; Yang, D. H.; Moon, H.-J.; Lee, J. B.; Bae, M. S.; Lee, S. C.; Lee, W. J.; Sun, I.-C.; Kwon, I. K., Gold nanoparticles surface-functionalized with paclitaxel drug and biotin receptor as theranostic agents for cancer therapy. *Biomaterials* **2012,** *33* (3), 856-866.

8.   Du, J.-Z.; Du, X.-J.; Mao, C.-Q.; Wang, J., Tailor-made dual pH-sensitive polymer–doxorubicin nanoparticles for efficient anticancer drug delivery. *Journal of the American Chemical Society* **2011,** *133* (44), 17560-17563.

9.   Allen, T. M.; Cullis, P. R., Drug delivery systems: entering the mainstream. *Science* **2004,** *303* (5665), 1818-1822.

10.   Kawasaki, E. S.; Player, A., Nanotechnology, nanomedicine, and the development of new, effective therapies for cancer. *Nanomedicine: Nanotechnology, Biology and Medicine* **2005,** *1* (2), 101-109.

11.   Wong, H. L.; Bendayan, R.; Rauth, A. M.; Xue, H. Y.; Babakhanian, K.; Wu, X. Y., A mechanistic study of enhanced doxorubicin uptake and retention in multidrug resistant breast cancer cells using a polymer-lipid hybrid nanoparticle system. *Journal of Pharmacology and Experimental Therapeutics* **2006,** *317* (3), 1372-1381.

12.   Kumari, A.; Yadav, S. K.; Yadav, S. C., Biodegradable polymeric nanoparticles based drug delivery systems. *Colloids and Surfaces B: Biointerfaces* **2010,** *75* (1), 1-18.

13.   Sahay, G.; Kim, J. O.; Kabanov, A. V.; Bronich, T. K., The exploitation of differential endocytic pathways in normal and tumor cells in the selective targeting of nanoparticulate chemotherapeutic agents. *Biomaterials* **2010,** *31* (5), 923-933.

14.   Duncan, R.; Richardson, S. C., Endocytosis and intracellular trafficking as gateways for nanomedicine delivery: opportunities and challenges. *Molecular pharmaceutics* **2012,** *9* (9), 2380-2402.

15.   Akinc, A.; Battaglia, G., Exploiting endocytosis for nanomedicines. *Cold Spring Harbor perspectives in biology* **2013,** *5* (11), a016980.

16.   Warner, I. M.; El-Zahab, B.; Siraj, N., Perspectives on moving ionic liquid chemistry into the solid phase. *Analytical chemistry* **2014,** *86* (15), 7184-7191.

17.   Magut, P. K.; Das, S.; Fernand, V. E.; Losso, J.; McDonough, K.; Naylor, B. M.; Aggarwal, S.; Warner, I. M., Tunable cytotoxicity of rhodamine 6G via anion variations. *Journal of the American Chemical Society* **2013,** *135* (42), 15873-15879.

18.   Couvreur, P., Nanoparticles in drug delivery: past, present and future. *Advanced drug delivery reviews* **2013,** *65* (1), 21-23.

19.   Shen, Y.; Jin, E.; Zhang, B.; Murphy, C. J.; Sui, M.; Zhao, J.; Wang, J.; Tang, J.; Fan, M.; Van Kirk, E., Prodrugs forming high drug loading multifunctional nanocapsules for intracellular cancer drug delivery. *Journal of the American Chemical Society* **2010,** *132* (12), 4259-4265.

20.   Park, K., Nanotechnology: What it can do for drug delivery. *Journal of controlled release: official journal of the Controlled Release Society* **2007,** *120* (1-2), 1.

21.   Fröhlich, E., The role of surface charge in cellular uptake and cytotoxicity of medical nanoparticles. *International journal of nanomedicine* **2012,** *7*, 5577.

22.   Cole, M. R.; Hobden, J. A.; Warner, I. M., Recycling antibiotics into GUMBOS: A new combination strategy to combat multi-drug-resistant bacteria. *Molecules* **2015,** *20* (4), 6466-6487.

23.   Tesfai, A.; El-Zahab, B.; Kelley, A. T.; Li, M.; Garno, J. C.; Baker, G. A.; Warner, I. M., Magnetic and nonmagnetic nanoparticles from a group of uniform materials based on organic salts. *Acs Nano* **2009,** *3* (10), 3244-3250.

24.   Merouani, S.; Hamdaoui, O.; Saoudi, F.; Chiha, M., Sonochemical degradation of Rhodamine B in aqueous phase: effects of additives. *Chemical Engineering Journal* **2010,** *158* (3), 550-557.

25.   Kutushov, M.; Gorelik, O., Low concentrations of Rhodamine-6G selectively destroy tumor cells and improve survival of melanoma transplanted mice. *Neoplasma* **2013,** *60* (3), 262-73.

26.   Ventura, S. P.; Marques, C. S.; Rosatella, A. A.; Afonso, C. A.; Gonçalves, F.; Coutinho, J. A., Toxicity assessment of various ionic liquid families towards Vibrio fischeri marine bacteria. *Ecotoxicology and environmental safety* **2012,** *76*, 162-168.

27.   Fearon, K. C.; Plumb, J. A.; Burns, H. J.; Calman, K. C., Reduction of the growth rate of the Walker 256 tumor in rats by rhodamine 6G together with hypoglycemia. *Cancer research* **1987,** *47* (14), 3684-3687.

CHAPTER 6
CONCLUSIONS AND FUTURE WORK

6.1. CONCLUSIONS

This dissertation discusses the chemotherapeutic potential of rhodamine based GUMBOS and concludes that the selective chemotherapeutic behavior observed previously in our group with the R6G nanoGUMBOS is observed for other rhodamine cation structures as well. The studies in Chapter 2 investigate the mechanism of selective toxicity and *in vivo* applications of R6G based nanoGUMBOS. These studies provide insight into a simple technique for development of more selective chemotherapeutics, and give further understanding to the potential clinical application of the nanoGUMBOS. As shown in Chapter 3, the toxicity of the nanoGUMBOS can be optimized by tuning the size of the nanoparticle. Using cyclodextrin to control the size of the nanoparticle suggested a size dependence on the chemotherapeutic toxicity, which is consistent with literature findings that suggest 80-100 nm as an optimal size for enhanced efficacy of nanomaterials employed biomedical applications. Furthermore, studies investigated in Chapters 4 and 5 indicate a structural dependence on the selective behavior of the examined nanomaterials. In this regard, while the GUMBOS derived from the zwitterion rhodamines displayed non-selective behavior, addition of a secondary cation on the carboxylic acid functional group led to selective behavior under the experimental conditions used in this work. Thus, from these studies, we can conclude that the GUMBOS concept can be applied to other hydrophobic cationic drugs to minimize their systemic toxicity.

6.2. FUTURE WORK

While this dissertation primarily focuses GUMBOS derived from rhodamine derivatives and their selective chemotherapeutic behavior, it would be interesting to examine if a similar behavior is also observed for other lipophilic cations. Since the rhodamines absorb light in the UV-

Vis range, it would be interesting to investigate this behavior in near infrared (NIR) dyes. NIR dyes absorb in the NIR region, which is known as the tissue transparent region, enabling use for both imaging and therapeutic purposes. This can be especially beneficial for fluorescence guided surgery applications. Furthermore, as the *in vivo* studies indicated a significant reduction in tumor volume, thus it would be of interest to examine if enhanced therapeutic efficacy is observed after addition of targeting ligands such as antibodies overexpressed on the breast cancer cells surface. Furthermore, for future examinations of the *in vivo* behavior, pathology studies of an untumored mouse treated with the nanoGUMBOS can provide further insight to the *in vivo* selectivity. Additionally, evaluation *in vivo* drug halflife within the blood plasma will provide further knowledge for possible clinical applications of the nanoGUMBOS. For future *in vivo* studies, use of the cyclodextrin templating method may also aid in minimizing the agglomeration observed in the results presented in this dissertation. In addition, the cyclodextrin (CD) templating can be modified to complex the cyclodextrin with the dye to assess the effect of CD as a drug delivery agent on the therapeutic properties of the nanoGUMBOS. Lastly, examination of the excretion of the cyclodextrin templated nanoparticles in contrast to the untemplated nanoparticles can provide further understanding of pharmacokinetic behavior of these nanomaterials.

VITA

Nimisha Bhattarai was born in Kathmandu, Nepal and immigrated to the United States at the age of 3. She grew up in Warrensburg, Missouri and attended Warrensburg high school where she gained a passion for chemistry and biology through both class work and numerous volunteer teaching opportunities. She later attended University of Central Missouri where she gained her first experience in chemistry research under Dr. Innocent Pumure. This research experience furthered her passion for chemistry and she began her graduate studies in Fall of 2013 at Louisiana State University in Professor Isiah Warner's research group. Nimisha plans to graduate with a Doctor of Philosophy in Chemistry from Louisiana State University in May of 2018.